Vascular calcification in chronic kidney disease

Vascular calcification in chronic kidney disease: vitamin K deficiency and new mediators

Sofía de la Puente-Secades

ISBN:
Printed by: Ridderprint
Cover design. Elena Fernández (@elenaf16)

Vascular calcification in chronic kidney disease: vitamin K deficiency and new mediators

DISSERTATION

to obtain the degree of Doctor at Maastricht University,
and Doctor rerum naturalium (Dr.rer.nat.) at the RWTH Aachen
on the authority of the Rector Magnifici,
Prof. dr. Pamela Habibović and Univ.-Prof. Dr. rer. nat. Dr. h.c. mult. Ulrich Rüdiger
in accordance with the decision of the Board of Deans,
to be defended in public
on Tuesday November 14th, 2023, at 13:00 hours

by

Sofía de la Puente-Secades

Supervisors:

Prof. dr. Leon Schurgers
Prof. dr. Joachim Jankowski (UKA)
Prof. dr. Juergen Floege (UKA)

Assessment committee:

Prof. dr. Rory Koene (Chair; Maastricht)
Prof. dr. Abraham Kroon (Maastricht)
Prof. dr. Michael Lehrke (Aachen)
Prof. dr. Wilhelm Jahnen-Dechent (Aachen)
Dr. Julie Klein (Toulouse)
Dr. Anja Verhulst (Antwerpen)

The research presented in this dissertation was funded with a grant from European Union's Horizon 2020 research and innovation programme under the Marie Sklodowska-Curie grant (agreement No 764474), CaReSyAn and SFB/TRR219 (Project ID- 322900939).
The work of this thesis was mainly performed at the Institute of Molecular Cardiovascular Research (IMCAR)-Uniklinik RWTH Aachen, Germany (head: Prof. Dr. Joachim Jankowski)

ABBREVIATIONS

ADP: Adenosine diphosphate

ALP: Alkaline phosphatase

Ang II: Angiotensin II

ApoB: Apolipoprotein B

ApoE: Apolipoprotein E

AT2: Angiotensin II type 2 receptor

ATP: Adenosine triphosphate

BCA: Bicinchoninic acid

BMP-2: Bone morphogenetic proteins

BSA: Bovine serum albumin

Ca^{2+}: Calcium ions

CAC: Coronary artery calcification

$CaCl_2$: Calcium chloride

CaSR: Calcium-sensing receptor

CBF: Calcification Blocking Factor

cDNA: Complementary deoxyribonucleic acid

CKD: Chronic kidney disease

CKD-EPI: Chronic Kidney Disease-Epidemiology Collaboration

CM: Calcifying medium

CM+VIF: Calcifying medium with addition of VIF

Co-IP: Co-immunoprecipitation

CPM: Calciprotein monomers

CPP-I: Primary Calciprotein Particles

CPP-II: Secondary Calciprotein Particles

CPPs: Calciprotein Particles

CRS: Cardiorenal syndrome

CT: Computer tomography

CVD: Cardiovascular diseases

Cy: Cyanine

Da: Dalton

DAPI: 4′,6-diamidino-2-phenylindole

ddH2O: Double-distilled water

DMEM: Dulbecco's modified Eagle's medium

dp-ucMGP : Unphospho- and uncarboxy- MGP

EC_{50}: Half maximal effective concentration

eNPP1: Ectonucleotide Pyrophosphatase/Phosphodiesterase 1
ERAD: Endoplasmic reticulum-associated protein degradation
FACS: Flow cytometry and fluorescence-activated cell sorting
FBS: Fetal bovine serum
FCS: Fetal calf serum
FGF23: Fibroblast growth factor 23
FITC: Fluorescein isothiocyanate
GFR: Glomerular filtration rate
GGCX: γ-glutamyl carboxylase
GGPP: Geranylgeranyl pyrophosphate
H_2DCFDA: 2',7'-dichlorodihydrofluorescein diacetate
hAoSMCs: Human aortic smooth muscle cells
HBSS: Hanks' Balanced Salt Solution
HDL: High-density lipoprotein
HMGCR: 3-hydroxy-3-methylglutaryl-coenzyme A reductase
HPLC: High-pressure liquid chromatography
IL: Interleukin
LDL: Low density lipoprotein
Lmna: Lamin A/C gen
MALDI-TOF/TOF: Matrix-assisted laser desorption/ionization time of flight/time of flight
MAPK: Mitogen-activated protein kinases
MGP: Matrix Gla protein
MK: Menaquinone
MOVAS: Mouse vascular smooth muscle cell
mRNA: Messenger ribonucleic acid
MSX2: Msh Homeobox 2
Na_2HPO_4/NaH_2PO_4: Sodium hydrogen phosphates
NaPi: Sodium/phosphate cotransporters
NCM: Non-calcifying medium
NF-κB: Nuclear factor kappa-light-chain-enhancer of activated B cells
NQO1: NAD(P)H Quinone Dehydrogenase 1
OCN: Osteocalcin
p-cMGP: Phospho- and carboxylated MGP
Pi: Inorganic phosphate
PIT-1/2: Sodium-dependent phosphate cotransporter-1 /2
PO_4^{3-}: Phosphate ions
PPi: Pyrophosphate

PTH: Parathyroid hormone

PTM: Post-translational modification

RAAS: Renin-Angiotensin-Aldosteron-System

RIPA: Radioimmunoprecipitation assay

ROS: Reactive oxygen species

RT-PCR: Real time-polymerase chain reaction

SCD: Schnyder Corneal Dystrophy

SD: Standard deviation

SDS: Sodium dodecyl sulphate

SEM: Standard error of the mean

Ser: Serine

SMCs: Smooth muscle cells

SOX9: SRY-Box Transcription Factor 9

STK: Serine-threonine kinase

Thr: Threonine

TNF-α: Tumor necrosis factor

UBIAD1: UbiA prenyl- transferase domain-containing 1

ucMGP: Uncarboxylated MGP

VDN: Vitamin D3 plus nicotine

VGCC: Voltage-gated channels

VIF: Vasoconstriction-Inhibiting Factor

Vit K: Vitamin K

VKDP: Vitamin K-dependent proteins

VKORC1: Vitamin K epoxide reductase complex subunit 1

VSMCs: Vascular smooth muscle cells

WHO: World health organization

α-SMA: α-Smooth Muscle Actin

Chapter 1

Introduction

1. INTRODUCTION

1.1. Chronic kidney disease

Chronic kidney disease (CKD) is a serious global health problem, during the last decades the number of worldwide deaths due to this disease has increased by almost 50% [1,2]. CKD is defined as increased proteinuria, which is the presence of proteins in the urine and is assessed by the urinary albumin-to-creatinine ratio. CKD is also defined as the impairment of the kidney function confirmed on two or more occasions at least 3 months apart [3].Kidney function is measured by calculation of the glomerular filtration rate (GFR) by the equation of the Chronic Kidney Disease-Epidemiology Collaboration (CKD-EPI) [4]. This equation takes into consideration sex, age, ethnic origin and serum creatinine concentration and classifies CKD into 5 stages [4]. Reduced kidney function is diagnosed as CKD if the GFR is below 60 mL/min/1.73 m^2 for at least three consecutive months [4,5]. The classification of the different CKD stages based on GFR can be observed in **Table 1**.

Table 1: Classification of CKD stages by the national kidney foundation [5].

Stages	GFR [mL/min/1.73 m^2]	Description
1	≥90	Kidney damage with normal or high GFR
2	60-89	Kidney damage with mild reduction of GFR
3A	45-59	Mildly to moderate reduction of GFR
3B	30-44	Moderate to severe reduction of GFR
4	15-29	Severe reduction of GFR
5	<15 (or dialysis)	Kidney failure

GFR decreases with age [6], but it is also influenced by other factors like diabetes and hypertension [2]. Data from different studies assessed that GFR rates higher than 75 mL/min/1.73 m^2 have a low risk for cardiovascular mortality, but this risk increases with the further decrease of the estimated glomerular filtration rates. For example, cardiovascular mortality was two times higher in patients with stage 3, and three times higher at stage 4, compared to individuals with normal kidney function [7]. In patients with CKD stage 3, the incidence of cardiovascular mortality is much higher than the incidence of kidney failure [7], which suggests that mortality in patients with mildly CKD is mainly related to the increased risk of cardiovascular diseases (CVD) rather than to the kidney failure itself, which makes CVD the major cause of death in CKD patients [3]. To summarize, patients suffering from chronic kidney disease have a highly increased risk of cardiovascular diseases [8,9].

1.2. Cardiovascular diseases

Cardiovascular diseases (CVD) are one of the major causes of human deaths worldwide and are responsible for more than 17.7 million deaths in 2016, according to the world health organization (WHO) [10]. CVD can be described as pathologies of the vessels, blood and heart and can be classified into two groups depending on whether they are related to the atherosclerotic process, such as ischaemic heart disease, coronary artery disease, cerebrovascular disease and diseases of the aorta and arteries, or not related to atherosclerosis, including congenital heart disease, rheumatic heart diseases, cardiomyopathies and arrhythmias [11]. The major pathological mechanisms that underlie CVD are inflammation, oxidative stress, thrombosis, vascular calcification and fibrosis [12].

Conventional risk factors for CVD are high concentrations of ApoB lipoproteins (mainly Low-Density Lipoprotein (LDL)), high blood pressure, smoking and diabetes [13]. To lower the risk of developing cardiovascular diseases, a healthy lifestyle is the main recommendation, which includes not smoking, a dietary sodium reduction, protein restriction, body weight management and having daily physical activity [3]. All of these approaches would only be effective if the recommendations are taken into account the during the early stage of CVD, the higher the stage, the less effective they are [13]. In case these recommendations are not enough, pharmacological interventions can be addressed [13]. Treatment with RAAS (Renin-Angiotensin-Aldosterone-System) inhibitors to low the pressure [3], and statins as a drug for lipid-lowering therapies (mainly LDL lowering therapies) are common therapies used in clinics [14,15].

To prevent the development of cardiovascular diseases, not only conventional cardiovascular risk factors should be controlled but also the prevention of the loss of kidney function should be considered. Cardiovascular diseases are also associated with impaired kidney function, regardless of age, sex or ethnic origin [3]. As mentioned before, CKD itself should be considered as a notable risk factor for CVD, but until now it has remained hidden, and only during the last years it is starting to be considered and described as one of the highest risk factors for CVD [13].

The clinical condition in which patients suffer at the same time from CKD and CVD is called cardiorenal syndrome (CRS). More precisely, patients with cardiorenal syndrome have a dysfunction at the same time of kidneys and heart, and the dysfunction of one of the organs induces the damage of the other [16]. Cardiorenal syndrome can also be classified in 5 types, based on the organ that is impaired the first (**Table 2**) [17]. This syndrome is influenced by

different pathological mechanisms like oxidative stress, fibrosis, inflammation and lastly phosphate and calcium misbalance, also called vascular calcification [8,16].

Table 2: Classification of cardiorenal syndrome by Ronco *et al.* 2014 [17].

Type	Name	Description
1	Acute CRS	Worsening cardiac function leading to acute kidney injury
2	Chronic CRS	Chronic heart failures causing CKD
3	Acute renocardiac syndrome	Worsening of kidney function leading to cardiac disorder
4	Chronic renocardiac syndrome	CKD leading to increase of cardiovascular events
5	Secondary CRS	Acute cardiac and kidney injury

The pathophysiological mechanisms that increase CVD risk in CKD are not fully elucidated. In early stages of CKD, vitamin D deficiency, smoking, dyslipidaemia, chronic inflammation and diabetes mellitus increase the risk of CVD, while hypertension and hypertrophy are risk factors for all stages of CKD to cause CVD [3]. In addition, in the mild to moderate stages of CKD, there are abnormalities in calcium and phosphate balance, triggered by uremic toxins among others, that will lead to soft tissue vascular calcification, atherosclerosis and more CVD [3].

1.3. Vascular calcification

It has been shown that one of the main predictors of CVD mortality in end-stage CKD is vascular calcification [18]. Vascular calcification is a pathological process in which there is a deposition of calcium phosphate salts in vascular tissues. This process can be compared to the bone formation process [19]. During vascular calcification development the vessel wall becomes stiffer, which increases blood pressure and negatively impacts blood circulation [20]. Vascular calcification is frequently occurring in the general population, and it is associated with high cardiovascular risk [21] and CKD [17], with 100% of the patients in CKD stage 5 on dialysis developing calcification in the aortic valve, mitral annulus or mitral valve [23]. Furthermore, in a

10-year follow-up study, individuals with no calcification detected via computed tomography showed less mortality than individuals that did show calcification [24].

1.3.1. Vascular layers: different types of vascular calcification

Vascular calcification can take place in different areas of the vessel wall. The wall consists of three layers (**Figure 1**) [25,26]: The inner layer, called the *intimal layer* or intima, is made up of endothelial cells, elastin and smooth muscle cells (SMCs). Intimal calcification, which is calcification of this layer, is driven by inflammation and lipid accumulation in the endothelial cells and results in atherosclerotic plaques, therefore it is also called atherosclerotic calcification [25,27]. Medial calcification, also called 'Monckenberg calcification', takes place in the *medial layer* which is made up of SMCs [28] and connective tissue. This type of vascular calcification is related to diabetes mellitus and CKD [19,25]. Medial calcification is driven by a breakdown in the extracellular matrix and deposition of minerals on the SMCs layer also linked to SMCs phenotypic change [29], which leads to stiffness of the wall and therefore hypertension and CVD. The lipid composition of calcification plaques is different between the intimal and the medial layer. While in the intimal layer there is a mix of cholesterol, cholesteryl esters and fatty acids, in the medial layer, and also in the bone, the fatty acids are the main component [30]. There is a third layer, called *adventitia* which is formed by myofibroblasts and has a connecting tissue function [25]. In patients no calcification has been found in this layer, only in *ex vivo* experiments [31].

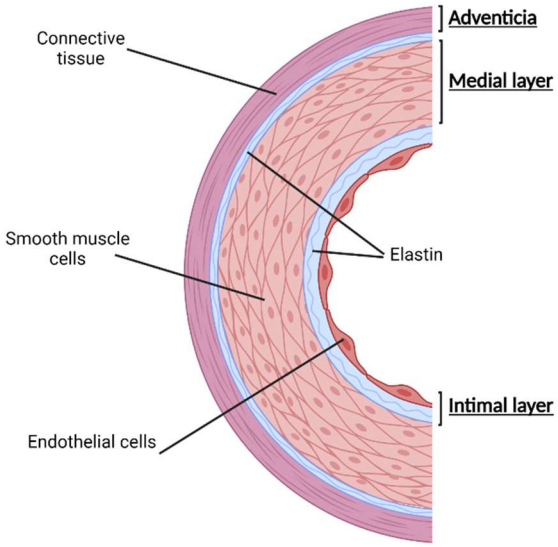

Figure 1: Schematic representation of the three layers of a vessel wall. Vessel wall is composed of intimal layer, mainly formed by endothelial cells, medial layer with smooth muscle cells, and adventitial layer formed by connective tissue. Adapted from Hammes *et al* 2015 [26].

1.3.2. Risk factors for the development of vascular calcification: calcium and phosphate

Well-known traditional risk factors for the development of vascular calcification are age, smoking, diabetes, hypercholesterolemia and hypertension [32]. For the non-traditional risk factors, misbalance in serum phosphate and calcium, with an increase in phosphate retention and excess of calcium excretion [33], is the main one in CKD patients [33]. Inflammation and reduced kidney function have been observed to be directly linked to calcification progression in CKD patients [34]. Other non-traditional risk factors are high doses of vitamin D intake, history of dialysis, systemic inflammation and deficiency of calcification inhibitors [33,35], as well as uraemia, hyperparathyroidism, premature senescence and oxidative [32].

Patients with CKD, accumulate uremic toxins due to the failure of the kidneys. These toxins are harmful substances that have shown a positive correlation with the development of vascular calcification, both *in vitro* and *in vivo* [36]. Uremic toxins create a uremic milieu that triggers different pathways leading to a misbalance of calcium and phosphate levels, and an increase of inflammation and oxidative stress that contributes to vascular calcification [36].

Calcium and phosphate are regularly taken via the diet. Normal *calcium concentration* in the serum of adults is approx. 8.9-10.1 mg/dL [37]. Calcium (Ca^{2+}) is reabsorbed in the kidney and is regulated by the parathyroid hormone (PTH) and vitamin D among other proteins. When there is elevated serum calcium, like in CKD patients, the expression levels of these two proteins are decreased and therefore the calcium reabsorption in the kidney is inhibited and there is an increase in renal calcium excretion [37]. Calcium uptake into the cells is via calcium channels, like the voltage-gated channels (VGCC) [38]. Extracellular Ca^{2+} activates a G-protein coupled receptor called calcium-sensing receptor (CaSR) [39,40], which maintains calcium homeostasis in the cells [40]. When this receptor is activated it decreases the levels of PTH [40]. Additionally, this activation has an anti-calcific effect, but the reason behind this effect is still not well understood [41]. It is known that the expression of CaSR is lost during vascular calcification [39,42]. Moreover, silencing of CaSR in SMCs increased calcium deposition while the overexpression of the receptor attenuated the process [43]. Furthermore, it has been observed that patients with CKD have lower levels of CaSR expression compared to the control group [43].

Normal *phosphate concentrations* in adults are within the range of 2.5-4.5 mg/dL [37]. Phosphate is absorbed in the gut, reabsorbed and excreted in the kidney, and finally excreted in the faeces. In the kidneys it is filtered through the glomerulus and reabsorbed via sodium/phosphate type 2 (NaPi) cotransporters that are expressed in the kidney and intestine

[44]. Phosphate homeostasis, the balance between the amount of phosphate absorbed in the intestine and excreted by the kidney, is a complex physiological mechanism in which different proteins and hormones are involved, like for example parathyroid hormone (PTH), fibroblast growth factor 23 (FGF23) / klotho and vitamin D [37,45]. PTH and FGF23 and its cofactor klotho decrease phosphate reabsorption by decreasing the abundance of sodium/phosphate transporters in the kidney, thereby increasing the excretion of phosphate, and lowering its serum levels. On the other hand, vitamin D increases its reabsorption in the proximal tube and improves the absorption in the intestine, raising the levels of phosphate [37,45]. In CKD, due to renal failure, phosphate homeostasis is impaired and there are high levels of phosphate which directly stimulate the upregulation of PTH and FGF23 to increase renal phosphate excretion [37,44]. Phosphate (Pi) is internalised into the cells via the sodium/phosphate type 3 (NaPi) cotransporters PIT-1 or PIT-2 [46]. Once inside the cell the metabolic processes (glycolysis, β-oxidation) incorporate Pi to ATP, which is then exported out of the cells via ATP channels. Extracellular ATP is hydrolysed via ectonucleotide Pyrophosphatase/Phosphodiesterase 1 (eNPP1) to AMP and pyrophosphate (PPi) which is an endogenous inhibitor of calcification. PPi can then be hydrolysed by tissue non-specific alkaline phosphatase (TNAP) to phosphate, increasing vascular calcification (**Figure 2**) [45,46]. Under CKD conditions, the phosphate misbalance is so strong that PPi is not potent enough to inhibit vascular calcification itself.

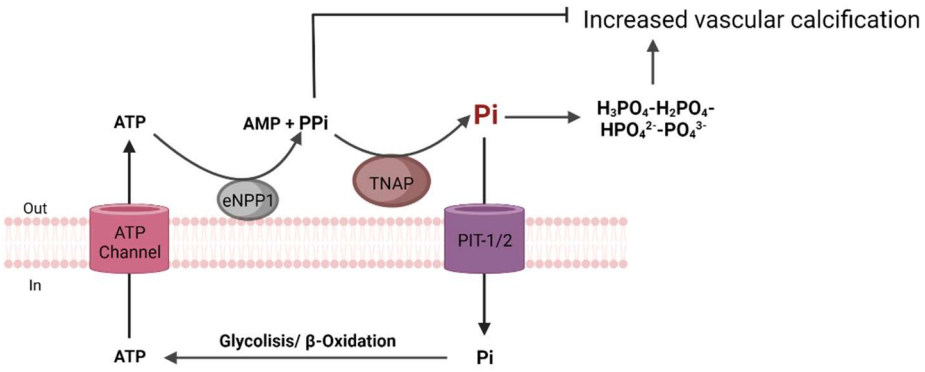

Figure 2: Phosphate transportation in a cell. Phosphate (Pi) is internalised into the cell throw transporters PIT-1/2 in the cell membrane. Once inside, Pi is incorporated to ATP during the metabolic processes (glycolysis, β-oxidation). When ATP is exported outside the cells via ATP channels, it is hydrolysed via ectonucleotide Pyrophosphatase/Phosphodiesterase 1 (eNPP1) to AMP and the endogenous inhibitor of calcification pyrophosphate (PPi). PPi can then be hydrolysed by tissue non-specific alkaline phosphatase (TNAP) to Pi and the respective phosphate ions (H_3PO_4-H_2PO_4-HPO_4^{2-}-PO_4^{3-}) increasing again the calcium deposition. Adapted from Villa-Bellosta *et al.* 2020 [46].

1.3.3. Vascular calcification: a passive or/and active process

Vascular calcification can be an active or passive process, both leading to the depositions of calcium phosphate. *Passive calcification* is independent of cellular activity and is just the deposition of calcium and phosphate on collagen and elastin fibrils leading to amorphous

calcification [47]. Calcium ions which are positively charged bind to the collagen and elastin due to their negative charge, once they bind, they become positively charged structures that attract negatively charged phosphates and carbonate ions and therefore triggering the calcification process by hydroxyapatite crystal nucleation and extracellular matrix calcification [47].

When calcium and phosphate ions (PO_4^{3-}) bind, they form hydroxyapatite particles, that later will bind to Matrix Gla protein (MGP) and Fetuin-A circulating in plasma, forming what are called Calciprotein Particles (CPPs). Fetuin-A and MGP bind to the particles due to its intrinsic negative charge, stabilizing them and forming what are called primary CPPs [48], under CKD conditions (hyperphosphatemia) primary CPPs make a transition to secondary CPPs which have an amorphous shape and are more difficult to be cleared (**Figure 3**) [48]. Elevated levels of CPP can be measured in CKD patients [48,49].

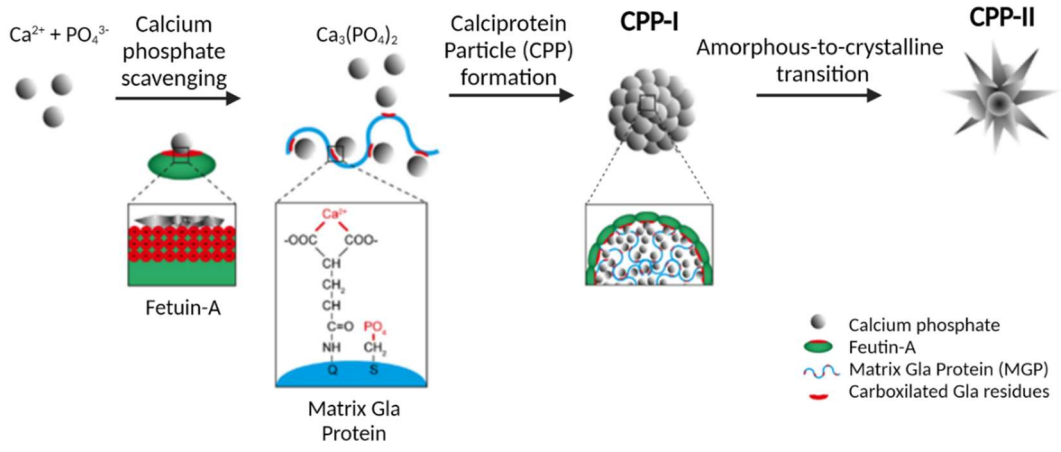

Figure 3: Calciprotein particles (CPP) formation under hyperphosphatemia conditions. Calcium and phosphate ions bind to fetuin-A and Matrix Gla Protein (MGP) forming primary CPPs (CPP-I). Under hyperphosphatemia conditions this primary CPPs make a transition to secondary CPPs (CPP-II), which would lead to development of calcification process. Modified from Kutikhin *et al.* 2021 [48].

Fetuin-A and MGP are well-known inhibitors of vascular calcification, they are able to inhibit the primary to the secondary transition of CPPs [48]. CPPs can be internalised by endothelial cells or SMCs. In both types of cells they increase ROS production, leading to an increase in inflammatory cytokines which finally leads to an upregulation of osteogenic genes related to vascular calcification [48].

On the other hand, *active vascular biomineralization* is regulated by cellular mechanisms and it is similar to the bone formation process. Active calcification is triggered by the release of matrix vesicles by SMCs, these matrix vesicles contain calcium and phosphate ions that allow the formation of calcium phosphate crystals in the interstitial space around collagen fibrils, leading to structure calcification [47].

Other mechanisms involved in the development of vascular calcification are the accumulation of calcium and phosphate in the extracellular matrix, the transdifferentiation of SMCs to osteoblast/chondrocyte-like cells, and SMC apoptosis and reduced proliferation [20,41]. Elastin degradation, inflammatory environment and oxidative stress also contribute to the development of vascular calcification [20,41].

1.3.4. Signalling pathways of vascular calcification

There are different pathways involved in vascular calcification, but still the complete mechanism for the development of vascular calcification is not known[41]. Under uremic conditions transporters PIT-1 and PIT-2, which transport phosphate into SMCs, are up-regulated. Once PIT-1 is activated it activates ERK1/2 MAP-kinase leading to the up-regulation of alkaline phosphatase (ALP) [41].

As mentioned before, under CKD and CVD conditions there is an increase in the inflammatory environment [36]. It has been shown that high phosphate concentrations induce a pro-inflammatory response by SMCs [50], SMCs then produce different pro-inflammatory molecules such as bone morphogenetic proteins (BMP-2), tumor necrosis factor alpha (TNF-α) or interleukins (IL-6). BMP-2 upregulates the expression of *MSX2*, and is directly linked to the upregulation of *PIT-1* expression [41]. TNF-α increases BMP-2 signalling and *MSX2* expression via the nuclear factor kappa-light-chain-enhancer of activated B cells (NF-κB) pathway [41]. IL-6 also plays an important role in vascular calcification, since it can activate the BMP-2 pathway and increases oxidative stress [51]. Under high phosphate and calcium concentrations, oxidative stress also plays an important role in the development of vascular calcification [38], it activates the ERK1/2 MAP-kinase [38] and p38-MAP-kinase pathways [52] and it also contributes to the increase of pro-inflammatory cytokines [50].

1.4. Regulators of vascular calcification: vitamin K

As mentioned before, in the past it was thought that vascular calcification is only a passive process, but for several years it is known that this process is highly regulated by multiple inducers and inhibitors. In healthy conditions, these inducers and inhibitors stay in balance, but when there are more inducers than inhibitors, vascular calcification is developed [53]. Some of the main regulators of vascular calcification are well-known and are shown in **Table 3:**

Table 3: Inducers and inhibitors of vascular calcification adapted from Schlieper *et al.* 2016 [53].

Inducers	Inhibitors
BMP-2, 4 and 6	Matrix Gla Protein
Osteocalcin	Fetuin-A
Alkaline phosphatase (ALP)	Pyrophosphate
Oxidative stress	BMP-7
Inflammatory cytokines (IL-6, IL-1, TNF-α)	Vitamin K
Apoptotic bodies	Magnesium
MMP-2, 3, and 7	

Among the known inhibitors of vascular calcification, vitamin K plays an important role, since some of the most known inhibitors of vascular calcification are vitamin K-dependent proteins (VKDP), like Matrix Gla Protein [54]. These VKDP need to be carboxylated to become active. During its recycling cycle, vitamin K in the hydroquinone form is oxidized to the epoxide form and acts as a cofactor of the γ-glutamyl carboxylase (GGCX) enzyme, activating VKDP [55] (**Figure 4**). Previous studies from our group have already shown a decreased activity of GGCX in kidneys from CKD rat models, which was related to an increase in vascular calcification, and this could be recovered after supplementation with vitamin K [56]. One of the most studied and known VKDP that inhibits vascular calcification is the Matrix Gla Protein. MGPs are activated after carboxylation by vitamin K and subsequent phosphorylation by casein kinase (p-cMGP) [57]. p-cMGP inhibits calcification by binding directly to the hydroxyapatite crystals, but also binding BMP-2 and therefore decreasing its activity [57]. In this context, it could be shown that the knockout of MGP *in vitro* leads to the development of vascular calcification, while a reduction of vascular calcification could be observed by overexpression of MGPs [58]. Furthermore, different studies have observed a positive correlation between the concentration of uncarboxylated MGP (ucMGP) and the degree of cardiovascular risk [59], vascular calcification [60] and CKD [61]. When there is a deficiency of vitamin K, MGPs cannot be carboxylated and cannot act as calcification inhibitors leading to an increase in vascular calcification and an increased risk of CVD [62]. Therefore, ucMGP is used as an indicator of vitamin K status [63].

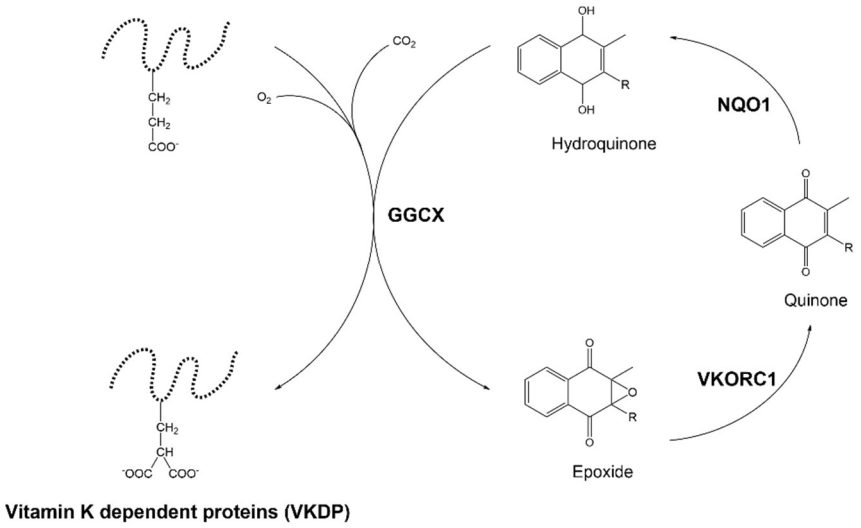

Figure 4: **Vitamin K recycling cycle.** Vitamin K in the hydroquinone form is oxidized to the epoxide by GGCX acting as a co-factor for the carboxylation of the vitamin K dependent proteins (VKDP). The epoxide form is converted to the hydroquinone again thanks to the enzymes vitamin K epoxide reductase complex subunit 1 (VKORC1), which forms the quinone form and afterwards NAD(P)H Quinone Dehydrogenase 1 (NQO1) converts quinone to hydrioquinone. Adapted from Nakagawa *et al.* 2018 [55].

Vitamin K has different isoforms with a common 2-methyl-1,4-naphthoquinone ring structure called menadione (also known as vitamin K3), and different side chains (**Figure 5**). Menadione is a metabolite of vitamin K1 after cleaving its side chain [64], and at the same time, it is a precursor of MK4 [65] (**Figure 6**). Vitamin K1, also called phylloquinone, has 4 units of phytyl in the side chain, and vitamin K2, also called menaquinone (MK), has a variable number of prenyl units in the side chains (**Figure 5**). Vitamin K2 can be divided into short-chain (MK4) or long-chain (MK7) depending on the number of these prenyl units [66].

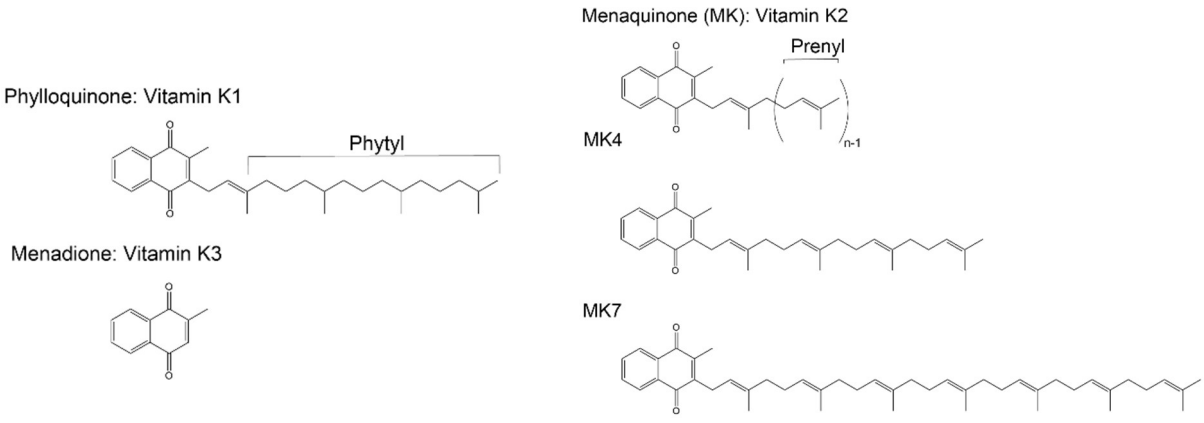

Figure 5: **Structures of the different vitamin K isoforms**. Phylloquinone: vitamin K1; menadione: vitamin K3; and the different menaquinones (MK): vitamin K2 isoforms MK4 and MK7. Adapted from Hirota *et al.* 2013 [65].

In the organism, the different vitamin K isoforms have different functions. Vitamin K1 mainly plays a role in blood coagulation, while vitamin K2 is important for the carboxylation of the

VKDP, and therefore, plays a role in the inhibition of vascular calcification [67]. Both vitamin K1 and K2 can be obtained through the diet, K1 mostly in green vegetables and K2 in food with bacterial processes, like fermented cheeses [66]. All vitamin K forms are taken up in the intestine and then absorbed by chylomicrons, vitamin K1 is transported into the liver where it carboxylates clotting factors, while vitamin K2, which has a longer half-life, is distributed through the entire body [66]. The daily recommended intake of K1 and K2 varies from 50-600 μg. Vitamin K1's daily dosage could be obtained via the diet, while vitamin K2 supplementation is recommended to reach these values [66].

In the metabolism, vitamin K1 can be converted to vitamin K2 by the enzyme UbiA prenyl-transferase domain-containing 1 (UBIAD1), which incorporates geranylgeranyl pyrophosphate (GGPP) to vitamin K3 (menadione) derived from the cleavage of vitamin K1 [68]. It is also known that UBIAD1 requires the binding of the enzyme 3-hydroxy-3-methylglutaryl-coenzyme A reductase (HMGCR) to carry out this enzymatic process [69,70] (**Figure 6**).

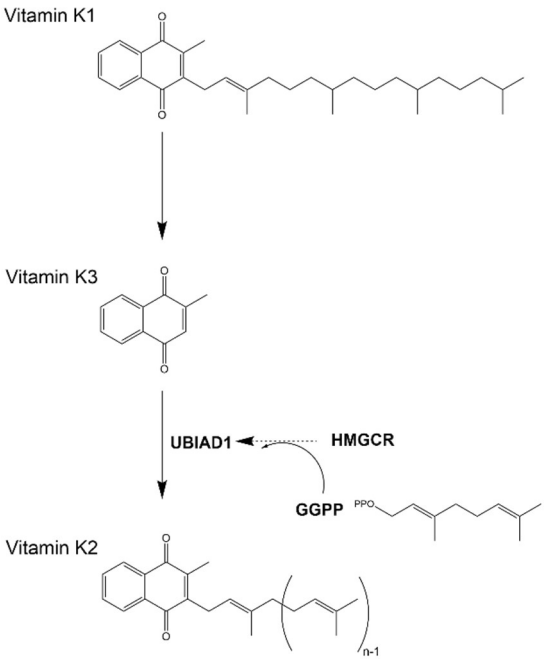

Figure 6: Conversion of vitamin K1 to vitamin K2. After the side chain of vitamin K1 is cleaved, vitamin K3 is converted to vitamin K2, via UBIAD1. HMGCR binds to UBIAD1, which adds GGPP (geranylgeranyl pyrophosphate) as a side chain to vitamin K3 leading to the formation of vitamin K2. Adapted from Schumacher *et al.* 2021 [70].

HMGCR enzyme is also involved in cholesterol synthesis and the mevalonate pathway. Therefore statins, a drug that binds and inhibits HMGCR, are used in patients with high cholesterol levels, but it has been found that treatment with statins increases vascular calcification in patients with cardiovascular diseases [71]. Furthermore, it has been shown that some lipophilic statins, inhibit the synthesis of MK4 by reducing UBIAD1 activity [68]. A change in the expression of any of these enzymes could be related to a vitamin K2 deficiency in CKD patients.

In CKD patients, a deficiency of vitamin K2, the isoform that carboxylates VKDP, could be shown [72,73], while the reason for this deficiency is still unknown. However, it is suspected that a potassium- and phosphate-poor diet, which many CKD patients consume, leads to a lower intake of this vitamin and thus to a deficiency of vitamin K in these patients [74]. In addition, the use of phosphate binders, especially sevelamer, also causes vitamin K deficiency, which is manifested by increased dephosphorylated-uncarboxylated MGP (dp-ucMGP) in end-stage CKD patients [75], probably due to the binding of sevelamer to fat-soluble vitamins [75]. Warfarin treatment in haemodialysis patients as anticoagulant could also lead to vitamin K deficiency [76] since it interferes with the enzyme vitamin K epoxide reductase complex subunit 1 (VKORC1) from the recycling cycle of vitamin K [57] (**Figure 4**). However, even without the use of antagonists, potassium- or phosphate-poor diet or phosphate binders, patients with advance CKD have shown a decreased plasma level of dp-ucMGP [77] .

Different trials with CKD patients on haemodialysis [78,79] or patients with type 2 diabetes and CVD [80], have showed that supplementation of vitamin K2, more specific MK7, improved the vitamin K status but did not show an improvement in vascular calcification progression, despite decreased dp-ucMGP levels [78,80]. Similar results were found in the “K4Kidneys trial”, where supplementation with MK4 in CKD patients, did not improve vascular stiffness [81]. In contrast, the supplementation of MK4 showed a decrease in arterial calcium content in rat models [82]. The recent published data from the “VitaVasK trial” with haemodialysis patients, showed that supplementation of K1 reduced the progression of thoracic and coronary aortic calcification as well as the levels of dp-ucMGP [83]. Furthermore, a currently on-going trial, called the “VitaK-CAC trail” where patients with coronary artery disease receive supplementation of MK7, is studying the effect of MK7 supplementation on the progression of vascular calcification [84].

1.5. Methods used for the detection of vascular calcification

To assess the degree of calcification in patients there are different diagnostic tools. The most common one is using computer tomography (CT) scanners that can estimate coronary artery calcification (CAC) and aortic calcification burden. Using these scanners, calcification can be quantified using different scores. One example is the Agatston score, which assigns calcium scores by measuring areas and densities of specks [85,86]. Lateral abdominal X-ray uses other scores like Kauppila or Adragao score, which are able to quantify calcification in aortas from the spine, hands and pelvis [87,88]. A method, not based on scores, but on the measurement of the formation of calcification particles themselves, is the T50 assay, which measures the time it takes for the transition from primary calciprotein particles (CPPs) to secondary calciprotein particles, by using light to distinguish the difference in turbidity between primary and secondary CPPs. The T50 assay allows the measurement of the serums capacity to inhibit this transition and therefore gives an indirect measurement of one of the strongest serum inherent calcification inhibitors Fetuin-A [89]. To assess hydroxyapatite crystals and microcalcification (hydroxyapatite crystals under 50 mm), ^{18}F-sodium fluoride intake is used. ^{18}F-sodium fluoride binds to both micro- and macrocalcifications (which are stable microcalcification aggregations), but they can be distinguished because the intake of ^{18}F-sodium fluoride ion in microcalcifications is higher compared to macrocalcifications [47].

1.6. Therapeutic approaches currently used to treat vascular calcification

There is still no clear treatment available against vascular calcification, but some therapeutic approaches are used to decrease its effect. Phosphate binders, like sevelamer, are able to reduce serum phosphate levels, but their benefit regarding vascular calcification is still not clear [90]. Furthermore, it has been observed that end-stage patients under sevelamer treatment have a decrease in vitamin K concentration [75]. Calcimimetics, which act on the calcium-sensing receptor, increasing its sensitivity, are able to reduce levels of parathyroid hormone via a feedback mechanism [42,91], but their effect on calcification development and CVD risk is still not clear [32]. Bisphosphonates, which bind to inorganic pyrophosphate, are used against dysregulated bone metabolism and have shown diverse results regarding vascular calcification in trials with CKD patients, and therefore their benefit against vascular calcification is still not clear [92]. Magnesium is a well-known inhibitor of calcification, *in vitro*, it inhibits CPPs formation [93] and *in vivo* it has been shown that magnesium supplementation reduced vascular calcification in nephrectomised rats [94]. Some clinical trials have shown an improvement in calcification propensity when a magnesium supplementation was given to the patients [95,96]. The MAGiCAL-CKD trial which is currently on-going is studying CAC progression in CKD patients supplemented with magnesium [97]. Vitamin D could also be considered as a treatment

option against vascular calcification, but actually both hypovitaminosis and hypervitaminosis D contribute to the development of vascular calcification [98,99]. High doses of vitamin D increase calcium and phosphate in serum, decrease fetuin-A and activate of pathways that trigger osteoblast transdifferentiation from SMCs [98]. On the other hand, low levels of vitamin D are linked to an increase in vascular calcification, due to the inability of vitamin D to decrease the inflammatory cytokines [50,99].

Recently, SNF472 has been described as a potent inhibitor of vascular calcification by binding to hydroxyapatite crystals [100]. The current phase 3 trial , “Calciphyx”, is ongoing for the use of SNF472 in haemodialysis patients as a treatment against calciphylaxis, where calcium deposits block blood vessels [101].

1.7. New mediators of vascular calcification: Chromogranin A and its peptide ‘Vasoconstriction-Inhibiting Factor’ (VIF)

As there are only limited therapeutic approaches available for the treatment of vascular calcification, the search for new approaches and mediators against this pathological mechanism has a particular interest.

Chromogranin A is a protein with a molecular weight of 48 kDa and 457 amino acids, found in the adrenal medulla. Higher concentrations of chromogranin A have been found in patients with cardiovascular or renal diseases, when they were compared to healthy individuals [102]. Under hypocalcemic conditions chromogranin A is released from the adrenal medulla together with parathyroid hormone [103]. Different peptides derived from chromogranin A have been described, with the most studied ones being vasostatin 1 and vasostatin 2, pancreastatin and catestatin [104]. All these peptides have a wide range of functions: vasostatins and catestatin have shown vasorelaxant as well as anti-bacterial and fungal properties among others, while pancreastatin has been described as anti-insulin peptide with pro-inflammatory properties [102]. Another peptide derived from chromogranin A, which was discovered by our group previously, is ‘Calcification Blocking Factor’ (CBF), and as the name suggests, it has inhibitory properties against vascular calcification [105].

Recently, the chromogranin A-derived peptide ‘Vasoconstriction-Inhibiting Factor’ (VIF) has been identified by our group. It was isolated from bovine adrenal glands after performing multiple chromatographic steps with reversed-phase and anion-exchange chromatography [106]. The fractions obtained after each chromatographic step were analysed in vasoregulatory assays and then the fraction showing the best vasoregulatory effect was further characterised.

After three chromatographic-vasoregulatory assay cycles, a homogenous fraction was obtained and analysed by matrix-assisted laser desorption/ionization time of flight/time of flight (MALDI-TOF/TOF) mass spectrometry. In this fraction, VIF was identified as a peptide derived from chromogranin A with a molecular weight of 3,919 Da. To study the vasoregulatory effect of VIF, *ex vivo* experiments were performed in rat kidneys perfused with angiotensin II. When the perfusion was done in the presence angiotensin II, a vasoconstriction inhibitory effect of VIF was observed [106]. VIF was able to decrease the half-maximal effective concentration and therefore, the maximal effect of angiotensin II when it was compared to the absence of VIF [106].

The same was done with human plasma and human VIF derived from chromogranin A was identified as a 35 amino acid peptide (97-131 chromogranin A) (**Figure 7**) with a molecular weight of 3,906 Da [106]. VIF concentration was measured in patients with CKD stage 5D and patients with heart failure, in both cases, VIF concentrations were higher when they were compared to the healthy controls (CKD vs healthy p-value=0.02; heart failure vs healthy controls: p-value=0.004) [106].

Figure 7: Schematic representation of VIF peptide. VIF peptide and its 35 amino acid sequence. Adapted from Salem *et al.* 2015 [106].

To study the mechanism of VIF inhibiting the vasoconstricting effect of angiotensin II, *ex vivo* experiments with perfused kidneys and *in vitro* experiments with endothelial cells were performed, both cultured with VIF and angiotensin II, in the presence or absence of the angiotensin II type 2 receptor (AT2) blocker PD123,319. The experiments with angiotensin II in the presence of both VIF and PD123,319 showed that PD123,319 abolished the VIF effect, and therefore, it was claimed that VIF binds in a non-competitive manner to AT2, inhibiting the effect of angiotensin II [106].

Other authors have shown that stimulation of the AT2 receptor inhibits phosphate-induced vascular calcification both *in vitro* and *ex vivo,* and this stimulation might be beneficial to reduce cardiovascular events in patients with CKD [107]. Recent studies with SMCs from wild-type mice and mice overexpressing the AT2 receptor, both cultured with high phosphate and angiotensin II, showed that overexpression of the AT2 receptor inhibits the development of vascular calcification, as well as the treatment with angiotensin II, decreases the calcium deposition [108]. *In vivo* experiments with ApoE and ApoE/AT2KO 5/6 nephrectomised mice revealed a decrease in calcium deposition after the treatment with angiotensin II [108]. Moreover,

angiotensin II prevents vascular calcification in human aortic smooth muscle cells cultured under high phosphate conditions by enhancing magnesium influx via activation of ERK1/2 kinases [109].

As mentioned before, peptides derived from chromogranin A have shown to have a wide range of different functions [102], but the VIF effect on the vascular calcification process has not been clarified until now.

1.8. Models to study vascular calcification

To study vascular calcification *in vitro, ex vivo* and *in vivo* models can be used:

(a) *In vitro* models: the most common used cells are primary vascular smooth muscle cells (VSMCs), which can change their phenotype into osteoblast/chondrocyte-like cells and promote vascular calcification by different pathways. Cell lines from mice or rat are used, like mouse vascular smooth muscle cell (MOVAS) or embryonic rat A7r5 and A10 [110]. Endothelial cells are also a model for vascular calcification, since these cells accelerate its progression, but the co-culture with SMCs gives much more reliable results [110]. For the induction of calcification itself, most of the culture media used have a low concentration of fetal bovine serum (FBS), and different stimuli are added: to trigger passive calcification leading to amorphous calcification, high concentrations of sodium hydrogen phosphates (Na_2HPO_4, NaH_2PO_4) or calcium chloride ($CaCl_2$) are used [111], while to activate the structure and bone related calcification a combination of β-glycerophosphate and ascorbic acid are added to the media [112].

In vitro models are convenient to start studying the basis of the calcification process, but of course, the tissue structure and the connection with other cell types are lost. Therefore, *ex vivo* models are also useful.

(b) *Ex vivo* models: the *ex vivo* models use vessel tissues, where aortic rings from mice and rats are the most used ones. In these rings, SMCs, endothelial cells and the aortic shape are still intact [110].

However, *in vivo* models are the ones that best mimic the natural process due to ability to mimic the pathology of the organism.

(c) *In vivo* models: in these models, mice and rats are mainly used to monitor the disease through time, since vascular calcification is also linked to aging [113]. Wistar rats and C57Bl/6 mice are the most used animals to induce vascular calcification in CKD models [32]. CKD can be induced in these animals by kidney reduction via nephrectomy (5/6 or 7/8 of the kidney), and/or vascular calcification is induced via the diet adding adenine, nicotine, vitamin D and/or phosphate [32,110]. In addition, vascular calcification can be induced by knocking out genes either from the intimal or the medial layer like for example ApoE$^{-/-}$, Klotho$^{-/-}$, Lmna$^{-/-}$ or Fetuin-A$^{-/-}$ models [110].

Chapter 2

Hypothesis and objectives of the thesis

2. HYPOTHESIS AND OBJECTIVES OF THE THESIS

Chronic kidney disease (CKD) is a serious global health problem: patients suffering from this disease have a highly increased risk of cardiovascular diseases (CVD) [9] and in particular a higher prevalence of vascular calcification. Vascular calcification is a pathological process in which there is a deposition of calcium phosphate salts in the vessels [47]. This deposition makes the vessel wall becomes stiffer, which increases blood pressure and negatively impacts blood circulation. Vascular calcification is strongly regulated by multiple inducers and inhibitors that are in balance under healthy conditions. However, when there is an increasing concentration of inducers, which is common in CKD, increased vascular calcification is observed in these patients [53].

Vitamin K is a well-known inhibitor of vascular calcification since it carboxylates the vitamin K-dependent proteins (VKDP) which directly inhibit vascular calcification [54]. CKD patients show a vitamin K2 deficiency, which is the isoform that carboxylates the VKDP. However, the reason for this deficiency in CKD patients is still unknown. During its recycling cycle, vitamin K in the hydroquinone form, is oxidized to the epoxide form and acts as a cofactor of the γ-glutamyl carboxylase (GGCX) enzyme activating the VKDP [114]. Due to vitamin K deficiency, VKDP are not carboxylated, leading to the development of vascular calcification and increased CVD risk in CKD patients [62]. In the metabolism, vitamin K1 is converted to vitamin K2 by the enzyme UbiA prenyltransferase domain-containing protein 1 (UBIAD1), which incorporates geranylgeranyl pyrophosphate (GGPP) to vitamin K-menadione derived from the cleavage of vitamin K1 [68]. In addition, for the activation of UBIAD1 a binding of 3-hydroxy-3-methylglutaryl-coenzyme A reductase (HMGCR) is necessary [69]. Therefore, the first part of the present study aims to investigate the uptake of different vitamin K isoforms and whether a change in the expression of the vitamin K converting enzymes and enzymes of the vitamin K recycling cycle could be related to vitamin K2 deficiency in CKD patients.

This thesis focuses on the following objectives:

a) **Analysis the uptake of different vitamin K isoforms (K1, MK4 and MK7) in CKD**
b) **Analysis the alteration of vitamin K converting enzymes UBIAD1 and HMGCR as a cause of vitamin K2 deficiency in CKD**
c) **Analysis the alteration of the enzymes involved in the vitamin K recycling cycle as a possible reason for vitamin K2 deficiency in CKD**

Besides vitamin K, chronic renal insufficiency leads to an imbalance of additional inducers and inhibitors of vascular calcification processes [53]. Knowledge of the mediators that inhibit or induce the process of vascular calcification is still in its infancy, so intervention options remain limited. Therefore, it is of great importance to find new mediators for a possible therapeutic approach. Our group could already identify and characterise different mediators that influence renal as well as cardiovascular processes. Recently, the chromogranin A-derived peptide ´Vasoconstriction-Inhibiting Factor´ (VIF) was identified and characterized as an inhibitor of AT2 receptor leading to an inhibition of vasoconstriction triggered by angiotensin II (Ang II) [106]. Stimulation of AT2 receptor inhibits phosphate-induced vascular calcification, as shown both *in vitro* and *ex vivo* [107]. Moreover, Ang II has shown an inhibitory calcification effect in SMCs [109]. Therefore, the second part of the present study aims to investigate whether VIF affects the inhibitory effect of Ang II on vascular calcification.

Based on this, the following objectives are also analysed in this thesis:

***a)* Investigation of the impact of VIF on the inhibitory effect of Ang II on vascular calcification**
***b)* Characterisation of VIF as a new mediator of vascular calcification by *in vitro*, *ex vivo,* as well as *in vivo* approaches**
***c)* Identification of the pathway mediating the inhibitory effect of VIF**
***d)* Identification of VIF binding partner**

Chapter 3

Methods and materials

3. MATERIALS AND METHODS

3.1. CKD animal models

CKD was induced in C57BL/6J mice via 5/6 nephrectomy, control mice had sham surgery. The two groups with 9 mice each had a continued vitamin K-rich diet (1 mg K1/kg, 500 µg MK4/kg, and 500 µg MK7/kg rodent chow (Ssniff, Germany) for 7 weeks. Animals were sacrificed using isoflurane (Abbvie, USA) 7 weeks after surgery and blood and organs (kidney, heart, brain, lung, liver and aorta) were harvested. Blood pressure was measured by the tail-cuff method (Coda, Kent Scientific, CT, USA). Next, CKD was induced in Wistar rats (Charles River Laboratories, USA) by 4 weeks of 0.75% adenine-containing diet (Altromin, Germany), followed by one week on the standard diet, followed by three weeks of 0.75% adenine. Control rats had 4 weeks of the standard diet. Serum urea in both experiments was measured by clinically laboratory routine (Vitros 250, Ortho Clinical Diagnostics, Institut für Versuchstierkunde, Aachen). The animal protocols were approved by the local ministry (LANUV 84-02.04.2011.A144 and 84-02.04.2017.A324).

3.2. Vitamin K quantification in animal tissues

For the extraction of vitamin K, snap-frozen tissues from mice were homogenated in a TissueLyser II (Qiagen, Germany) and later on vitamin K was extracted by hexane followed by cleaning using a Sep-Pak plus silica cartridge (Waters, Germany). Vitamin K was eluted with 3% diethyl ether in hexane that was evaporated in an argon stream and diluted in isopropanol for injection in high-pressure liquid chromatography (HPLC; Merck Hitachi, Japan). Vitamin K was separated in reversed-phase HPLC with a Max RP C12 column (Phenomenex, USA) as the stationary phase and with isocratic methanol at pH 5 was used as a mobile phase. Vitamin K1, MK4 and MK7 were detected at 246 nm and quantified by external standards (Vitamin K1 and MK4 from Sigma-Aldrich, Germany, and MK7 from Santa Cruz, USA).

3.3. Immunofluorescence staining in rat and human kidney sections

Immunofluorescence staining was performed using deparaffinised kidney sections from control and CKD rats, and healthy and CKD human kidneys. Deparaffinization was done in xylene (VWR Chemicals, USA), and dehydrated in decreasingly concentrated isopropanol (100% and 96%, 70% and 50%) (Roth, Germany) for 5 min each. Antigen retrieval was performed by boiling in citrate buffer for 20 min. Blocking was performed with 1% BSA (Bovine serum albumin) (Roth, Germany) for 30 min at room temperature. HMGCR antibody 1:50 (GTX32134, Genetex, Irvine, USA) was enhanced by adding biotinylated anti-mouse IgG (BA-

200 Vector labs, USA) UBIAD1 antibody (SC-271595, Santa Cruz, USA) was incubated 1:100 overnight at 4°C. Secondary antibodies were streptavidin-FITC 1:33 (SA-5001, Vector labs, USA) for HMGCR and anti-rabbit Cy3 1:300 (711-165-152 Dianova, Germany) for UBIAD1. Synaptopodin antibody 1:20 (61094, PROGEN Biotechnik GmbH, Germany) was incubated overnight at 4ºC, and then secondary antibody anti-mouse Cy3 1:300 (715-165-150 Dianova, Germany) was added. VKORC1 antibody was incubated overnight at 4ºC 1:100 (PA5-34358, Invitrogen, USA), and then anti-rabbit AF647 1:200 (711-605-152, Dianova, Germany) was added. NQO1 antibody 1:50 (orb228572, Biorbyt, United Kingdom) was enhanced by adding biotinylated anti-rabbit IgG (BA-1,000-1.5 Vector labs, USA) and the secondary antibody was streptavidin-FITC 1:33 (SA-5001, Vector labs, USA). Nuclei were counterstained with DAPI (D-1306, Molecular Probes, the Netherlands). Finally, the slides were mounted with VECTASHIELD® Mounting Media (Vector labs, USA) and images were taken on the Nikon A1 laser confocal microscope (Nikon, Japan). The quantification was done using ´ImageJ´ software (National Institutes of Health, USA). For HMGCR, UBIAD1 and NQO1 the relative expression was normalized to the tubule area, and VKORC1 was normalized to the relative expression of synaptopodin or the tubule area.

3.4. Human nephrectomy specimens

Kidney sections were provided by the urology department from Eschweiler Hospital from patients undergoing (partial) nephrectomy due to kidney cancer. The local ethics committee of the University Hospital RWTH Aachen approved all human tissue protocols (EK-016/17). All patients provided informed consent and the study was performed in accordance with the Declaration of Helsinki.

3.5. mRNA isolation and cDNA synthesis from rat kidneys

RNA was extracted from rat kidneys by the Qiagen RNeasy kit (Qiagen, Germany), according to manufacturers' instructions. The amount of RNA was quantified using a Nanovue Plus Spectrophotometer (GE Healthcare, Germany) at 260 and 280nm. cDNA was synthesized after incubating 300 ng total RNA from each sample with 100 µmol/L oligo dT primer (Eurofins, Germany) at 70°C for 5 min. Afterwards, samples were incubated at 37°C for 1 h with M-MLV RT 5x Buffer, M-MLV RT Enzyme and dNTPs Mix (Promega, USA) to achieve cDNA synthesis. In the final step, samples were diluted in a 1:8 ratio in RNase free water (Braun, Germany).

3.6. Quantitative real-time polymerase chain reaction (RT-PCR)

Quantitative real-time PCR (RT-PCR) was performed using SYBR Green dye (Powerup, Applied Biosystems, Germany). A total of 10 µL per reaction was used comprising 5 µL SYBR green (Powerup, Applied Biosystems, Germany), 1 µL of 2 mmol/L forward primer, 1 µL of 2 mmol/L reverse primer and 3 µL of the cDNA sample. The reactions were performed in a QuantStudio3 Real-Time PCR System I (Thermo Fisher Scientific, USA). The protocol for the RT-PCR cycle was as follows: Hold stage with one interaction at 50ºC for 2 min followed by 95ºC for 10 min. The "PCR stage" had 40 interactions at 95ºC for 15 sec followed by 60ºC for 1 min. Finally, the "Melt Curve Stage" had 1 interaction at 95ºC for 15 sec, followed by 60ºC for 1 min and again 95ºC for 15 sec. All primers used for the RT-PCR were synthesized by (Eurofins, Germany). **Table 4** shows the PCR primers used in this study. The reactions were performed in duplicates in order to obtain accurate Ct values. All data were analysed by the "2(-ΔΔCt)" (cycle threshold) method, comparing all the values with the housekeeping gene (*PPIA* for rat genes and *β-actin* for human samples).

Table 4: Primers used for gene expression analysis.

Target	Sequence (5´-3´)
PPIA forward (rat)	CAAATGCTGGACCAAACACAA
PPIA reverse (rat)	TTCACCTTCCCAAAGACCACAT
HMGCR forward (rat)	CCTCCATTGAGATCCGGAGG
HMGCR reverse (rat)	AAGTGTCACCGTTCCCACAA
UBIAD1 forward (rat)	AAGTGCGCCTCCTATGTGTT
UBIAD1 reverse (rat)	CAGGAGTGAGTGAGGCACTG
β-actin forward (human)	CAACCGCGAGAAGATGAC
β-actin reverse (human)	GTCCATCACGATGCCAGT
BMP-2 forward (human)	GAGGTCCTGAGCGAGTTCGA
BMP-2 reverse (human)	ACCTGAGTGCCTGCGATACA
MSX2 forward (human)	AAGAAAACAGGGCTTGGTGCCTC
MSX2 reverse (human)	GCGCAAGTTCCGTCAGAAACAG
SOX9 forward (human)	AGCTCTGGAGACTTCTGAACGA
SOX9 reverse (human)	GTTCTTCACCGACTTCCTCCG

Target	Sequence (5´-3´)
PIT1 forward (human)	TACAGGCCGGAATCCTTATG
PIT1 reverse (human)	AGCGTGGACTTGAAAGAGGA
Osteocalcin forward (human)	CGATAGGCCTCGTGAAAGC
Osteocalcin reverse (human)	GGCAGCGAGGTAGTGAAGAG
α-*SMA* forward (human)	CAGCCAAGCACTGTCAGGAAT
α-*SMA* reverse (human)	CACCATCACCCCCTGATGTC
IL-6 forward (human)	GCAAGTCTCCTCATTGAATCC
IL-6 reverse (human)	GCAACAATTCCTGGCGATACCTC

3.7. Von Kossa histological staining of human and rat kidney sections for calcification

Von Kossa staining was performed to visualize calcified areas in kidney sections from human and rat kidney sections. Therefore, the slides were deparaffinised as previously described and then incubated with 5% silver nitrate (Sigma-Aldrich, Germany) in the presence of UV light at 405 nm for 12 min, washed three times with double-distilled water (ddH_2O), incubated in the presence of 5% sodium thiosulfate (Sigma-Aldrich, Germany) in water for 1 min, and washed three times with ddH_2O. Next, nuclear fast red (Merck, Germany) was added to the slides for 5 min. The slides were then rinsed, dehydrated with ethanol, incubated for 5 min in xylol, and covered with Vitro-Clud (Langenbrinck, Germany). Calcification was visualized using a Leica DM5500B microscope equipped with a digital imaging system. Staining was determined by the positively stained area as a percentage of the total kidney section, using ´ImageJ´ software (National Institutes of Health, USA).

3.8. Post-translational modification analysis by mass spectrometric imaging (MALDI imaging) of kidney sections from rats

For the MALDI imaging measurement, sections of 5 µm from kidney tissues were made and mounted on indium tin oxide conductive-coated slides (Bruker Daltonics, Germany). The samples were deparaffinised by using xylene (VWR Chemicals, USA) for 5 min twice, and hydrated with isopropanol for 5 min with descending ethanol concentrations (100% and 96%, 70% and 50%) (Roth, Germany) for 2 min each and at last ddH_2O for 5 min. The sections were coated with a trypsin solution (25 ng/µL in 20 mmol/L ammonium bicarbonate, Lonza,

Switzerland), incubated for 2 h at 50°C and coated with α-cyano-4-hydroxycinnamic acid (Bruker Daltonics, Germany) as matrix (10 mg/mL dissolved in 70% acetonitrile/ 0.2% Trifluoroacetic acid). The coating process was performed by using a sprayer for MALDI imaging (HTX TM-Sprayer: TMSP-M3, HTX Technologies, USA). MALDI data accumulation was performed using a TOF-TOF-mass spectrometer (Rapiflex; Bruker-Daltonics, Germany) equipped with a Smartbeam^{TM} 3D laser with a 10 kHz repetition rate and controlled by the Flex-Control 4.0 (Bruker-Daltonics, Germany). Mass spectra were acquired with 200 laser shots for each raster point and a digitizer rate of 2.5 GS/s in reflector positive mode. Analyses were taken in mass range 600-3,000 Da by using a raster width of 100 µm.

3.9. Cell culture of human aortic smooth muscle cells (hAoSMCs)

Primary human aortic smooth muscle cells (hAoSMCs) were obtained from Promocell (Germany) (**Table 5**). The cells were isolated from plaque-free regions of the human aorta and were claimed to be stained positive for smooth muscle *β* -actin. HAoSMCs were cultured in "smooth muscle cell growth medium 2" (Promocell, Germany). The growth medium was supplemented with 100 U/mL penicillin and 100 µg/mL streptomycin (Thermo Fisher Scientific, USA). HAoSMCs were cultured at 37°C and 5% CO2 saturation in a humidified atmosphere with refreshing media every 48 h. Cells from passage P4 until P9 were used for experiments.

Table 5: HAoSMCs used for the experiments.

Lot number	Age	Sex	Race	Health status
411Z027.3	58	Male	Caucasian	Diabetes Type II
437Z012.2	55	Male	Caucasian	Diabetes Type II
452Z011.4	68	Male	Caucasian	Diabetes Type II
458Z016.6	51	Female	Caucasian	--
437Z016.2	51	Female	Caucasian	--

3.10. Splitting and seeding of hAoSMCs

After reaching a 90% confluence, the cells were washed with phosphate-buffered saline (PBS) (Sigma-Aldrich, Germany) and to detach the cells accutase (Sigma-Aldrich, Germany) was added. The flask was incubated at 37°C for 3 min to detach the cells from the bottom of the flask. The detachment by accutase was stopped by adding growth medium.

The suspension was collected and centrifuged in a Heraeus Multifuge 3SR (Thermo Fisher Scientific, USA) at 300g for 5 min at room temperature. Subsequently, the supernatant was

removed, and the pellet was re-suspended in 1 mL growth medium. 10 µL of this suspension were loaded into a Neubauer chamber (Paul Marienfeld GmbH & Co. KG, Germany) and the number of cells was counted under the microscope (Leica Biosystems GmbH, Germany). Afterwards, the cell suspension was diluted with growth medium, depending on the desired number of cells per well and the number of wells. The 48 wells plates were cultured with approx. 3 x 10^3 cells/well, the 24 well plates with approx. 7 x 10^3 cells/well and the 12 well plates with approx. 10 x 10^3 cells/well each, depending on the donor and the experiment to perform (all culture plates used were purchased from Falcon/Corning, USA).

3.11. Peptide synthesis

The VIF peptide used for this thesis was ordered and synthesized from Campro (Scientific GmbH, Germany) using the solid-phase method with a purity higher than 90%.

3.12. Calcification induction in hAoSMCs

HAoSMCs were grown to 90% confluence and were seeded into 48 well plates (3 x 10^3 cells/well). Cells were cultivated in Dulbecco's modified Eagle's medium (DMEM) high glucose containing 4.5 g/L glucose, L-glutamine, and sodium bicarbonate without sodium pyruvate (Sigma-Aldrich, Germany), supplemented with 100 U/mL penicillin and 100 µg/mL streptomycin. DMEM was supplemented with 2.5% fetal calf serum (FCS) (Bio & Sell GmbH, Germany). 2.5 mmol/L phosphates were used to induce calcification (calcifying medium; CM), using 1:1 of disodium hydrogen phosphate (Na_2HPO_4) (Merck, Germany) and sodium dihydrogen phosphate (NaH_2PO_4) (Roth, Germany). The calcifying medium was supplemented with angiotensin II (Sigma-Aldrich, Germany) (max. concentration 100 nmol/L) and VIF (max. concentration 100 nmol/L). As reference medium, DMEM supplemented with 2.5% FCS and containing 0.9 mmol/L phosphate was used (non-calcifying medium; NCM). The hAoSMCs were cultured at 37°C and 5% CO_2 saturation in a humidified atmosphere from one till 7 days replacing the medium after 48 h.

3.13. Calcification induction in rat thoracic aortic rings

The animal experiments were approved by the regional ethics committee and conformed to the Guide for the Care and Use of Laboratory Animals (permit number 40002A4). 8-10 weeks old male Wistar rats (Janvier, France) were anaesthetised with 4-5% isoflurane (Abbvie, USA) in an anaesthesia induction chamber to fall asleep. The thoracic aortas were gently dissected and cut into 3-4 mm segments. The endothelial layer of the thoracic aortic ring was manually damaged by scratching using a conventional pipette tip and the dry weight of each aortic ring

was determined using a precision scale (ABT 230-5DNM, KERN GmbH, Germany). The thoracic aortic rings were incubated with DMEM containing 4.5 g/L glucose, L-glutamine, and sodium bicarbonate without sodium pyruvate (Sigma-Aldrich, Germany), supplemented with 2.5% FCS and 2.8 mmol/L phosphate to induce calcification (calcifying medium; CM). The calcifying medium was supplemented with VIF (max. concentration 100 nmol/L). As reference medium, DMEM supplemented with 2.5% FCS and containing 0.9 mmol/L phosphate was used (non-calcifying medium, NCM). The thoracic aortic rings were incubated for 7 days while the medium was replaced after 48 h.

3.14. Animal model of elastocalcinosis

An animal model of elastocalcinosis (calcification of medial elastic fibers) with proven increased arterial calcification [115,116] was chosen to assay the effects of VIF *in vivo*. Animal experiments were approved by the regional ethics committee ´Comité d'éthique pour l'expérimentation animale Languedoc Roussillon N°36´, with the agreement number (APAFIS 2018072715539434#17270v4). Three groups of six weeks old Wistar rats (Charles River Laboratories, Germany) were given a regular rat chow (A04, Safe, France) and spring water (calcium 60 µmol/L, Mont Roucous, France) *ad libitum* for one week before experiments. Two groups received VIF (31 µg/kg per day) and a vehicle (saline), respectively, infused through an osmotic pump (Alzet 2004, Charles River Laboratories, USA) implanted under the skin. VIF treatment was initiated three or four days before induction of elastocalcinosis (vitamin D3 plus nicotine, or VDN rats) with a single injection of vitamin D3 (300,000 IU/kg, i.m.) and two gavages of nicotine (25 mg/kg, 5 mL/kg) on the same day, as previously described [115,116]. Untreated rats served as control rats (sham operation and saline administration). Four weeks later, rats were anaesthetised with ketamine-xylazine (Medistar, Germany), and a catheter was inserted into the right carotid artery for blood pressure measurement. After 10-15 min of equilibration, systolic, diastolic, mean arterial, and pulse (systolic-diastolic) pressures were determined. The aorta was gently dissected, adventitial fat removed, and cut into segments (3-4 mm) for further analysis.

3.15. Quantification of calcium content

To quantify the calcium content, hAoSMCs and aortic rings were washed three times with PBS and were decalcified using 1 mmol/L HCl for 24 h. The calcium content in the supernatant was determined with the o-cresolphthalein complexone method, in which o-cresolphtalein forms a purple complex after binding to the calcium ions, according to the manufacturer's protocol from RANDOX (RANDOX LABORATORIES, UK). The measurement was done in 96 well plates (Corning GmbH HQ, Germany) measuring the absorbance with a spectrometer (infinite m200,

Tecan group AG, Switzerland) at 572 nm. Cell content was then extracted in 1 mmol/L NaOH (Roth, Germany) with 0.2% sodium dodecyl sulphate (SDS) (Sigma-Aldrich, Germany) and the protein content of the cells was measured by the micro bicinchoninic acid (BCA) protein assay kit (Thermo Fisher Scientific, USA), according to the manufacturer's protocol, here BCA forms purple-coloured complexes after binding to Cu^{+}, which is formed when Cu^{2+} is reduced by proteins in an alkaline environment. Afterwards, the absorbance was measured in a spectrometer at 562 nm. The calcium content was normalized to the total protein content of the cells or the dry weight of the aortic rings.

3.16. Histological calcification staining

Alizarin red and von Kossa staining were performed to visualize calcified areas in hAoSMCs and on the aortic rings. Therefore, cells and aortic rings were fixed with 1 mL of 4% paraformaldehyde (Sigma-Aldrich, Germany) for 1 h. The rings were dehydrated and embedded in paraffin (Sakura Finetek, USA), and 5 µm slices were prepared by a microtome (Leica RM 2250, Germany). The slices were placed on a glass slide, deparaffinised in xylene (VWR Chemicals, USA), and dehydrated in decreasingly concentrated isopropanol (Roth, Germany) solutions before staining. For alizarin red staining, aortic rings were incubated with 2% Alizarin red S (Sigma-Aldrich, Germany) for 20 min in darkness and cells for 5 min in darkness. Afterwards, alizarin red was removed after multiple washing steps till clear crystals were seen under the microscope. Von Kossa staining has been previously described. All slides were then rinsed, dehydrated with ethanol, incubated for 5 min in xylol (VWR Chemicals, USA), and covered with Vitro-Clud (Langenbrinck, Germany). Calcification was visualized using a Leica DM5500B microscope equipped with a digital imaging system. Staining was determined by the positively stained area in cells or by the area stained as a percentage of the total aortic area section, using ´ImageJ´ software (National Institutes of Health, USA).

3.17. mRNA isolation and cDNA synthesis from hAoSMCs

For the synthesis of cDNA, hAoSMCs were seeded into 12 well plates (10 x 10^3 cells/well). Cells were incubated in the corresponding condition for 48, 72 or 120 h. The total mRNA was extracted from hAoSMCs using Zymoresearch Quick-RNATM MicroPrep kit (Zymoresearch, Germany). The steps were performed according to the manufacturer's instructions. Afterwards, the RNA content was determined with a Nanodrop (Thermo Fisher Scientific, USA). Reverse transcription was performed using 600 ng total RNA, 100 µmol/L oligo dT primer (Eurofins, Germany) at 70°C for 5 min. Afterwards, samples were incubated at 37°C for 1 h with M-MLV RT 5x Buffer, M-MLV RT Enzyme and dNTPs Mix (Promega, USA) to

achieve cDNA synthesis. In the final step, samples were diluted in a 1:8 ratio in RNAase-free water (Braun, Germany).

3.18. Interleukin-6 (IL-6) determination by enzyme-linked immunosorbent assay (ELISA)

The secretion of IL-6 was quantified following the enzyme-linked immunosorbent assay according to the manufacturer's protocol (Invitrogen, USA). HAoSMCs were seeded into 48 well plates (7 x 10^3 cells/well). Cells were cultured in a non-calcifying medium (NCM) and calcifying medium in the absence (CM) and presence of VIF (CM+VIF; 100 nmol/L). After 48 h, the supernatant was collected and diluted 1:100 for ELISA measurement. Absorbance was measured at a wavelength of 450 nm and subtracting 570 nm in the spectrophotometer (infinite m200, Tecan group AG, Switzerland).

3.19. PamGene array for the kinase activity profile

The phosphorylation serine-threonine kinase (STK) was analysed in the lysate of hAoSMCs using the PamChip® Ser/Thr Kinase assay (STK; PamGene International, The Netherlands). Each STK-PamChip® array contains 144 individual phosphosites that are peptide sequences derived from substrates for Ser/Thr kinases. HAoSMCs were seeded in 12 well plates (10 x 10^3 cells/well) and after 48 h of stimulation with the corresponding condition (NCM, CM and CM+VIF 100 nmol/L), the cells were washed with cold PBS and 120 µL of M-PER™ Mammalian Extraction Buffer containing Halt Phosphatase Inhibitor Cocktail and EDTA-free Halt Protease Inhibitor Cocktail (1:100 each, Thermo Fisher Scientific, USA) were added. The cells were scratched, and 8 well pro condition were pulled and collected. The samples were centrifuged for 15 min at a maximum speed in a pre-cooled centrifuge at 4ºC (Eppendorf 5417R, Germany). Afterwards, the supernatant lysate was collected, and the protein amount was measured following the protocol for DC protein assay (Bio-Rad, USA). Afterwards, 2 µg of sample and 400 µmol/L ATP were applied per array together with an antibody mix to detect the phosphorylated Ser/Thr. During the STK assay, the kinases of the sample will phosphorylate the substrates on the chip thanks to the presence of ATP, the antibody mix is used to detect the phosphorylated serine and threonine residues. After incubation for an hour at 30ºC, where the sample is pumped back and forth through the porous material to maximize binding kinetics and minimize assay time, a secondary FITC-conjugated antibody is used to quantify the phosphorylation signal. Imaging was done using a LED imaging system and the spot intensity at each time point was quantified (and corrected for local background) using the BioNavigator software version 6.3 (PamGene International, The Netherlands). Upstream Kinase Analysis (UKA) [117], a functional scoring method (PamGene) was used to rank kinases

based on combined specificity scores (based on peptides linked to a kinase, derived from 6 databases) and sensitivity scores (based on treatment-control differences). Results for the up/down-regulation are expressed as the median kinase statistic with a median final score as significance.

3.20. Western blotting

HAoSMCs were seeded into 24 well plates (7 x 10^3 cells/well). After stimulation with the corresponding condition (NCM, CM and CM+VIF 100 nmol/L), cells were lysed with radioimmunoprecipitation assay (RIPA) (Thermo Fisher Scientific, USA) lysis buffer including EDTA-free Halt Protease Inhibitor Cocktail (1:10; Sigma-Aldrich, Germany) and Halt Phosphatase Inhibitor Cocktail (1:10; Sigma-Aldrich, Germany). The lysates were centrifuged at 13,000g at 4°C for 15 min and the supernatants were collected. The protein amount was measured following the protocol for DC protein assay (Bio-Rad, USA). Afterwards, 20 µg of protein from each sample were diluted in ddH_2O containing 100 mmol/L DTT (Sigma-Aldrich, Germany) and 1x LämmLie (Bio-rad, USA) and were resolved by 12% SDS–polyacrylamide (Roth, Germany) gel electrophoresis (self-made), transferred to nitrocellulose membranes (GE healthcare-LifeScience, United Kingdom), and blocked with 5% BSA (Roth, Germany) for 1 h at room temperature. The following primary antibodies were used to detect protein levels: anti p-P38 antibody 1:1,000 (9211S, Cell signaling, Germany), anti p-ERK1/2 antibody 1:2,000 (4370S, Cell signaling, Germany), anti tubulin 1:1,000 (2144, Cell signaling, Germany). The blots were incubated overnight at 4°C. The secondary anti-rabbit antibody 1:1,000 (7074S, Cell signaling, Germany) was used and incubated for 1 h at room temperature. Immunoreactive bands were visualized via enhanced chemiluminescence using develop solution SuperSignal™ West Pico Chemilumineszenz-Substrat 1:1 (Thermo Fisher Scientific, USA) in ChemiDoc Imager from Bio-Rad (Bio-Rad, USA), and densitometry was performed using Image Lab software 5.0 (Bio-Rad, USA).

3.21. Measurement of reactive oxygen species (ROS)

The ROS production was determined following the Detection Assay Kit according to the manufacturer's protocol (Biovision, USA). The assay detects peroxyl and hydroxyl radicals using the fluorescent probe 2',7'-dichlorodihydrofluorescein diacetate (H_2DCFDA). HAoSMCs were plated at a density of 2.5 x 10^4 cells/well in black 96-well plates with transparent bottom. After 24 h the cells were incubated in a non-calcifying medium (NCM) and calcifying medium in the absence (CM) and presence of VIF (CM+VIF; 100 nmol/L) for 24 h. Then, the medium was removed, and the cells were washed twice with serum-free DMEM high glucose (Sigma-Aldrich, Germany). The probe (H_2DCFDA) was diluted (1:1,000) in serum-free DMEM high

glucose and added to cells for 45 min. Cells were then washed twice with Hanks' Balanced Salt Solution (HBSS) (Fisher Scientific, USA) and were incubated with 100 µL HBSS for 24 h. Fluorescence was measured at an excitation wavelength of 495 nm and an emission wavelength of 529 nm in the spectrophotometer (infinite m200, Tecan group AG, Switzerland). Next, the cells were lysate with Tris-Triton X (10 mmol/L Tris (Roth, Germany), 1:20 Triton- X100 (Sigma-Aldrich, Germany). Finally, the fluorescence values were normalised to the protein amount measured with micro bicinchoninic acid (BCA) protein assay kit (Thermo Fisher Scientific, USA).

3.22. Calciprotein particle (CPP) quantification

For CPPs quantification the supernatant of 48 well plates (3 x 10^3 cells/well) was taken after 48-72h stimulation with the corresponding condition (NCM, CM and CM+VIF 100 nmol/L). The supernatant was centrifuged for 10 min at 4ºC and 20,000g (Sigma 3k30, Sigma-Aldrich, Germany) and the pellet was resuspended in 50 µL sodium chloride (VWR Chemicals, USA). Then 1 µL of each sample was placed in a Formvar/Carbon 200 Mesh Copper membrane (Sigma-Aldrich, Germany) and analysed under the electron microscope TEM Zeiss Leo 906 at 60kV (Omega, USA).

3.23. Endocytosis and uptake assay of CPP in hAoSMCs

Bovine fetuin-A-derived CPM were prepared in a solution containing 400 µL of 2.5 mg/mL fetuin-A (F2379) in 140 mmol/L sodium chloride (VWR Cheminals, USA) mixed with additional 100 µL 140 mmol/L sodium chloride and 250 µL 24 mmol/L phosphate buffer (pH 7.4) (Roth, Germany). After thorough mixing 250 µL of 40 mmol/L calcium chloride solution (pH 7.4) (Roth, Germany) was added and mixed again. The final concentrations per 1 mL mixture were 1 mg bovine fetuin-A, 6 mmol/L phosphate, and 10 mmol/L calcium. CPM formation proceeded at 37ºC for 10 min. This reaction contains CPP-1, CPM and free fetuin-A monomer. The complete mixture was desalted using spin filtration devices with a 3,000 MW cutoff (Vivaspin 2, VS0251, Sartorius AG, Germany). CPP-1 were separated using spin filtration devices with a 300,000 MW cutoff (Vivaspin 2, VS0291, Sartorius AG, Goettingen, Germany). The flow through contains a mixture of about 10% CPM and about 90% free fetuin-A monomer, which could not be further separated. The separated CPM/fetuin-A monomer fraction was called CPM for simplicity. Because the CPM preparation contained a large portion of free fetuin-A monomer, an additional fetuin-A monomer control was included in all assays. CPPs were prepared from an identical protein-mineral mixture. CPP-1 and CPP-2 were harvested by centrifugation (20,000g for 15 min at 4ºC) after 10 min and overnight incubation, respectively. Cells were seeded in 24 well plates (7 x 10^3 cells/well) and kept overnight. The next day, the cells were

incubated for 1 h with 100 µg Alexa488-labelled (Invitrogen, USA) fetuin-A monomer, CPP-1, or CPP-2 or with a combination of CPP-1 and CPP-2. CPM were applied in 100 µg amounts. Cells were washed twice with PBS and observed under a DMI6000B fluorescence microscope (Leica, Germany). After cell detaching fluorescent fetuin-A monomer, CPM, and CPP uptake were measured by flow cytometry using FACSCalibur (BD Biosciences, USA) and analysed by FlowJo Single Cell Analysis Software v10 (BD Biosciences, USA).

3.24. Co-immunoprecipitation (Co-IP) of VIF and Calcium-sensing Receptor (CaSR)

Co-immunoprecipitation (Co-IP) was performed in hAoSMCs lysates. HAoSMCs grown till 90% confluence in T125 flask were collected using 800 µL CHAPSO buffer ((50 mmol/L Tris-HCl (Roth, Germany), 1% Triton-X-100 (Sigma-Aldrich, Germany), 2% CHAPSO (Sigma-Aldrich, Germany), 100 mmol/L NaCl (Roth, Germany), 15 mmol/L EGTA (Honeywell, USA) and 0.02% NaN_3 (Sigma-Aldrich, Germany), 100 µL EDTA-free Halt Protease Inhibitor Cocktail (1:10; Sigma-Aldrich, Germany) and 100 µL Halt Phosphatase Inhibitor Cocktail (1:10; Sigma-Aldrich, Germany). Lysates were shaken for two hours at 4ºC. 100 µL of 1 mg/mL VIF was added to the cell lysates and incubated overnight at 4ºC. The pool of cell lysates with VIF was incubated either alone, with 30 µL of mouse IgG1 Isotype Control antibody (5415, Cell signaling, Germany), or with 30 µL of anti-CaSR antibody (sc-47741, Santa Cruz, USA) overnight at 4ºC. The next day, 35 µL of Pierce Protein A/G Magnetic Beads (Thermo Fisher Scientific, USA) were added to the lysates with antibodies and incubated again overnight at 4ºC. After 24 h, CaSR was eluted from the beads after washing in a magnetic stand (Thermo Fisher Scientific, USA) and using 30 µL of NaCl 1 mol/L. VIF was detected after the desalting step using a ziptip C18 (Merck, Germany) following the manufacturer's instruction, except the following solutions were modified: wetting solution and elution buffer were 80% acetonitrile (Sigma-Aldrich, Germany), and the washing solution was 0.1% trifluoroacetic acid (Merck, Germany). Subsequently, samples were immediately analysed via MALDI-TOF/TOF mass spectrometer (Ultraflex III, Bruker Daltonics, Germany) for the search of VIF. For CaSR detection, samples were separated via electrophoresis using 12% Criterion™ Tris-Tricine Gel (Bio-rad, USA). Afterwards, the gels were stained using 0.1% Coomasie Brilliant Blue r-250 (Sigma-Aldrich, Germany) in 50% methanol (Sigma-Aldrich, Germany) and 10% acetic acid (Roth, Germany) for 2h. Later on, the gels were destained with 50% methanol (Sigma-Aldrich, Germany) and 10% acetic acid (Roth, Germany) overnight. The next day the gels between the marks of 75 and 250 kDa were cut into small pieces and let in 100 µL of 50 mmol/L ammoniumhydrogencarbonate (Sigma-Aldrich, Germany) / acetonitril (Sigma-Aldrich, Germany) 1:1 for 10 min at 25ºC, followed by 10 min at 25ºC in 100 µL of 50 mmol/L ammoniumhydrogencarbonate (Sigma-Aldrich, Germany) ~pH 7. Finally, they were digested

in 100 µL of 50 mmol/L ammoniumhydrogencarbonate (Sigma-Aldrich, Germany) ~pH 7 and 1 µL of Sequencing Grade Modified Trypsin (Promega, USA) overnight at 37ºC. CaSR was detected the next day after another desalting step using Ziptip (Merck, Germany) and using MALDI-TOF/TOF mass spectrometer (Ultraflex III, Bruker Daltonics, Germany).

3.25. Flow cytometry and fluorescence-activated cell sorting (FACS) analysis for apoptosis assay

Apoptosis assay was performed in hAoSMCs seeded in 24 well plates (10 x 10^3 cells/well) after 7 days of stimulation with the corresponding condition (NCM, CM and CM+VIF 100 nmol/L) and with refreshing medium every 48 h. After 7 days the supernatant of the cells was collected into FACS tubes (Sarstedt, Germany) and the cells were detached with accutase for 5 min. To stop the reaction Hanks buffer at pH 7.4 (containing Hanks balanced salt solution (HBSS, Thermo Fisher Scientific, USA), 0.3 mmol/L EDTA (Sigma-Aldrich, Germany) and 0.06 % BSA (Roth, Germany) was added to the wells. The cells were transferred to the FACS tubes and centrifuged at 300g at 20ºC for 5 min (Heraeus Multifuge 3SR, Thermo Fisher Scientific, USA). After discarding the supernatant, the cells were washed with Hanks buffer again and centrifuged. Finally, the samples were resuspended in binding buffer at pH 7.4 containing 0.1 mol/L HEPES (Lonza, Switzerland), 1.4 mol/L NaCl (VWR Chemicals, USA) and 25 mmol/L $CaCl_2$ (Merck, Germany). Next, annexin V-FITC (1:100; BD Pharmingen, USA) was added and incubated for 15 min at RT and darkness. 10,000 events were measured in BD FACSCanto™ II System (BD Biosciences, USA) and the percentage of annexin V positive cells was analysed by FlowJo Single Cell Analysis Software v10 (BD Biosciences, USA).

3.26. Statistical analyses

Statistical analysis was performed using GraphPad Prism 9 (GraphPad Software, USA), and the data were represented as mean ± SD for the *in vivo* experiments and as mean ± SEM for the cells experiments. Multiple comparison analysis of variance (ANOVA) for a single factor (one-way) or multiple factors (two-way) was performed to determine differences between treatment groups and the reference group. In both, Bonferroni t's multiple comparisons were used as a post-test. An unpaired t-test was applied to check for differences between two groups for parametric data. Simple linear regression was used to study the correlation of non-parametric data with a confidence interval of 95%. Differences at $p<0.05$. *p <0.05, **p≤0.01, ***p≤0.001, ****p≤0.0001 were considered to be statistically significant.

Chapter 4

Results

4. RESULTS

4.1. CKD mice model to study vitamin K deficiency

To study vitamin K deficiency in CKD, C57BL/6J mice with 5/6 nephrectomy and C57BL/6J mice with sham operation as control were used. Both groups underwent a 7 week diet containing different vitamin K isoforms (vitamin K1 (K1), menaquinone 4 (MK4), and menaquinone 7 (MK7)). Afterwards, the organs (liver, kidney, aorta, heart, lung, brain and serum) were harvested, and vitamin K isoforms were extracted and isolated from each organ via reversed-phase chromatography and analysed via HPLC for their quantification (**Figure 8**).

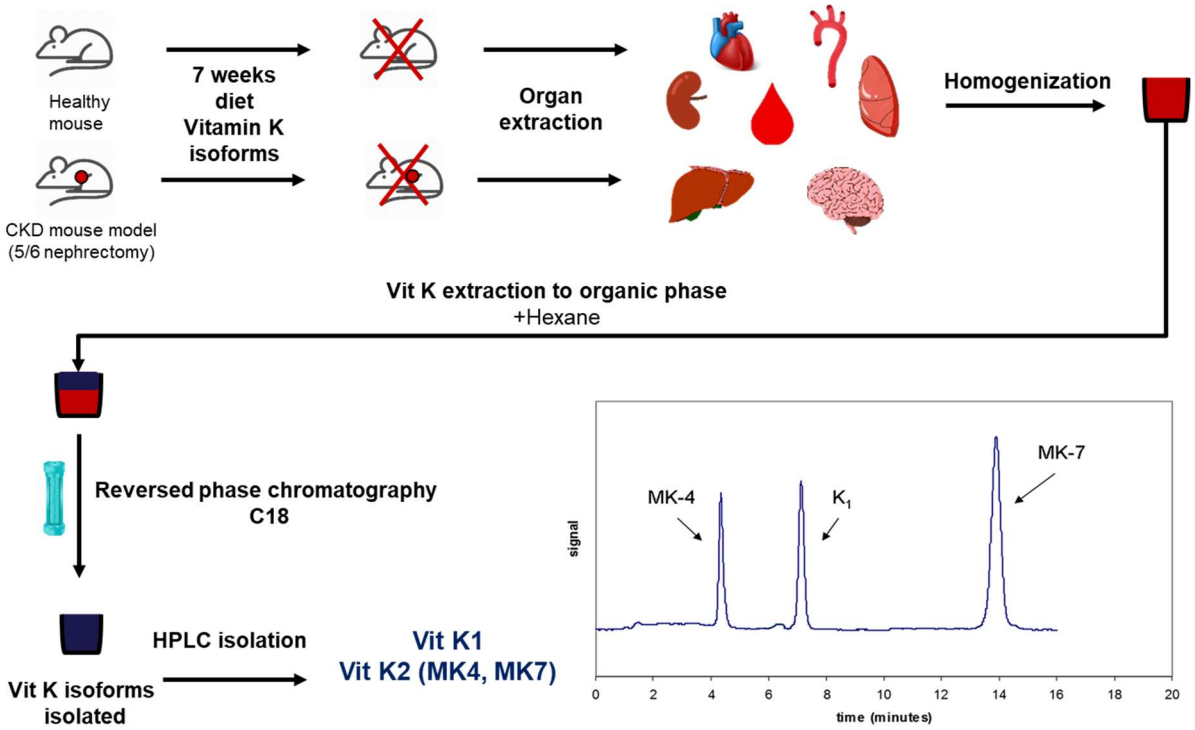

Figure 8: Scheme of C57BL/6J mice model used to study vitamin K deficiency in CKD. C57BL/6J mice had either a sham surgery or a 5/6 nephrectomy followed by 7 weeks diet of the different vitamin K (Vit K) isoforms (1 mg K1/kg, 500 μg MK4/kg and 500 μg MK7/kg rodent chow). After the sacrifice the organs were harvest and vitamin K extracted via reversed phase chromatography in a C18 column. The different vitamin K isoforms were isolated via HPLC and later quantify by using internal standards.

CKD in the 5/6 nephrectomy group was confirmed by measuring urea in their serum after 7 weeks, showing an increase in the 5/6 nephrectomy group compared to the control group (**Figure 9**). Concentrations of the different vitamin K isoforms in the organs of CKD and control mice were isolated via HPLC and quantified using internal standards.

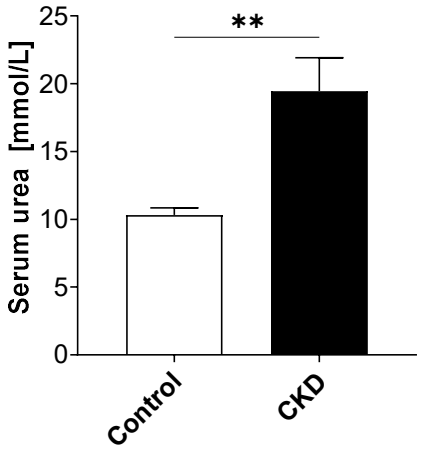

Figure 9: **Serum urea concentration of control and CKD mice models.** Control (white bar) and CKD (black bar) mice serum urea concentration at the end of the experiment (7 weeks). Data are shown as mean ± SD, **p≤0.01 compared to the control group, based on unpaired t-test assuming equal SD (N=3 per group). *Measurement provided by the Institut für Versuchstierkunde.*

4.1.1. Concentrations of vitamin K1 and MK4 and MK7 isoforms in the organs of control and CKD mice

In the studied tissues the highest concentration of all the vitamin K isoforms was found for vitamin K1 in the liver in both the CKD and control group (>15,000 ng/g tissue). However, no difference between the groups was observed (**Figure 10A**). Furthermore, K1 concentration was much higher compared to the isoforms MK4 and MK7 in the liver (**Figure 10A**). In addition, the highest MK7 concentration was also found in the liver in both groups (approx. 2,000 ng/g tissue) with no significant difference between the two groups (**Figure 10A**). The highest MK4 concentration was found in the kidney and aorta (2,000-3,000 ng/g tissue) (**Figure 10B and 10C**). In the kidneys of CKD mice, a significant decrease in MK4 was observed compared to control mice (**Figure 10B**).

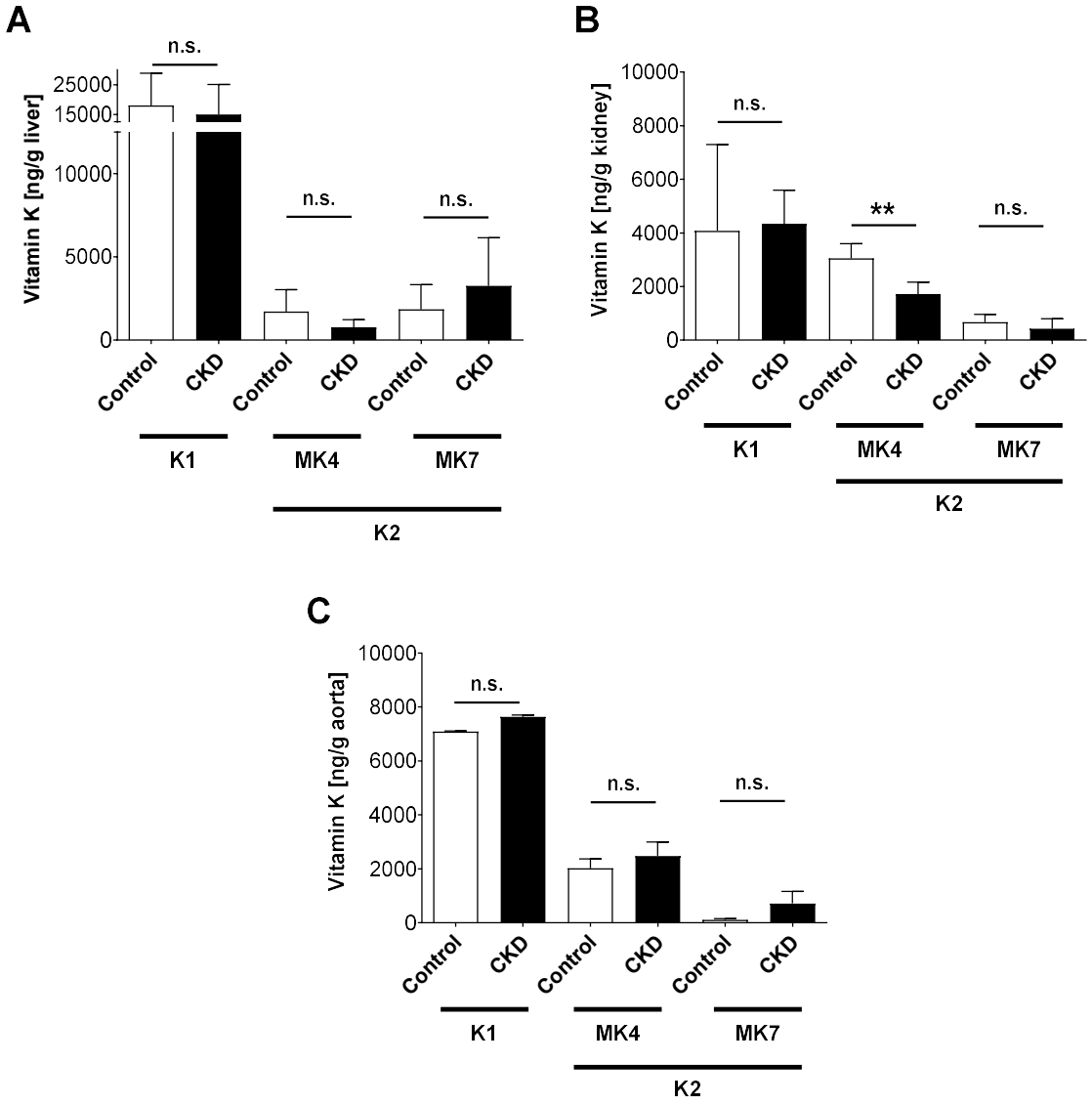

Figure 10: Quantification of the vitamin K isoforms concentrations in control and CKD mice. Vitamin K1 (K1), menaquinone 4 (MK4), and menaquinone 7 (MK7) concentrations were measured in livers, kidneys and aortas from control (white bar) and CKD mice (black bar) via HPLC, after sacrificed. Data are shown as mean ± SD, **p≤0.01 compared to the control group, based on unpaired t-test assuming equal SD (N=7-8 per group).

No significant difference between the groups was found in other tissue samples (**Figure 11 A-D**). The concentrations of all the isoforms were low in serum and lung (<1,000 ng/g tissue), but especially in the brains (<500 ng/g brain) (**Figure 11 B-D**).

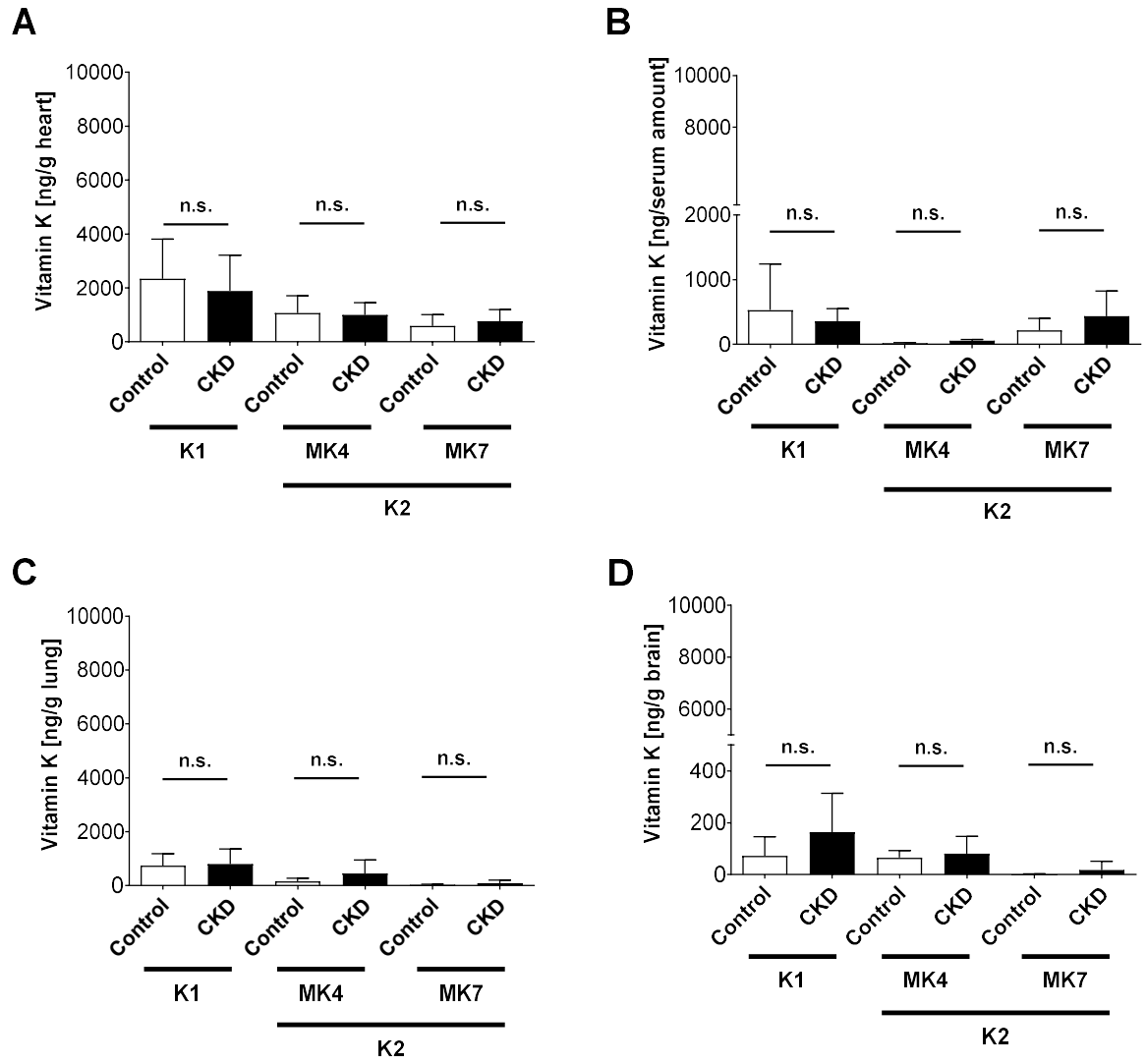

Figure 11: Quantification of the vitamin K isoforms concentrations in control and CKD mice. Vitamin K1 (K1), menaquinone 4 (MK4), and menaquinone 7 (MK7) concentrations were measured in hearts, serum, lungs and brains from control (white bar) and CKD mice (black bar) via HPLC, after sacrificed. Data are shown as mean ± SD, compared to the control group, based on unpaired t-test assuming equal SD (N=7-8 per group).

4.2. Vitamin K-related enzymes in kidneys from CKD rat model

In order to find an explanation for the decrease in MK4 concentration in CKD kidneys, the expression of the two enzymes involved in the conversion of vitamin K1 to vitamin K2 [68,69], HMGCR and UBIAD1, was studied in kidneys of Wistar rats. To induce CKD in Wistar rats, the animals underwent a 7 week diet regime consisting of 4 weeks of adenine diet followed by 2 weeks of standard diet and finished off with 1 week of adenine diet. The control group got 7 weeks of the standard diet. After 7 weeks the rats were sacrificed and immunofluorescence co-staining of HMGCR and UBIAD1 enzymes was done on the kidney sections from both groups **(Figure 12).**

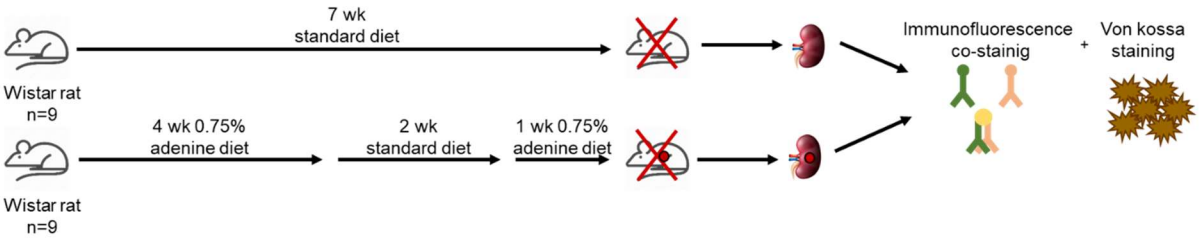

Figure 12: Scheme of adenine-CKD rat model used to study the vitamin K-related enzymes in kidneys. Wistar rats went under either 7 weeks standard diet or 4 weeks adenine diet, with 2 weeks break in between and followed by 1 more week of adenine diet to induce CKD. After 7 weeks the rats from both groups were sacrificed, and immunofluorescence co-staining and von Kossa staining were done in kidney sections of both groups.

CKD was confirmed by measuring urea concentration in the serum of the animals after 7 weeks of diet. An increase was observed in the CKD group when compared to the control group (**Figure 13**).

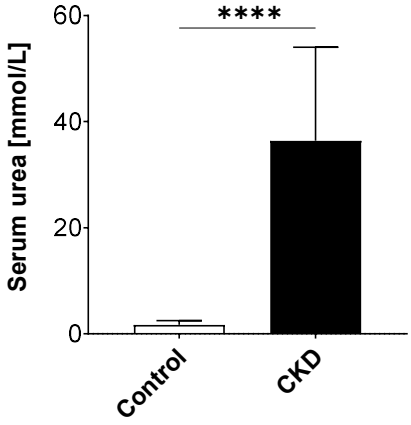

Figure 13: Serum urea concentration of control and CKD rat models. Control (white bar) and CKD (black bar) rats serum urea concentration at the end of the experiment. Data are shown as mean ± SD, ****p≤0.0001 compared to the control group, based on unpaired t-test assuming equal SD (N=7 per group). *Measurement provided by the "Institut für Versuchstierkunde" (RWTH Aachen).*

4.2.1. Vitamin K converting enzymes: HMGCR and UBIAD1 co-staining in kidney sections from control and CKD rats

Co-staining of FITC labelled HMGCR (green) and Cy3 labelled UBIAD1 (red), showed expression of both enzymes in the kidney tubules, with a decreased expression in the CKD group compared to the control one (**Figure 14**).

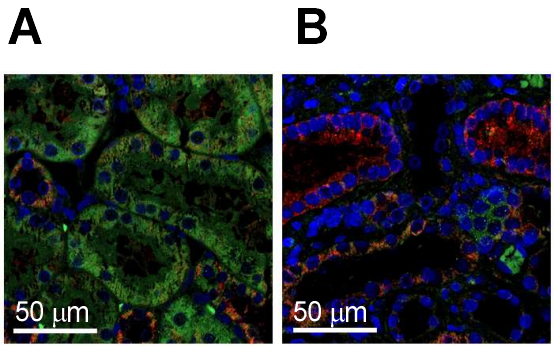

Figure 14: HMGCR and UBIAD1 co-staining in the kidneys of control and CKD rats. Immunofluorescence representative images of control (**A**) and CKD (**B**) rat kidneys stained with FITC-HMGCR (green), Cy3-UBIAD1 (red) and DAPI (blue) (magnification: 40x; scale bar: 50 µm).

To quantify the staining of the enzymes on the surface of the tubules, ´ImageJ´ software (National Institutes of Health, USA) was used.

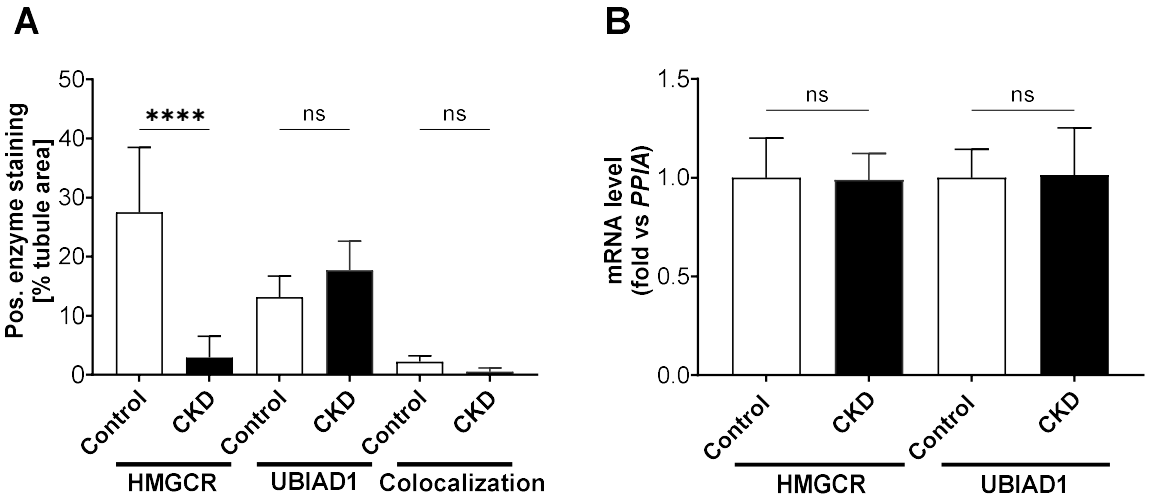

Figure 15: Quantification of HMGCR and UBIAD1 positive staining in control and CKD rats. Quantification of HMGCR, UBIAD1 and colocalization of both enzymes stained area in kidney sections from control (white bars) and CKD (black bars) rats shown as a percentage of the total tubule area. Data are shown as mean ± SD, ****p≤0.0001 compared to the control group, based on one-way ANOVA (**A**). Relative quantification of HMGCR and UBIAD1 mRNA levels in rat kidneys from control (white bars) and CKD (black bars) groups. Data are shown as mean ± SD normalised to housekeeping gene PPIA and compared to the control group, based on one-way ANOVA (**B**). Sidaks correction was used as a post-test (N=8-9 per group).

A significant decrease in positive staining of HMGCR in the kidney tubules from CKD rats was found, while no differences in the expression of UBIAD1 between the two groups, nor the co-staining of both enzymes were observed (**Figure 15A**). Furthermore, gene expression of HMGCR and UBIAD1 was also analysed by real-time PCR, showing no difference between CKD and control rats (**Figure 15B**).

HMGCR enzyme is needed for the synthesis of MK4 [68], and the MK4 isoform is important for the carboxylation of vitamin K-dependent proteins that inhibit vascular calcification [56]. Therefore, after observing the strong decrease in protein level for HMGCR in CKD rat kidneys compared to control rats, calcium deposition in the kidneys was analysed. For this, kidney sections from control and CKD rats were stained with von Kossa staining (**Figure 16**).

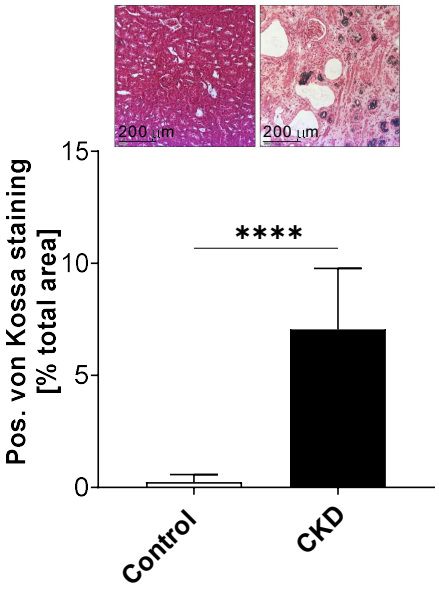

Figure 16: Von Kossa staining of kidney sections from control and CKD rats. Representative images of von Kossa staining in control (left) and CKD (right) rat kidneys (magnification: 2.5x; scale bar: 200 µm) and its quantification in control (white bar) and CKD (black bar) rat kidneys as a percentage of the total area section. Data are shown as mean ± SD ****p≤0.0001 compared to the control group, based on unpaired t-test (N=8-9 per group).

Kidney slides from CKD rats had calcium deposits, clearly seen after von Kossa staining (**Figure 16**). Quantification of the von Kossa staining in kidney sections showed a significant increase in the CKD group (**Figure 16**), with an approx. 4 times larger calcified area in the CKD rats compared to the control group.

Furthermore, a negative correlation could be found between the expression of HMGCR and von Kossa staining in the rat kidneys (**Figure 17A**), while no correlation was observed for UBIAD1 and von Kossa staining (**Figure 17B**).

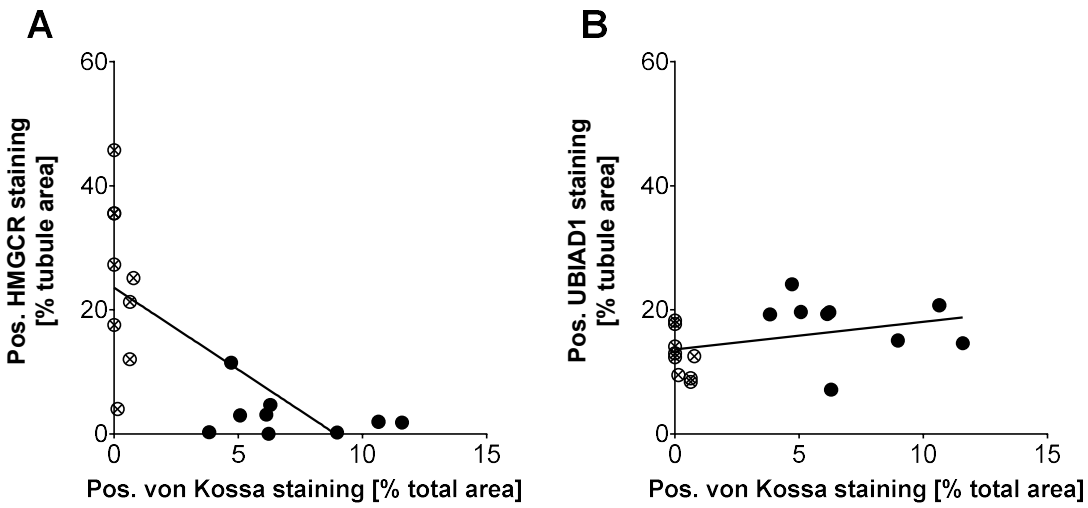

Figure 17: Correlation between positive staining of HMGCR and UBIAD1 enzymes on the surface on the tubules and von Kossa staining in control and CKD rats. Correlation between HMGCR positive staining area and von Kossa positive staining in kidney sections from control (white dots) and CKD (black dots) rats. Correlation analysis was performed: r=-0.7215 and **p≤0.01 (**A**). Correlation between UBIAD1 positive staining area and von Kossa positive staining in kidney sections from control (white dots) and CKD (black dots) rats. Correlation analysis was performed: r=0.3627 and non-significant p-value (**B**). (N=8-9 per group)

4.2.2. Post-translational modifications of HMGCR enzyme in CKD rat kidneys

An increased uremic toxin concentration in CKD patients has already been reported [118]. Uremic toxins lead to post-translational modifications in proteins, which could affect their activity and expression [119]. Therefore, to further study the decrease in HMGCR expression, post-translational modifications of this enzyme were analysed by MALDI imaging.

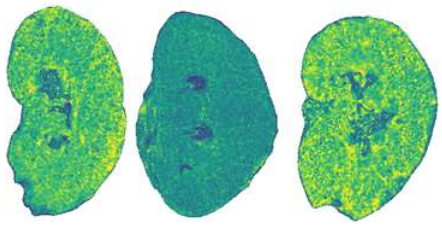

Figure 18: Carbamylation of HMGCR enzyme in CKD kidneys. Representative images of the post-translational modification carbamylation, in HMGCR enzyme ("*VSLGLAEDVSK*") analysed via MALDI imaging in CKD rat kidneys. Carbamylated residues (yellow colour) are found in lysines in most of the CKD kidneys studied. The colour scale represents the mass intensity of the modification found, the more yellow, the higher intensity of the modified sequence. *MALDI image measurement done by Dr. Julianne Hermann from IMCAR institute (RWTH Aachen)*

In CKD rat kidneys, analysed by MALDI imaging, carbamylated lysine residues were found in the HMGCR enzyme. After digestion, carbamylation was found in the sequence *"VSLGLAEDVSK*" which correlates to amino acids 298 to 308 of HMGCR. The non-modified sequence has a molecular weight of 1120 kDa, and when the lysine 308 (*K*) is carbamylated its molecular weight changes to 1160.63 kDa, which is the molecular weight of the post-

translational modification referred to as carbamylation (43 kDa). Carbamylated HMGCR was distributed all around the kidney surface (represented in yellow in **Figure 18**).

4.2.3. Vitamin K recycling enzymes: VKORC1 and NQO1 staining in kidney sections from control and CKD rats

To further study vitamin K2 (MK4) deficiency in CKD kidneys, the expression of the recycling enzymes VKORC1 and NQO1 was studied.

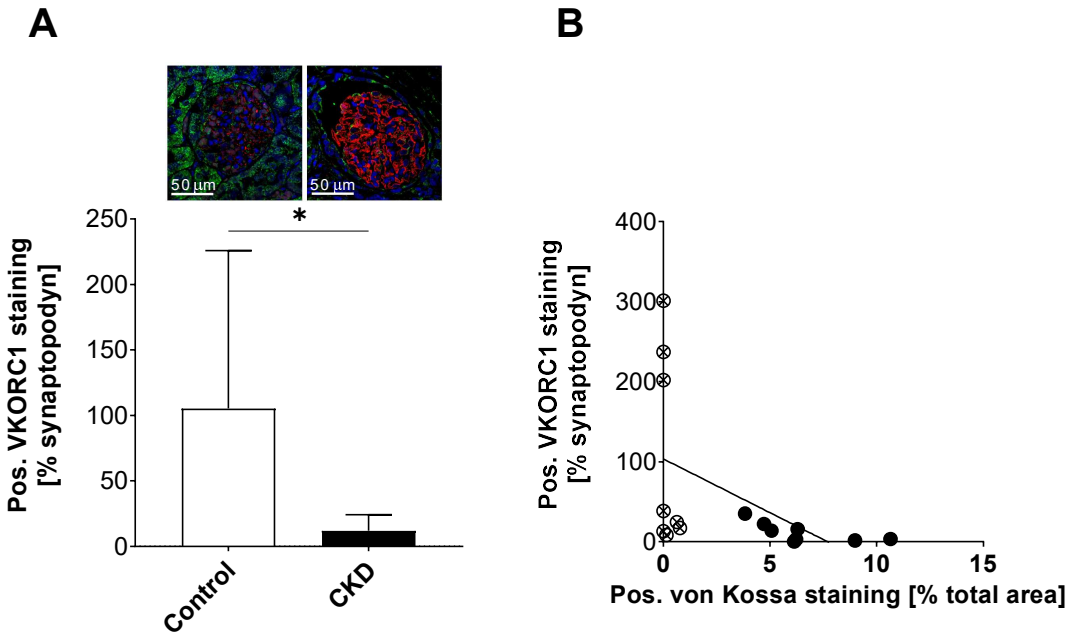

Figure 19: VKORC1 positive staining and its correlation with von Kossa staining in control and CKD rat kidneys. Immunofluorescence representative images of control (left) and CKD (right) rat kidneys stained with synaptopodin (Cy3, red), VKORC1 (AF647, shown as green) and DAPI (blue) (magnification: 40x; scale bar: 50 µm) and the quantification of the VKORC1 stained area in control (white bar) and CKD (black bar) rat kidneys as a percentage of synaptopodin positive staining in the kidney sections. Data are shown as mean ± SD, *p<0.05 compared to the control group, based on unpaired t-test (N=8-9 per group) (**A**). Correlation between VKORC1 positive staining area and von Kossa positive staining in kidney sections from control (white dots) and CKD (black dots) rats. Correlation analysis was performed: r=-0.5057; *p<0.05 (**B**).

Immunofluorescence co-staining of Cy3 labelled synaptopodin (red), and AF647 labelled VKORC1 (green), showed that VKORC1 was present in close vicinity to the glomeruli in kidneys and mainly in the tubules (**Figure 19A**). Here, a significant decrease in the VKORC1 staining in the CKD group compared to the control group was observed (**Figure 19A**). Furthermore, a negative correlation was observed between positive VKORC1 staining and the presence of calcium crystals in the kidneys (**Figure 19B**).

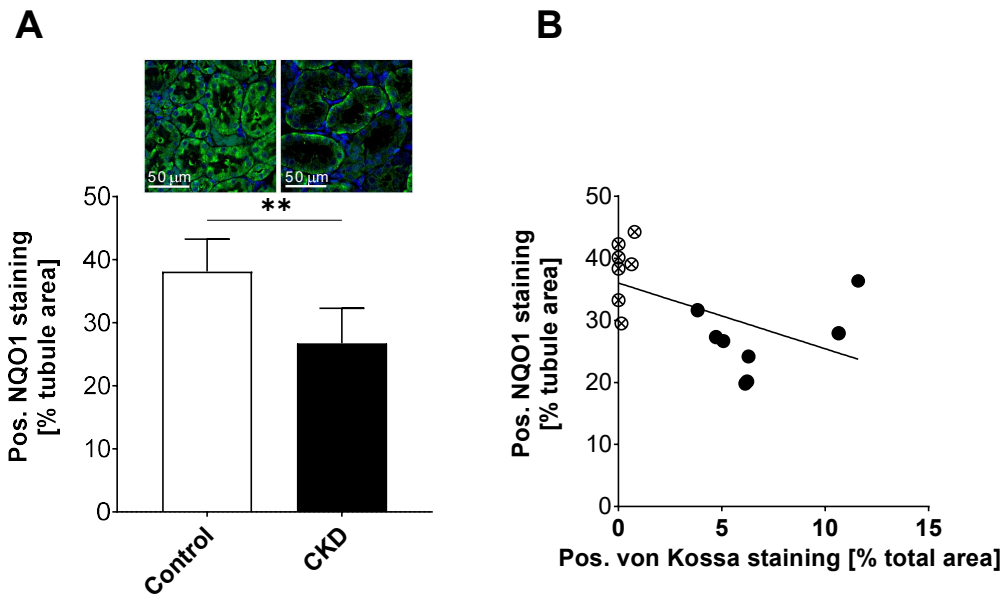

Figure 20: NQO1 positive staining and its correlation with the positive von Kossa staining in the control and CKD rat kidneys. Representative immunofluorescence images of control (left) and CKD (right) rat kidneys stained with NQO1 (FITC, green) and DAPI (blue) (magnification: 40x; scale bar: 50 µm) and the quantification of the NQO1 stained area in control (white bar) and CKD (black bar) rat kidneys as a percentage of tubule area in the kidney sections. Data are shown as mean ± SD, **p<0.01 compared to the control group, based on unpaired t-test (N=6-7 per group) (**A**). Correlation between NQO1 positive staining area and von Kossa positive staining in kidney sections from control (white dots) and CKD (black dots) rats. Correlation analysis was performed: r=-0.5343; *p<0.05 (**B**).

Immunofluorescence staining of FITC labelled NQO1 (green) showed that this enzyme is present in the tubules of the kidneys (**Figure 20A**). Here, a significantly decreased staining for NQO1 in the CKD kidneys compared to the control group was observed (**Figure 20A**). Moreover, a negative correlation between the positive NQO1 staining and the presence of calcium crystals in the kidneys of CKD rats was observed (**Figure 20B**).

4.3. Vitamin K-related enzymes in kidneys from CKD individuals

4.3.1. Vitamin K converting enzymes: HMGCR and UBIAD1 co-staining in kidney sections from healthy and CKD individuals

To confirm the data observed in the rat CKD model, the same immunofluorescence staining in kidney sections from healthy and CKD patients was performed. The CKD patients had a GFR between 33 and 46 mL/min/1.73 m^2 and healthy individuals between 99 and 107 mL/min/1.73 m^2.

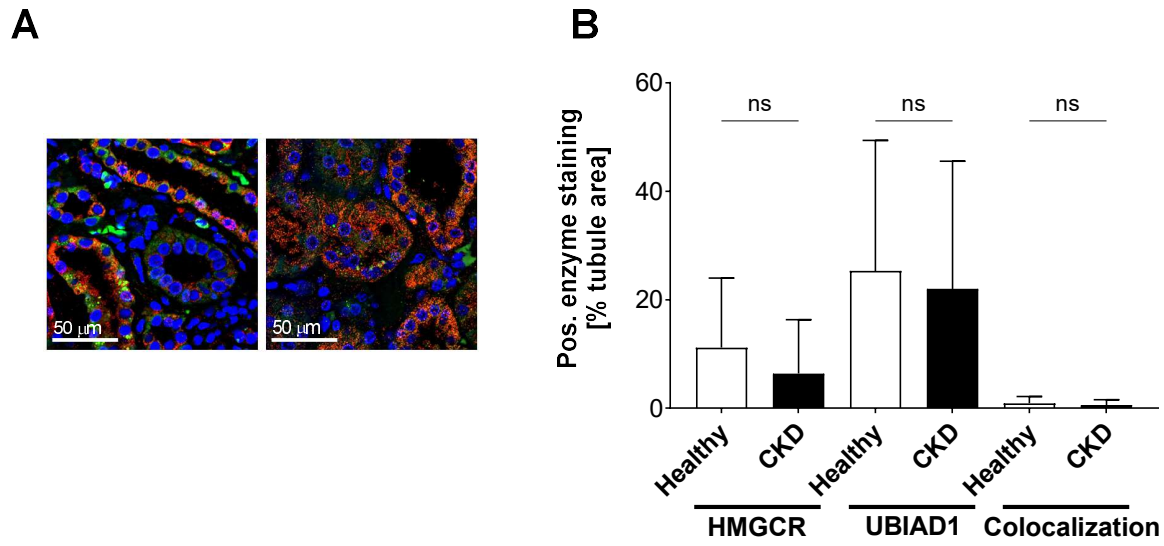

Figure 21: HMGCR and UBIAD1 co-staining in the kidneys of healthy and CKD individuals. Representative immunofluorescence images of healthy (left) and CKD (right) human kidneys stained with HMGCR (FITC, green), UBIAD1 (Cy3, red) and DAPI (blue) (magnification: 40x; scale bar: 50 µm) (**A**). Quantification of HMGCR, UBIAD1 and co-staining of both enzymes stained area in kidney sections from healthy (white bars) and CKD (black bars) patients as a percentage of the total tubule area. Data are shown as mean ± SD, ****p≤0.0001 compared to the healthy group, based on one-way ANOVA. Sidaks correction was used as a post-test (N=4-6 per group) (**B**).

Similar to the rat staining, immunofluorescence staining of FITC labelled HMGCR (green) and Cy3 labelled UBIAD1 (red), in human kidney sections showed that these enzymes are mainly expressed in the tubules (**Figure 21A**), however, no significant difference in the percentage of positively stained enzymes could be shown between the sections from CKD patients and healthy subjects (**Figure 21B**).

Subsequently, von Kossa staining of the human kidney sections was done to quantify the degree of calcification in the kidneys.

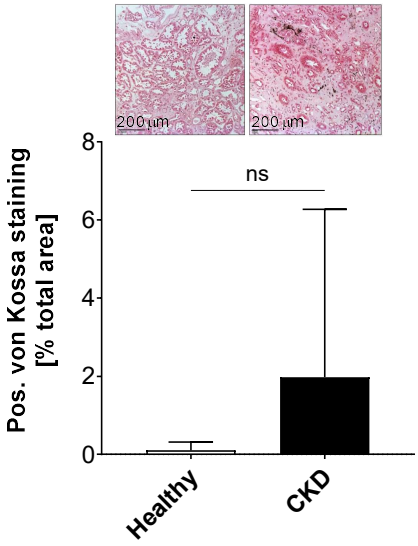

Figure 22: Von Kossa staining of kidney sections from healthy and CKD individuals. Representative images of von Kossa staining in healthy and CKD human kidneys (magnification: 2.5x; scale bar: 200 µm) and its quantification in healthy (white bar) and CKD (black bar) human kidneys as a percentage of the total area section. Data are shown as mean ± SD ****p≤0.0001 compared to the healthy group, based on unpaired t-test (N=4-6 per group).

CKD patients did not show a significant increase in calcium crystals in kidneys in comparison with the healthy group (**Figure 22**), even if the CKD patients had low GFR and thus, higher calcium deposition was expected.

4.3.2. Vitamin K recycling enzymes: VKORC1 and NQO1 staining in kidney sections from healthy and CKD individuals

In RNA sequencing data analysis, vitamin K converting enzymes*, HMGCR* and *UBIAD1*, and the enzymes involved in the vitamin K recycling cycle, *GGCX, NQO1* and *VKORC1*, have been analysed in CKD and healthy human kidney sections [120]. In this study previously performed by our group, of all the enzymes analysed related to vitamin K metabolism, there was only found a significant difference in the expression of *VKORC1*, with a lower expression in CKD patients [120].

Therefore, the expression of this enzyme was analysed at protein level by co-staining of VKORC1 and synaptopodin (a marker for podocytes) in the human kidney sections.

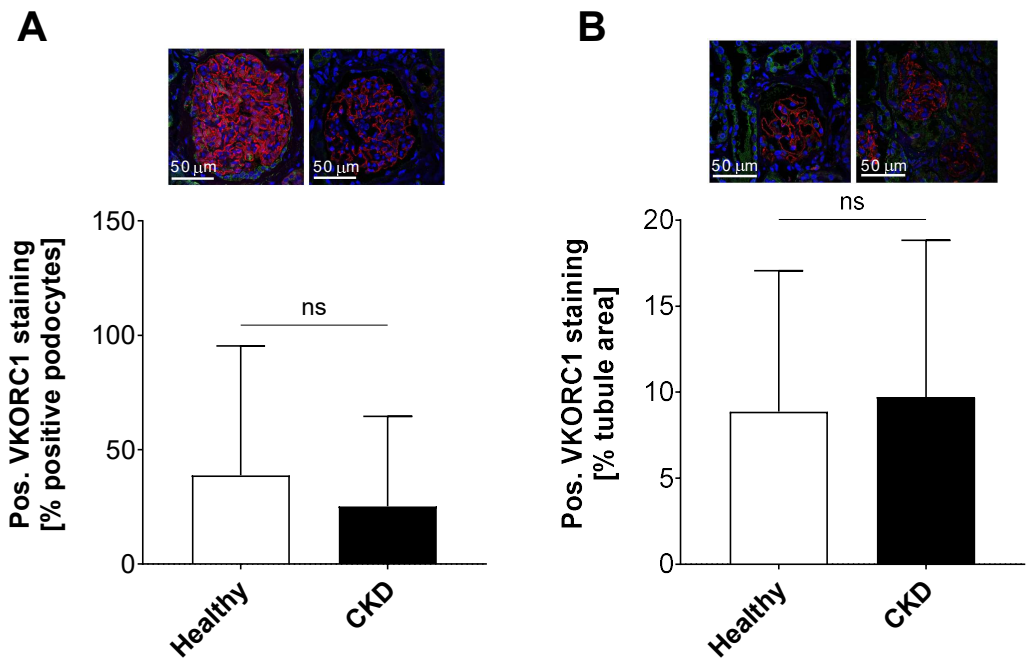

Figure 23: VKORC1 positive staining in healthy and CKD individuals. Representative immunofluorescence images of healthy and CKD human kidney glomeruli (**A**) and tubules (**B**) stained with VKORC1 (green), synaptopodin (red) and DAPI (blue) (magnification: 40x; scale bar: 50 µm) and the quantification of the VKORC1 stained area in healthy (white bar) and CKD (black bar) human kidneys as a percentage of podocytes positive staining in the kidney sections (**A**) and as a percentage of total tubules area in the kidney sections (**B**). Data are shown as mean ± SD compared to the healthy group, based on unpaired t-test (N=4-6 per group).

The immunofluorescence co-staining of Cy3 labelled synaptopodin (red) and AF647 labelled VKORC1 (green), showed a very weak staining in the glomeruli of the kidneys in both healthy and CKD patients (**Figure 23A up**), with no difference between the two groups (**Figure 23A down**). Positive staining of VKORC1 was found on the tubules of the kidney (**Figure 23B up**), however, no significant difference between CKD patients and healthy subjects could be detected (**Figure 23B down**).

NQO1 staining was also performed in CKD and healthy individuals but no staining could be observed either for healthy or for CKD samples (data not shown).

The present data show that vitamin K deficiency in CKD is mainly due to the decreased expression of vitamin K converting enzymes, which leads to a decreased synthesis of vitamin K2 and therefore a decreased carboxylation of the vitamin K-dependent enzymes that are directly responsible for the inhibition of vascular calcification, finally leading to increased vascular calcification in CKD patients. Therefore, the search and development of new drugs for the prevention and therapy of vascular calcification in CKD patients has a big interest and is still needed, in this context the chromogranin A-derived peptide VIF could be an interesting target as a drug for vascular calcification.

4.4. New mediator of vascular calcification: VIF

4.4.1. VIF effect on angiotensin II inhibition of calcium deposition

Since the chromogranin A-derived peptide VIF was characterized as being able to inhibit angiotensin II-induced vasoconstriction by affecting the angiotensin II type 2 (AT2) receptor [106] and Kukida *et al.* suggested that stimulation of the AT2 receptor inhibits phosphate induced vascular calcifications [107], the impact of VIF on the inhibitory effect of angiotensin II (Ang II) on vascular calcification was investigated. For this purpose, an *in vitro* vascular calcification assay was used. HAoSMCs were cultured using non-calcifying medium (NCM) (containing 0.9 mmol/L phosphate) as well as calcifying media (CM) (2.5 mmol/L phosphate) in the absence or presence of angiotensin II and VIF (100 nmol/L each).

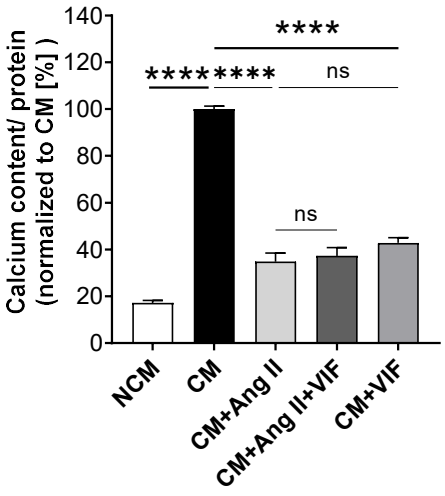

Figure 24: VIF effect on angiotensin II inhibition of calcium deposition in hAoSMCs. Quantification of calcium content on hAoSMCs incubated in non-calcifying conditions (NCM) and under calcifying conditions in the absence (CM), presence of angiotensin II (CM+Ang II), a combination of angiotensin II and VIF (CM+Ang II+VIF) or VIF (CM+VIF). Data are shown as mean ± SEM, ****p≤0.0001 compared to CM or to CM in the presence of angiotensin II, based on one-way ANOVA. Bonferroni's multiple comparisons were used as a post-test (N=4 per group).

Figure 24 shows a 60% inhibition of calcium deposition after the addition of Ang II, while the addition of VIF had no significant influence on this effect. Moreover, when the cells were incubated with VIF in the absence of Ang II, a strong inhibitory effect of VIF was also observed.

4.4.2. *In vitro* and *ex vitro* characterization of calcification inhibition by VIF

After noticing the potency of VIF to inhibit vascular calcification in hAoSMCs when it was added at a concentration of 100 nmol/L, a dose-response experiment *in vitro* (hAoSMCs) and *ex vivo* (rat aortic rings) was done.

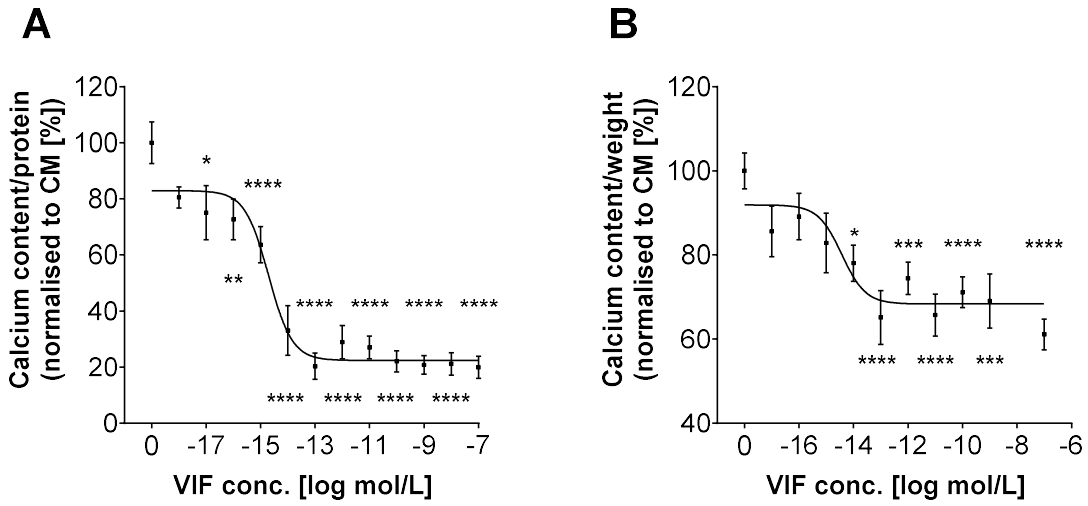

Figure 25: VIF effect on calcium deposition in *in vitro* and *ex vivo* models of vascular calcification. Dose-response effect of VIF on Ca^{2+} content of hAoSMCs (**A**) and isolated thoracic aortic rings (**B**) incubated under calcifying conditions in the absence (0) or presence of increasing concentrations of VIF ($1x10^{-18}$ to $1x10^{-7}$ mol/L). Data are shown as mean ± SEM, *p ≤0.05, **p≤0.01, ***p≤0.001, ****p≤0.0001 compared to the calcifying condition in the absence of VIF, based on one-way ANOVA. Bonferroni's multiple comparisons were used as a post-test (N=3-6 per group).

Both the *in vitro* and *ex vivo* models showed a dose-response effect for VIF (**Figure 25**), with an EC_{50} of $1x10^{-15}$ mol/L.

The inhibitory effect of VIF on vascular calcification was confirmed with alizarin red staining in the *in vitro* model with hAoSMCs cultured using non-calcifying medium (NCM) (containing 0.9 mmol/L phosphate) as well as calcifying media (2.5 mmol/L phosphate) in the absence (CM) or presence of VIF (CM+VIF) (100 nmol/L) (**Figure 26**).

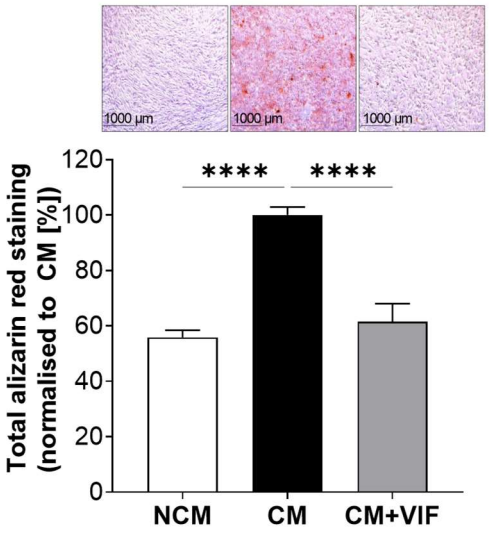

Figure 26: **Alizarin red staining in hAoSMCs incubated in non-calcifying conditions (NCM) and under calcified conditions in absence (CM) or presence of VIF (CM+VIF).** Representative images of alizarin red (magnification: 4x; scale bar: 1000 µm) and the quantification of the total stained area in hAoSMCs incubated in non-calcifying conditions (NCM; white bar) and under calcifying conditions in the absence (CM; black bar) or presence of VIF (100 nmol/L) (CM+VIF; grey bar) using cetylpyridinium chloride (**B**). Data are shown as mean ± SEM, ****p≤0.0001 compared to CM in the absence of VIF, based on one-way ANOVA. Bonferroni's multiple comparisons were used as a post-test (N=6 per group).

The staining of hAoSMCs with alizarin red showed the presence of calcium phosphate crystals, represented by red crystals under the microscope when they were cultured under calcifying conditions (CM). Incubation of hAoSMCs under calcifying conditions and in the presence of VIF (CM+VIF) inhibited the formation of these red crystals (**Figure 26**). Quantification of the alizarin red deposition with cetylpyridinium confirmed the alizarin red staining observations under the microscope. hAoSMCs cultured under calcifying conditions in the presence of VIF (CM+VIF) showed a 40% reduction of alizarin crystals compared to the cells cultured under calcifying conditions in the absence of VIF (CM) (**Figure 26**).

Alizarin red and von Kossa staining in *ex vivo* rat aortic rings cultured under non-calcifying (NCM) and calcifying conditions in the absence (CM) or presence of VIF (100 nmol/L) (CM+VIF) also showed the inhibitory effect of VIF on vascular calcification *ex vivo* (**Figure 27**).

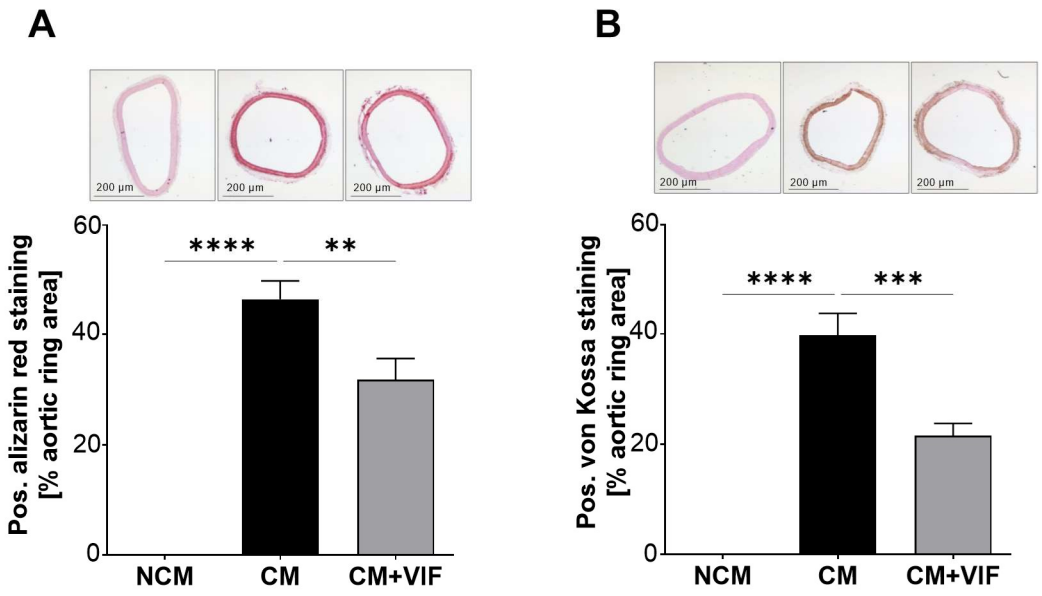

Figure 27: Alizarin red and von Kossa staining in aortic rings incubated in non-calcifying conditions (NCM) and under calcified conditions in absence (CM) or presence of VIF (CM+VIF). Representative images of alizarin red staining (**A**) and von Kossa staining (**B**) (magnification: 2.5x; scale bar: 200 µm) and its corresponding quantification of the stained area in thoracic aortic rings incubated in non-calcifying conditions (NCM; white bar) and under calcifying conditions in the absence (CM; black bar) or presence of VIF (100 nmol/L) (CM+VIF; grey bar) as a percentage of the total aortic area section. Data are shown as mean ± SEM, **p≤0.01, ***p≤0.001, ****p≤0.0001 compared to CM in the absence of VIF, based on one-way ANOVA. Bonferroni's multiple comparisons were used as a post-test (N=4 per group).

Staining of rat aortic rings with both alizarin red and von Kossa showed deposition of calcium phosphate crystals in the media layer of the vessel wall when the rings were cultured only under calcifying conditions (CM and CM+VIF), represented by red (alizarin red) or brown (von Kossa) crystals under the microscope. Incubation of the rat aortic rings under calcifying conditions in the presence of VIF (CM+VIF) decreased the formation of these crystals (**Figure 27**). Quantification of the stained areas in the rings confirmed the alizarin red and von Kossa staining observations under the microscope, aortic rings cultured under calcifying conditions in the presence of VIF (CM+VIF) showed a 10-20% reduction in the deposition of the crystals compared to the rings cultured under calcifying conditions in the absence of VIF (CM) (**Figure 27**).

4.4.3. *In vivo* characterization of calcification inhibition by VIF

In collaboration with the INSERM institute in Montpellier (France) the VIF effect was investigated *in vivo* in rats. A VDN (vitamin D3 plus nicotine) rat model of elastocalcinosis [115,116] was used. VDN rats were infused with or without VIF with an osmotic pump (31 µg/kg per day) implanted under the skin for 4 weeks. Rats with sham operation and saline administration were used as a control. After the sacrifice, the aortas were taken for alizarin red and von Kossa staining.

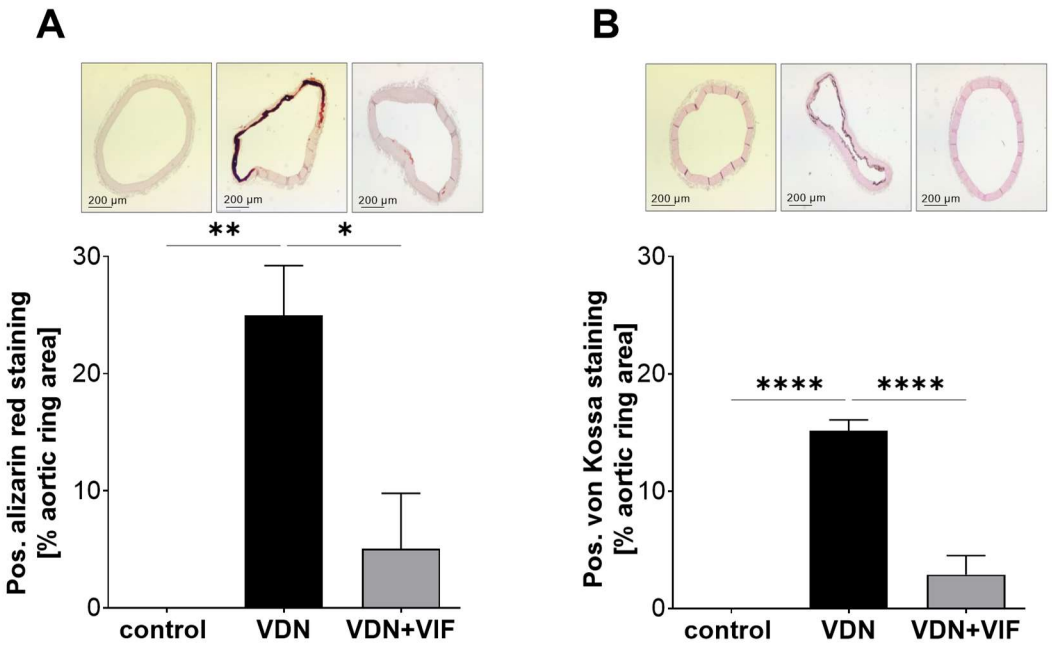

Figure 28: **Alizarin red and von Kossa staining in aortic rings from control, VDN rats and VDN infused with VIF (VDN+VIF).** Representative images of alizarin red staining (**A**) and von Kossa staining (**B**) of thoracic aortic rings of Wistar rats (magnification: 2.5x; scale bar: 200 µm) and its corresponding quantification of the stained area in thoracic aortic rings of Wistar rats (control; white bar) and VDN Wistar rats treated by a vehicle (VDN; black bar) or treated by VIF infused (31µg/kg per day for 4 weeks) (VDN+VIF; grey bar) via an osmotic pump as a percentage of the total aortic area section. Data are shown as mean ± SEM, *p ≤0.05, **p≤0.01, ****p≤0.0001 compared to the VDN in the absence of VIF, based on one-way ANOVA. Bonferroni's multiple comparisons were used as a post-test (N=4 per group).

Both stainings showed a significant increase of 20-30% in vascular calcification in the aortas of VDN rats, which was significantly reduced to 0-10% by treatment with VIF (**Figure 28**).

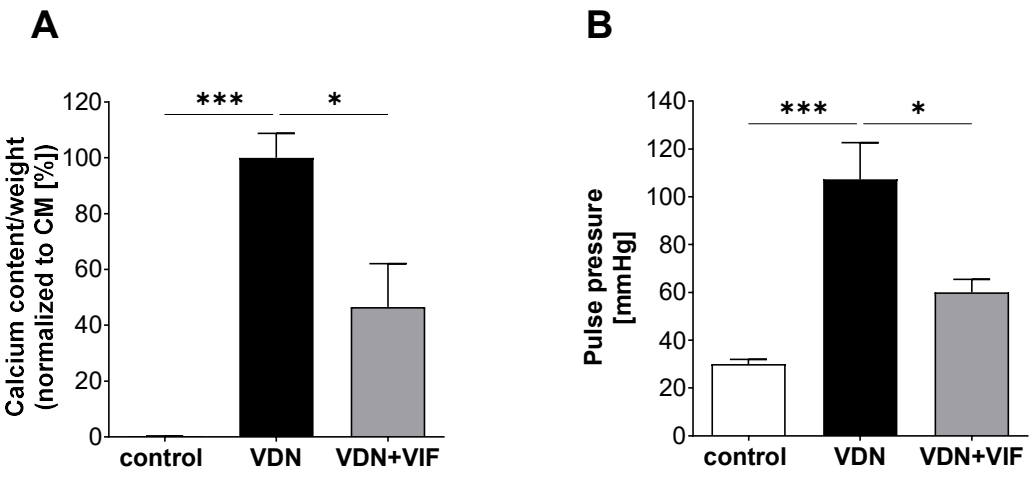

Figure 29: Calcium content and pulse pressure in aortas from control, VDN rats and VDN infused with VIF (VDN+VIF). Quantification of calcium content of thoracic aorta (**A**) and carotid arterial pulse pressure (**B**) of Wistar rats (control; white bar) and VDN Wistar rats treated by a vehicle (VDN; black bar) or treated by VIF infused (31µg/kg per day for 4 weeks) (VDN+VIF; grey bar). Data are shown as mean ± SEM, *p ≤0.05, ***p≤0.001 compared to the VDN in the absence of VIF, based on one-way ANOVA. Bonferroni's multiple comparisons were used as a post-test (N=4 per group). *Measurements done by Dr. Nathalie Gayrard from INSERM–Montpellier (France).*

Furthermore, the decrease in calcium deposition in the VIF infused rats could be confirmed by quantification of the calcium content in the aortas. This showed a 50% reduction of calcium deposition as a result of VIF treatment (**Figure 29A**). Since a correlation between vascular calcification and hypertension has been described [121], the effect of VIF on pulse pressure was investigated next in this rat model. A 50% reduction in VDN-induced pulse pressure could be observed by treating the animals with VIF (**Figure 29B**).

4.4.4. VIF effect on the expression of the genes involved in the development of vascular calcification in hAoSMCs

To further elucidate the inhibitory mechanism of VIF on the inhibition of vascular calcification, the expression of vascular calcification related genes [41] was analysed in hAoSMCs via real-time PCR, after three and five days incubation under calcifying or non-calcifying conditions and in the absence or presence of VIF (**Figure 30**).

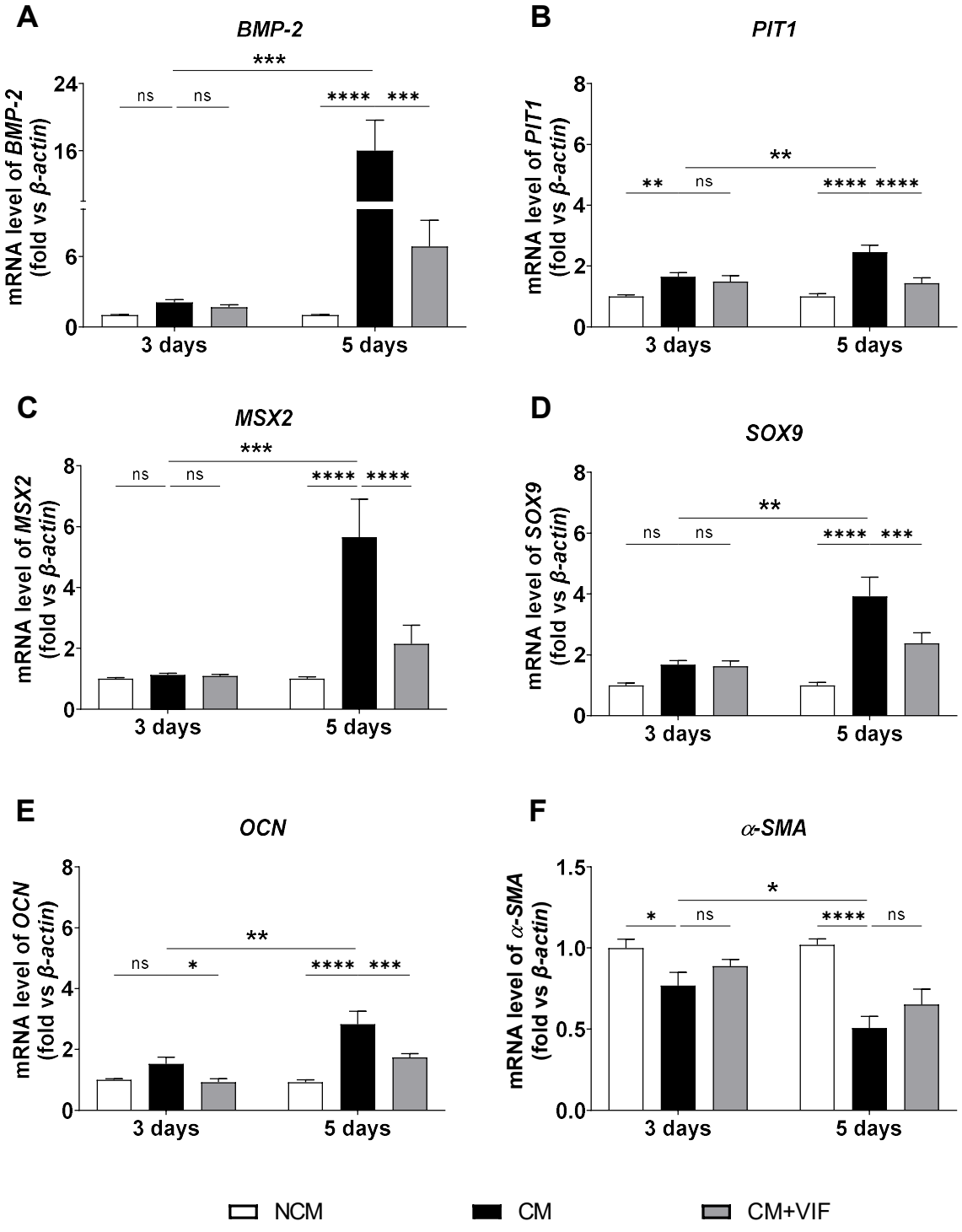

Figure 30: VIF effect on the expression of genes involved in the development of vascular calcification in hAoSMCs. Relative quantification of bone morphogenetic protein 2 (*BMP-2*) (**A**), sodium-dependent phosphate cotransporter-1 (*PIT1*) (**B**), transcription factor Msh homeobox 2 (*MSX2*) (**C**), SRY-Box Transcription Factor 9 (*SOX9*) (**D**), osteocalcin (*OCN*) (**E**), and α-Smooth Muscle Actin *(α-SMA*) (**F**) expression by real time-PCR. hAoSMCs were incubated in non-calcifying conditions (NCM; white bar) and under calcifying conditions in the absence (CM; black bar) or presence of VIF (100 nmol/L) (CM+VIF; grey bar) for three or five days. Data are shown as mean ± SEM. *p<0.05, **p≤0.01, ***p≤0.001, ****p≤0.0001 normalised to housekeeping gene *β–actin* and compared to CM in the absence of VIF, based on two-way ANOVA for the different conditions, and unpaired t-test for comparisons between CM. Bonferroni's multiple comparisons were used as a post-test (N=4-6 per group).

After incubating the cells with calcifying medium (CM) for three days, only a significant change in the gene expression of sodium-dependent phosphate cotransporter-1 (*PIT1*) and α-Smooth Muscle Actin (α-*SMA*) was observed (**Figure 30B and 30F**) when it was compared to non-calcifying medium (NCM). Furthermore, three days of treatment with VIF only showed a reduction in osteocalcin (*OCN*) gene expression (**Figure 30E**).

However, after an incubation time of five days with calcifying medium, a significant increase in gene expression was observed for all genes (**Figure 30A-E**) except α-*SMA*, which showed a decrease in gene expression (**Figure 30F**). Treatment of hAoSMCs with VIF for five days at a concentration of 100 nmol/L showed a significant reduction in the expression of all these calcification-related genes (**Figure 30A-E**), while no significant change was observed for α-*SMA* (**Figure 30F**).

4.4.5. VIF effect on the expression and secretion of IL-6 by hAoSMCs under calcifying conditions

Under calcifying conditions, SMCs secrete inflammatory cytokines like tumour necrosis factor-α (TNF-α), interleukin-1β (IL-1β) and interleukin-6 (IL-6) that upregulate calcification-related genes [50]. Therefore, the expression and secretion of inflammatory cytokines TNF-α, IL-1β and IL-6 was studied in hAoSMCs cultured under calcifying conditions and in the absence or presence of VIF (100 nmol/L) (**Figure 31**).

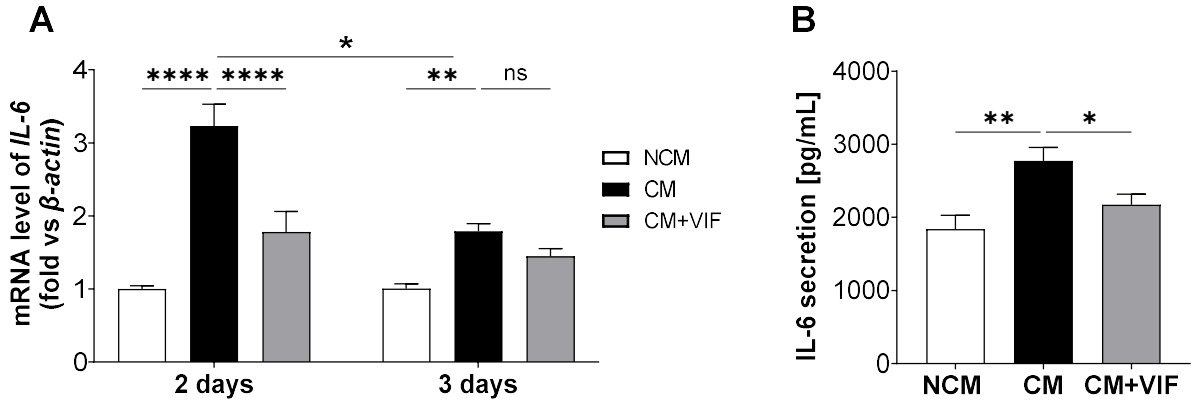

Figure 31: VIF effect on the expression and secretion of IL-6 by hAoSMCs. Relative quantification by RT-PCR of *interleukin-6* (*IL-6*) gene expression in hAoSMCs incubated in non-calcifying medium (NCM; white bar) or calcifying medium in the absence (CM; black bar) or presence of VIF (100 nmol/L) (CM+VIF; grey bar) for two or three days. Data are shown as mean ± SEM normalised to housekeeping gene *β-actin*, *p<0.05, **p≤0.01, ****p≤0.0001 compared to CM in the absence of VIF, based on two-way ANOVA for the different conditions, and unpaired t-test for comparisons between CM. Bonferroni's multiple comparisons was used as a post-test (N=4 per group) (**A**). Relative quantification by ELISA of IL-6 secretion in the supernatant of hAoSMCs incubated in non-calcifying medium (NCM; white bar) or calcifying medium in the absence (CM; black bar) or presence of VIF (100 nmol/L) (CM+VIF; grey bar) for two days. Data are shown as mean ± SEM, *p<0.05, **p≤0.01 compared to CM in the absence of VIF, based on one-way ANOVA. Bonferroni's multiple comparisons were used as a post-test (N=4 per group) (**B**).

While no significant change in *TNF-α* and *IL-1β* expression was observed in cells cultured under calcifying conditions compared to non-calcifying conditions (data not shown), a significant upregulation of *IL-6* expression was observed in cells cultured under calcifying conditions (CM) for two and three days. However, the increase after three days was less pronounced in comparison to the increase after two days. Moreover, the co-incubation with VIF showed a significant reduction of this effect only after two days of incubation (**Figure 31A**). Furthermore, a significant increase on IL-6 secretion was measured by ELISA in the supernatant of hAoSMCs cultured under calcifying conditions for two days. In the presence of VIF, this secretion was significantly reduced (**Figure 31B**).

4.4.6. VIF effect on the activation and phosphorylation of P38 and ERK1/2 MAP kinases in hAoSMCs under calcifying conditions

Mitogen-activated protein kinases (MAP kinases) such as P38 and ERK1/2 are directly linked to the calcification process [41,122] by activating IL-6 production [123]. Therefore, the activity of these two kinases was analysed via PamGene analysis, in hAoSMCs cultured under non-calcifying conditions and under calcifying conditions in the absence or presence of VIF (100 nmol/L) (**Table 6**).

Table 6: Kinase ranking scores for STK kinases in hAoSMCs analysed by PamGene. HAoSMCs were incubated in non-calcifying medium (NCM) or calcifying medium in the absence (CM) or presence of VIF (100 nmol/L) (CM+VIF) for two days. Kinase ranking scores were obtained using PamGene analysis based on the median final score and median kinase statistic and are shown as median kinase statistic for P38, ERK1 and ERK2 (N=3 per group).

Kinase	CM vs NCM	CM+VIF vs CM
P38	**0.51**	**-7.69**
ERK2	**0.39**	-4.50
ERK1	0.34	-4.41

PamGene analysis showed a significant upregulation of the phosphorylating activity for P38 and ERK2 MAP kinases (bold numbers), and a slight upregulation for ERK1. The phosphorylating activity of P38 was significantly decreased (negative and bold value) in the presence of VIF, while for ERK1/2 the decrease was not significant (**Table 6**).

To corroborate this effect, phosphorylation and thus activation of P38 and ERK1/2 MAP kinases were analysed by Western blot using lysates from hAoSMCs incubated in non-calcifying medium or calcifying medium in the absence or presence of VIF (100 nmol/L) for two days (**Figure 32**).

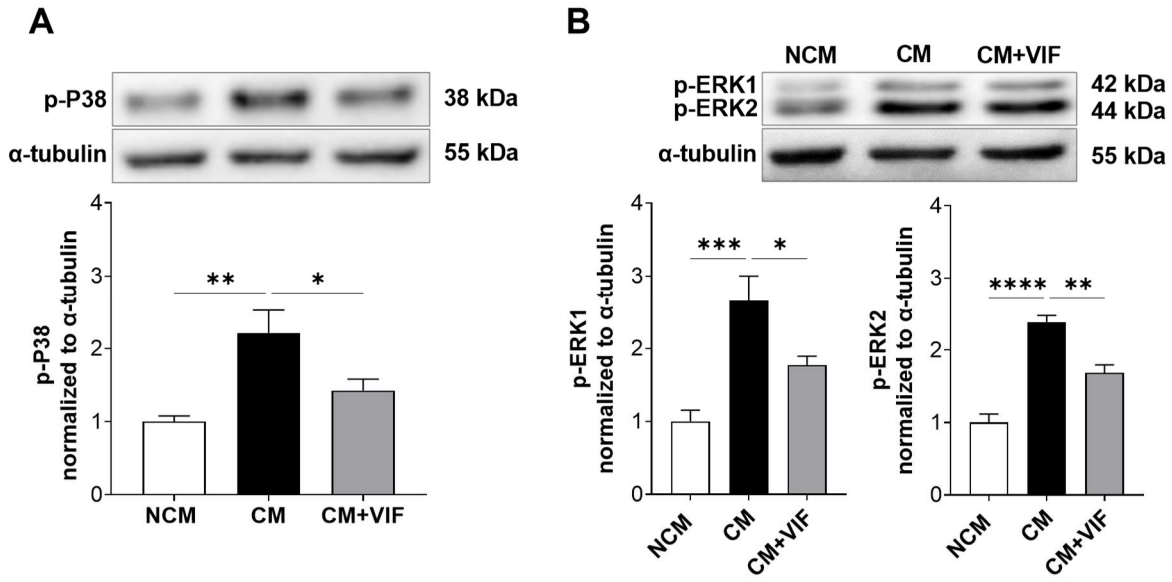

Figure 32: VIF effect on the P38 and ERK1/2 MAP kinase activation. Representative Western blots of phosphorylated P38 (**A**) and ERK1/2 (**B**) in hAoSMCs and the corresponding quantification (**C**) and (**D**) respectively, incubated in a non-calcifying medium (NCM; white bar) or calcifying medium in the absence (CM; black bar) or presence of VIF (100 nmol/L) (CM+VIF; grey bar) after two days. Data normalised to housekeeping gene α-tubulin are shown as mean ± SEM, *p<0.05, **p≤0.01, ***p≤0.001, ****p≤0.0001 compared to CM in the absence of VIF, based on one-way ANOVA. Bonferroni's multiple comparisons were used as a post-test (N=5-6 per group).

A significant increase in the kinase activation induced by calcifying conditions was observed for P38 MAPK (**Figure 32A**) as well as for ERK1/2 MAPK (**Figure 32B**) after two days. The phosphorylation was significantly reduced for all three kinases in the presence of VIF (100 nmol/L) (**Figure 32**).

4.4.7. VIF effect on ROS production in hAoSMCs under calcifying conditions

Under calcifying conditions there is a production of reactive oxygen species (ROS), that activate the phosphorylation and activation of the kinases [52], as shown in **Table 6** and **Figure 32**. Therefore, the production of ROS by hAoSMCs cultured in calcifying media in the absence and presence of VIF was analysed (**Figure 33**).

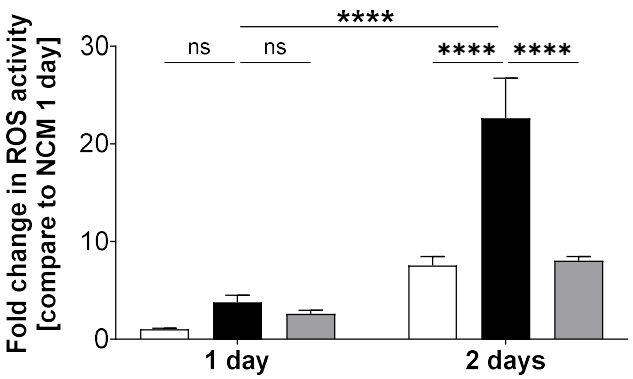

Figure 33: VIF effect on ROS production in hAoSMCs. Quantification of ROS activity in hAoSMCs incubated in non-calcifying conditions (NCM; white bars) and under calcifying conditions in the absence (CM; black bar) or presence of VIF (100 nmol/L) (CM+VIF; grey bar) after one and two days. Data are shown as mean ± SEM. , ****p≤0.0001 compared to CM in the absence of VIF, based on one-way ANOVA. Bonferroni's multiple comparisons were used as a post-test (N=7 per group).

After one day of culture under calcifying conditions, there was no significant increase in the production of ROS by the hAoSMCs, however, one day later, cells which were cultured in CM showed a significant increase in ROS production, which was decreased when the cells were cultured in presence of VIF (100 nmol/L) (**Figure 33**).

4.4.8. VIF effect on phosphate-mediated apoptosis in hAoSMCs

High phosphate concentrations induce apoptosis of vascular SMCs [124], which has been suggested as the underlying mechanism of vascular calcification [41,125,126]. Thus, to investigate the effect of VIF on apoptosis, hAoSMCs cultured under calcifying conditions in the absence or presence of VIF were analysed via flow cytometry by counting the positive annexin V cells, which is a marker for apoptosis marker.

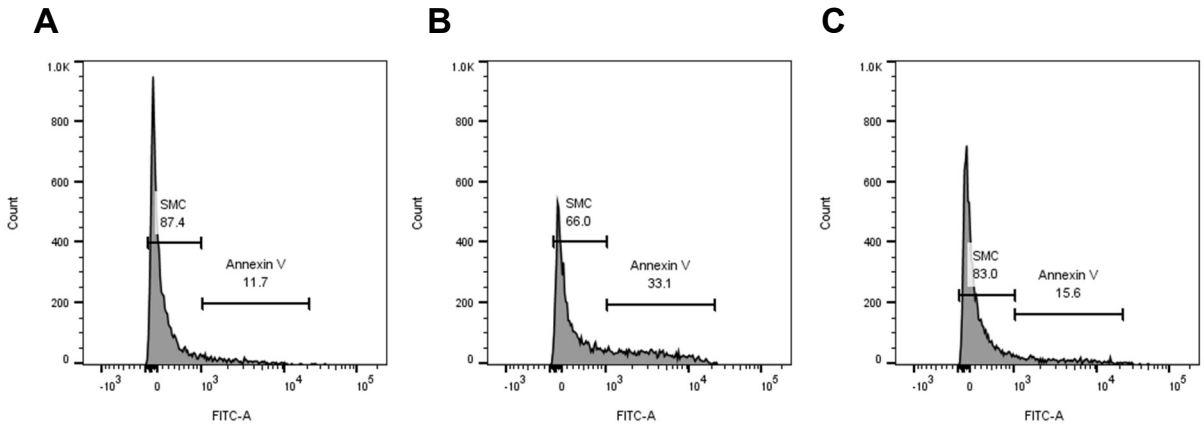

Figure 34: VIF effect on phosphate-mediated apoptosis in hAoSMCs. Flow cytometry histograms showing the percentage of FITC-annexin V positive cells in a hAoSMCs population cultured in non-calcifying conditions (**A**) and under calcifying conditions in the absence (**B**) or presence of VIF (100 nmol/L) (**C**).

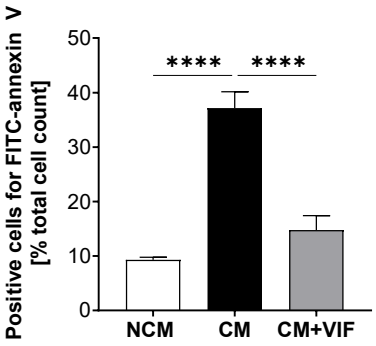

Figure 35: VIF effect on phosphate-mediated apoptosis in hAoSMCs. Flow cytometry quantification of FITC-annexin V positive cells in a hAoSMCs population when hAoSMCs are incubated in non-calcifying conditions (NCM; white bar) and under calcifying conditions in the absence (CM; black bar) or presence of VIF (100 nmol/L) (CM+VIF; grey bar) for 7 days. Data are shown as mean ± SEM, ***p≤0.001, ****p≤0.0001 compared to CM in the absence of VIF, based on one-way ANOVA. Bonferroni's multiple comparisons were used as a post-test (N=4 per group).

Figures 34-35 shows the percentage of annexin V-positive cells in a population of hAoSMCs. HAoSMCs cultured under non-calcifying conditions have an annexin V positive cell population of approximately 10% (**Figure 34A and 35**). When cells are cultured under calcifying conditions, the population of annexin V positive cells, which are apoptotic cells, increases until 40% (**Figure 34B and 35**). Addition of VIF to calcifying media decreases the population of apoptotic cells (**Figure 34C**) to percentages similar to non-calcifying media (**Figure 35**).

4.4.9. VIF effect on the formation and uptake of primary and secondary calciprotein particles (CPPs)

Since vascular calcification is driven by the formation of CPPs [48,127], the formation and uptake of these particles was analysed in the supernatant of hAoSMCs in the absence or presence of VIF. The formation of primary and secondary CPPs was analysed by electron microscope. (**Figure 36**).

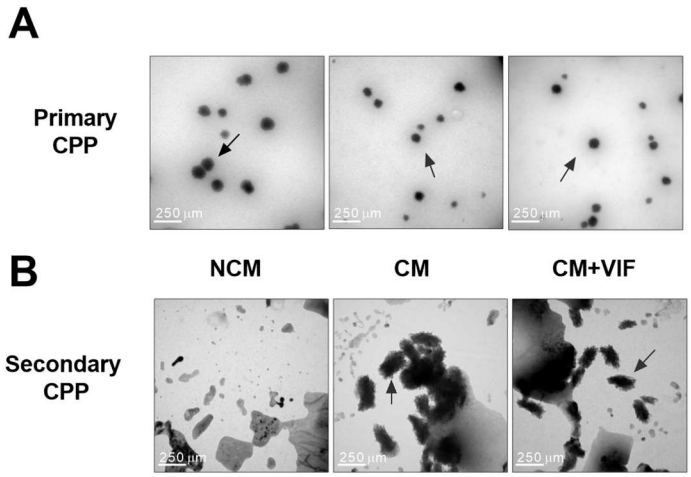

Figure 36: **VIF effect on the formation of primary and secondary CPPs by hAoSMC.** Representative images pointing (black arrows) the formation of primary (**A**) or secondary (**B**) CPPs in the supernatant of hAoSMCs incubated in non-calcifying conditions (NCM) and under calcifying conditions in the absence (CM) or presence of VIF (100 nmol/L) (CM+VIF) taken by electron microscope (magnification: 60000x; scale bar: 250 µm). *Measurement done in collaboration with the microscopy department of Uniklinik RWTH Aachen.*

Primary CPPs were formed in the supernatant of all the conditions tested (**Figure 36A**). However, secondary CPPs were only formed when cells were cultured under calcifying conditions (CM and CM+VIF) (**Figure 36B**). Inhibition of the formation of secondary CPPs by VIF was not detected.

To analyse the uptake of CPPs, hAoSMCs were incubated with Alexa488-labelled calciprotein monomers (CPM) and primary and secondary CPPs. The uptake of the particles was analysed after different time points using flow cytometry. Labelled fetuin-A monomers were used as a negative control.

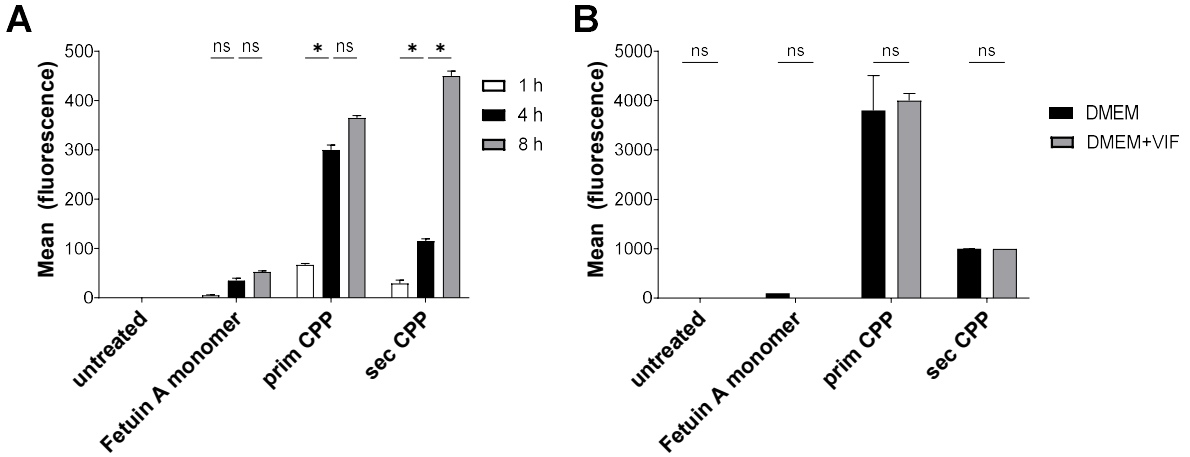

Figure 37: VIF effect on the uptake of primary and secondary CPPs by hAoSMC. Uptake of fetuin A monomer, primary CPPs (prim CPP) and secondary CPPs (sec CPP) by hAoSMCs at different time points, data are shown as mean ± SEM, *p<0.05 compared to one hour, based on two-way ANOVA. (**A**); and after four hours in absence (DMEM; black bar) and presence or presence of VIF (100 nmol/L) (DMEM+VIF; grey bar) data are shown as mean ± SEM, compared to DMEM in absence of VIF, based on one-way ANOVA. (**B**). Bonferroni's multiple comparisons were used as a post-test (N=2 per group). *Measurement done in collaboration with Dr. Sinna Köppert from Biointerface Laboratory in Aachen.*

Figure 37A shows a maximum uptake of primary CPPs after four hours. For secondary CPPs, this increased uptake was observed after four and eight hours of incubation, while an increase in cell death was observed after eight hours (data not shown). Therefore, the effect of VIF on CPPs uptake after four hours was analysed next.
There was no difference in the uptake of CPPs, both the primary and the secondary, when the cells were cultured in the presence of VIF (100 nmol/L) compared to the cells that did not receive VIF (**Figure 37B**).

4.4.10. VIF binding partner

A calcium misbalance is one of the main drivers of vascular calcification [36], with high concentrations of calcium leading to vascular calcification in CKD patients [37]. Extracellular calcium can activate the Calcium-sensing receptor (CaSR) [39], and it has been observed that activation of this receptor decreases vascular calcification [42]. Therefore, CaSR was studied as a binding partner of VIF in hAoSMCs. Co-immunoprecipitation of VIF with CaSR in hAoSMC lysates was performed and then analysed via mass spectrometry.

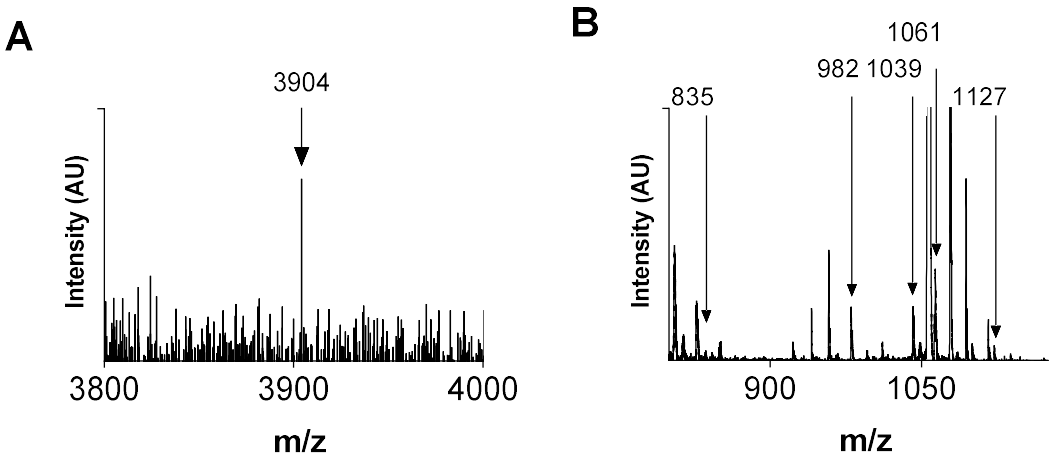

Figure 38: Co-immunoprecipitation of VIF and CaSR in hAoSMCs. Mass spectrometry spectra from VIF (**A**) and the representative identified fragments of Calcium-sensing receptor (CaSR) after trypsin digestion (**B**). *Mass spectrometry data obtained by Prof. Dr. Vera Jankowski from IMCAR institute (RWTH Aachen).*

Using mass spectrometry, VIF was detected with a mass/charge ratio (m/z) of 3,904 (**Figure 38A**) in the hAoSMC lysates incubated with CaSR antibody and VIF. In the same samples, CaSR was detected, after trypsin digestion, by identifying its fragments with a corresponding mass/charge ratio (m/z) of 835 m/z, 982 m/z, 1039 m/z, 1061 m/z, 1127 m/z (**Figure 38B**). In comparison, in hAoSMC lysates incubated with VIF and IgG antibody (negative control), no mass-signal was detected. Hence, these data show an interaction between VIF and CaSR.

Chapter 5

Discussion

5. DISCUSSION

The first part of the present thesis aimed to investigate the reason behind vitamin K2 deficiency in CKD patients, beyond the diet. To address this, the tissue content of different vitamin K isoforms in a CKD rat model was studied, as well as the expression of the enzymes involved in the conversion of vitamin K1 to vitamin K2 and the enzymes involved in the vitamin K recycling cycle. The second part of the thesis aimed to investigate whether VIF has an effect on the angiotensin II inhibitory effect on vascular calcification, and to further characterise VIF in the vascular calcification processes.

One reason for vitamin K deficiency in CKD patients is the low intake of this vitamin due to low potassium and phosphate diet [74]. This diet followed by many CKD patients includes low leafy and dairy product intake, which are rich in vitamin K1 and K2, respectively [74]. However, in this thesis, we studied the causes of vitamin K deficiency in CKD beyond the diet. In this thesis a mouse model of CKD by 5/6 nephrectomy, receiving a diet with different isoforms of vitamin K *ad libitum* was set-up. By measuring the tissue content of the different isoforms, it is possible to study where the isoforms are transported, in which organ they are required and metabolised, thereby indicating an organ-specific function of each isoform.

Our results showed that vitamin K1 was the most abundant isoform in all analysed tissues, compared to MK4 and MK7, in both the control and CKD group. The highest vitamin K1 content was found in livers, as expected since vitamin K1 carboxylates clotting factors in the liver [66]. The highest MK4 concentration was found in the aortas and kidneys. In these tissues carboxylation of vitamin K-dependent proteins is needed to inhibit vascular calcification [55]. The highest MK7 concentration was also measured in livers. The lowest concentrations of all isoforms were observed in the lungs and brains. However, the low concentration of vitamin K2 isoforms in brain contradicts previous findings [128,129], and recently a neuroprotective function in the brain has been described for MK4 [129]. For MK7, the low concentration could be explained by the long side chain of the menaquinone, which makes it harder to pass the blood-brain barrier. Additionally, no difference in tissue content of all isoforms was observed between CKD and control mice, with exception of MK4 in kidneys, for which the concentration was significantly decreased in CKD mice compared to the control group. McCabe *et al*. have already found changes in MK4 concentrations in different organs, in an adenine model of CKD rats fed only with vitamin K1 [128]. But to date, no study has been done comparing the tissue content of different isoforms in a CKD model after supplementing all of them in the diet. Our study is thus the first one to show a decreased concentration of MK4 in the kidneys of CKD (5/6 nephrectomy) mice compared to a control group, after the intake of three different isoforms of vitamin K.

The results of this study were recently published in the journal 'Kidney international' [120]. These data empathise that vitamin K-deficiency in CKD is not only due to diet, but is also related to its transport or metabolism.

In order to investigate the transport of vitamin K isoforms, our group studied their transportation by lipoproteins, in CKD haemodialysis patients and healthy individuals [120]. In this recently published study, we have shown that high-density lipoprotein (HDL) is the lipoprotein responsible for the transport of the MK4 and MK7 isoforms [120]. In uremic HDL particles from haemodialysis patients, we saw a decrease in MK7 incorporation compared to the incorporation in HDL particles from healthy subjects. Moreover, the *in vitro* data confirmed that HDL particles from haemodialysis patients do not incorporate MK7 as good as HDL from healthy subjects. This might explain why different clinical trials, done with MK7 as supplementation, have failed to improve vitamin K status [78] or to slow down the development of vascular calcification [79].

To analyse the impairment in the vitamin K metabolism, the vitamin K converting enzymes HMGCR and UBIAD1 in an adenine nephropathy rat model were studied. UBIAD1 is directly involved in the enzymatic conversion of vitamin K1 to vitamin K2 [130], but it needs the binding of HMGCR to fulfil this process [131]. Furthermore, to synthesize vitamin K2, UBIAD1 incorporates geranylgeranyl diphosphate (GGPP), which is a metabolite from the cholesterol pathway (also known as the mevalonate pathway), in which HMGCR is also involved [131]. In this thesis, we performed co-staining of both enzymes in rat kidneys, and we could see a significant decrease in the staining for HMGCR in the tubules from the CKD rats, while the gene expression of both enzymes showed no difference. No difference in *UBIAD1* gene expression contradicts previous findings from McCabe *et al.* in a CKD rat model, where a decrease at both the gene and protein level of UBIAD1 was found in kidneys of adenine rats [128]. The reason for this disagreement might be the different percentages of adenine used in their (continuous 0.25% adenine diet) and our (0.75% adenine diet with two weeks standard diet in between) model. Furthermore, in this thesis, the decrease in HMGCR staining correlates with an increase in calcium content in the kidneys of CKD rats. Although this calcium deposition is not vascular calcification and it is called nephrocalcinosis, it is thought that it is also driven by the misbalance of calcium and phosphate homeostasis, and it is regulated by mediators like Matrix Gla Protein, meaning that vitamin K also plays an important role here [132].

A decrease in HMGCR leads to a decrease in GGPP production [70], which is needed for the synthesis of vitamin K2 from vitamin K1, and therefore would also explain the decreased concentration of vitamin K2 (MK4) found in CKD kidneys.

The post-translational modification (PTM) of HMGCR described in this thesis, a carbamylation of lysine 301, is probably caused by the increase in uremic toxins under CKD conditions [119], and more specifically, by the increase in urea content [133,134] observed in CKD rats. This PTM could affect the binding between HMGCR and UBIAD1 and therefore, decrease the synthesis of vitamin K2 in CKD, explaining the decrease in MK4 concentration found in kidneys. In addition, it has been described that due to mutations in *UBIAD1*, which are common in Schnyder Corneal Dystrophy (SCD), HMGCR and UBIAD stay bound and are not degraded [69]. This permanent binding of HMGCR and UBIAD1 makes them avoid endoplasmic reticulum-associated protein degradation (ERAD) [69], leading to an accumulation of cholesterol, which is the main problem in SCD patients [131]. However, to date, there are not enough data available about this dystrophy and the vitamin K status of the patients. Nevertheless, *in vitro* studies have observed that most of the UBIAD1 mutations, associated with SCD, have a minimal effect on both MK4 biosynthesis and carboxylation of vitamin K-dependent proteins, finding only one mutation directly related to MK4 deficiency [135]. Another study in SCD patients has found increased plasma levels of dp-ucMGP, which would also correlate with low vitamin K status [136]. No further information regarding UBIAD1 is published to date. However, taking into account these previous studies on SCD [69,131,135,136], we hypothesise that there is a permanent or incorrect binding between HMGCR and UBIAD1, probably caused by the PTM in HMGCR under CKD conditions, that affects and decreases vitamin K2 synthesis. More studies on HMGCR-UBIAD1 binding and vitamin K status would be needed. Staining for HMGCR and UBIAD1 does not reflect protein expression or functionality, thus, further experiments to analyse the activity and function of these proteins would be needed to confirm our findings.

Another limiting step in the vitamin K metabolism is the vitamin K recycling cycle, where three enzymes, γ-glutamyl carboxylase (GGCX), vitamin K epoxide reductase complex subunit 1 (VKORC1) and NAD(P)H Quinone Dehydrogenase 1 (NQO1) are involved [55]. A deficiency in GGCX activity in kidneys from CKD rats has already been described by previous work from our group [56]. Although no changes in activity were detected in VKORC1 and NQO1 in this study [56], McCabe *et al.* observed a decrease in *VKORC1* gene expression in kidneys from the CKD rat model, which could be counteracted when the CKD rats were supplemented with vitamin K1 [128]. The results of this thesis showed a decrease in both VKORC1 and NQO1 staining in the kidneys of CKD rats. The decrease in both enzymes again correlates with an increase in calcium deposition in the kidneys. Our data are in line with the *in vivo* model of spontaneous vascular calcification, developed by Michaux *et al.*, in which a mutation of *VKORC1* leads to vitamin K deficiency and increased vascular calcification [137]. In addition, *in vitro* experiments in tubular kidney cells (HK2 cells), demonstrated an increase in calcium

deposition when *VKORC1* was silenced [138]. No studies on NQO1 regarding vitamin K and vascular calcification have been done to date.

Of the enzymes studied in the CKD rat model, HMGCR had the strongest decrease in staining and the highest negative correlation to calcium deposition in kidneys. Therefore, it is an interesting target for further studies in CKD. A deeper analysis to study the degree of calcification in vessels from CKD subjects, and its relationship with these enzymes should also be addressed. HMGCR, UBIAD1, VKORC1 and NQO1 are mainly expressed in the endoplasmic reticulum of epithelial cells in the tubules [139] (Human Protein Atlas, www.proteinatlas.org). Each CKD sample analysed, showed clear pathological structures, with huge dilation or atrophy in the tubules, or even absent glomeruli [140]. This might be an additional reason for the overall decrease in staining of the enzymes studied, although all the calculations in this thesis have been normalised to the tubule area.

Current experiments in our group are focused on the stimulation of the activity of these enzymes in CKD patients: for example for GGCX, previously reported as decreased activity in CKD [56], we aim to increase its activity and thereby improving the vitamin K status, resulting in a better carboxylation of vitamin K-dependent proteins, and a reduction of vascular calcification.

The main limitation of the first part of this thesis was the low number of human samples. This might explain the inability to translate the staining in rodent tissues to human kidneys. Co-staining of HMGCR and UBIAD1 in human kidney samples did not show a significant difference between healthy and CKD patients, although a clear tendency with a decrease in staining for HMGCR in CKD patients was observed. The von Kossa staining in kidneys from CKD patients showed that even with low GFR values (range 33-46 mL/min/1.73 m^2), these patients did not have an increase in calcium deposition in kidneys compared to the healthy individuals. These results disagree with previous data, where increased calcium deposition was observed in CKD patients compared to healthy individuals [141,142]. This thesis and the corresponding publication [120] demonstrate the first analysis of these two enzymes in CKD patients.

RNA sequencing data analysis, recently published by our group [120], of each enzyme related to the vitamin K metabolism (*GGCX, NQO1* and *VKORC1* as well as *HMGCR* and *UBIAD1*), only showed a decreased *VKORC1* expression in podocytes from CKD patients [120]. In this thesis, VKORC1 staining has been analysed in kidney sections of CKD patients and healthy controls. However, no difference was found between the two groups, either in the podocytes

or in the epithelial cells in tubules. Nevertheless, similar to the CKD rat model, the CKD patients also showed a reduced amount of tubules compared to the healthy individuals. This might be translated as a general decrease in VKORC1, due to the lower number of tubules in CKD patients. Surprisingly, NQO1 staining was not observed at all, probably due to a low affinity of the primary antibody used.

The results of this thesis combined with the previously published data [56,120], reaffirm that vitamin K metabolism is highly altered under CKD conditions. Increased uremic toxins as a result of CKD, probably cause post-translational modifications of enzymes involved in vitamin K metabolism (i.e. carbamylation of HMGCR), ultimately leading to vitamin K deficiency in CKD patients.

The data from the first part of the thesis show the impairment of the enzymes involved in the vitamin K metabolism in CKD, leading to a decreased concentration of vitamin K2 (MK4) in the kidneys. Specifically, CKD rats showed reduced HMGCR, VKORC1 and NQO1 staining compared to the control group (Figure 39). A bigger sample size for CKD patients and healthy individuals is needed to corroborate these findings. Nevertheless, this thesis shows for the first time a direct link between a decrease in the enzymes involved in vitamin K metabolism, the decreased MK4 content and increased calcium deposition in CKD kidneys.

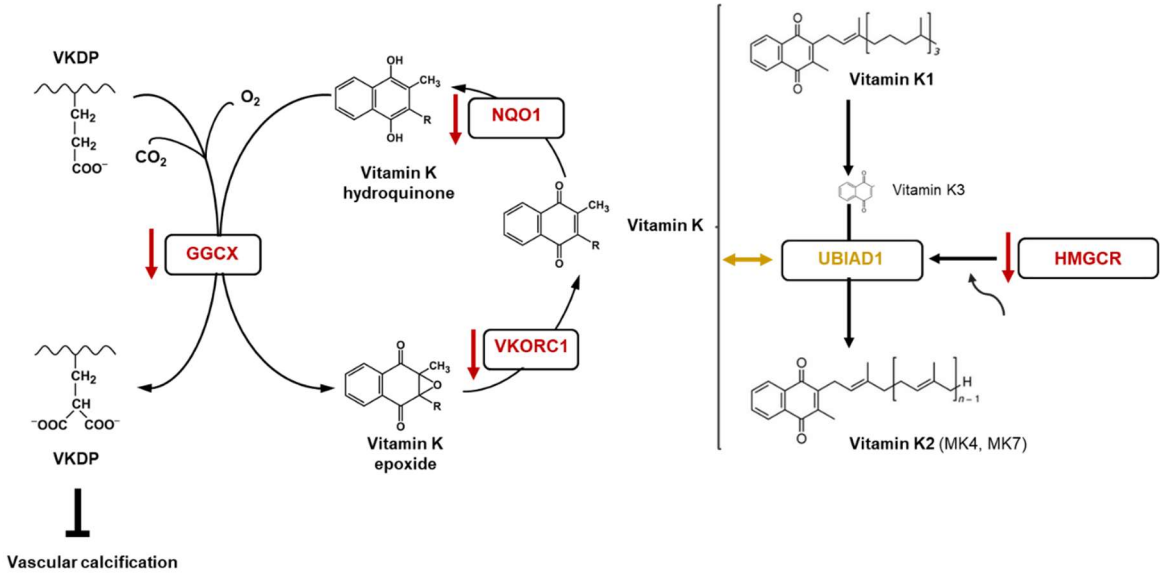

Figure 39: Schematic representation of vitamin K recycling cycle and vitamin K converting enzymes altered under CKD conditions. Decreased positive staining of HMGCR, VKORC1 and NQO1 in CKD model leads to a decreased vitamin K2 (MK4) content and increased calcification extent in kidneys. A reduction of GGCX activity in CKD has already been published [56]. No differences are found for UBIAD1 enzyme.

All these findings open new therapeutic approaches for vitamin K supplementation in CKD patients to reduce the risk of cardiovascular diseases, especially vascular calcification. However, no treatment options against the development of vascular calcification are known so far. Thus, the second part of this thesis focused on the search for new mediators of vascular calcification, finding VIF as a potent inhibitor.

VIF has been previously described as 'Vasoconstriction-Inhibiting Factor' since it decreases the vasoconstriction effect of angiotensin II, by binding to the same receptor, AT2 receptor [106]. Angiotensin II has been described as an inhibitor of vascular calcification [109], and stimulation of the AT2 receptor also leads to inhibition of this process [107]. Therefore, in the search for new mediators of vascular calcification, the present study aimed to determine whether VIF influences the inhibitory effect of angiotensin II on vascular calcification, as well as to further characterise VIF in vascular calcification processes. As a result, after incubating hAoSMCs with high phosphate concentrations to induce vascular calcification, and in the presence of angiotensin II, the combination of angiotensin II and VIF, or only VIF, it was seen that VIF did not affect the angiotensin II inhibition of vascular calcification. In addition, VIF was as potent inhibitor as angiotensin II. The potent inhibitory effect of VIF was confirmed *ex vivo*, in rat aortic rings cultured with high phosphate concentrations, as well as *in vivo* in the aortas of Wistar rats treated with vitamin D3 and nicotine, used as a model of medial arterial calcification and hyper pulsatility [115,116]. All the models studied in this thesis showed a decrease in calcium deposition when VIF was added to the calcifying media. Moreover, VIF has a dose-response effect against vascular calcification with an EC_{50} around 10^{-15} mol/L in both *in vitro* and *ex vivo* calcification assays, which is a really low concentration, meaning that VIF is a potent inhibitor of vascular calcification. These EC_{50} values are similar to the EC_{50} values from the peptide 'Calcification Blocking Factor (CBF)' [143], but the percentage of inhibition *in vitro* is higher with VIF (70% inhibition when VIF is added to calcified media compared to 30% inhibition in presence of CBF). EC_{50} value for VIF is much lower than the EC_{50} of the SNF472 drug [96], which is currently in phase 3 trial for the treatment of calciphylaxis in CKD patients [97], indicating a major potency of VIF compared to SNF472.

To unravel the mechanism of this potent inhibitor of vascular calcification, the most common genes related to the development of vascular calcification (*BMP-2, PIT1, MSX2, SOX9* and *OCN*) [41] were firstly studied. The addition of VIF to calcifying conditions decreased the expression of all these genes when it was compared to calcifying media, while no difference was observed for α*-SMA*, a marker of smooth muscle cells [144]. Subsequently, it was observed, that in hAoSMCs cultured under calcifying conditions, VIF decreased the up-regulation of the expression and concentration of IL-6, an inflammatory cytokine that activates the expression

of the vascular calcification-related genes [50]. Therefore, VIF inhibits the expression and secretion by SMCs of inflammatory cytokines under calcifying conditions. Other cytokines secreted by SMCs in presence of high concentrations of phosphate, thus linked to calcification processes, are tumour necrosis factor-α (TNF-α) and interleukin-1β (IL-1β) [50], but neither the expression nor the secretion of them could be detected in any of the conditions analysed in this thesis, probably due to low concentrations of these cytokines in the supernatant.

Mitogen-activated protein kinases (MAP kinases) P38 and ERK1/2 are active when they are phosphorylated under calcifying conditions [41,122], and as a result, they increase the expression and secretion of IL-6 [123]. In the presence of VIF, the phosphorylation status and activity of these MAP kinases were decreased, compared to their activity in hAoSMCs cultured under high phosphate conditions. P38 and ERK1/2 are activated when the production of ROS (reactive oxygen species) is increased [52]. Therefore, ROS production by hAoSMCs in calcifying media, in the absence or presence of VIF was analysed. This ROS production was increased after two days of incubation under calcifying conditions as was expected [38,50], and incubation in the presence of VIF decreased ROS levels to the levels of non-calcifying conditions. Furthermore, VIF also decreases the population of apoptotic cells in hAoSMCs cultured under high phosphate conditions, which is in agreement with the inhibitory calcification effect of VIF, since high phosphate leads to secretion of apoptotic bodies from hAoSMCs that will lead to apoptotic cell dead [124].

All these results show the potent ability of VIF to inhibit the most common calcification pathways in SMCs. Vascular calcification is initiated by primary and secondary calciprotein particles (CPPs) [48], therefore, the formation and uptake of primary and secondary CPPs by hAoSMCs in the absence and presence of VIF was studied, but, VIF did not interfere with any of these processes.

Vascular calcification is driven by excessive incorporation of calcium into the cells [38]. Ca^{2+} uptake into the cells occurs via calcium channels like voltage-gated channels (VGCC) [38], but surface plasmon resonance experiments with VGCC and VIF did not show an interaction between them (data not shown in this thesis). Extracellular Ca^{2+} activates the calcium-sensing receptor (CaSR) [39,40], and its activation leads to a decrease in vascular calcification [41]. Therefore, CaSR was studied as binding partner of VIF. Standard detection of co-immunoprecipitation using Western blot, could not be performed due to the big difference between the molecular weight of VIF (3,905 Da) and CaSR (121,000 Da). Nevertheless, co-immunoprecipitation using mass spectrometry to detect VIF and CaSR, has shown the interaction between VIF and this receptor. The loss of CaSR expression in SMCs leads to an

increase in calcium deposition [39], while its overexpression ameliorates this process [43]. Although the exact mechanism linking CaSR and vascular calcification is still not known in detail [41], the activation of CaSR by calcimimetics increases the levels of the calcification inhibitor Matrix Gla Proteins (MGP) [145]. We hypothesise that VIF could work as a calcimimetic of CaSR, leading to a decrease in vascular calcification. The detailed mechanism of this binding and how this leads to a decrease of vascular calcification has to be further investigated.

CKD patients have an increased concentration of VIF in plasma [106], which could mean that VIF is produced by the body to counteract vascular calcification derived from the increase in uremic toxins under CKD conditions. Correlation analysis between VIF concentration and vascular calcification in CKD patients should be addressed to confirm these findings.
Using *in vitro* and *ex vivo* studies our group has recently discovered the active fragment of VIF, VIF 22-28 (paper under submission). This short fragment of 7 amino acids, represents a possible and beneficial therapeutic agent against vascular calcification due to its better pharmacological properties compared to the full peptide.

In summary, in the second part of this thesis, it was found that VIF is a very potent inhibitor of vascular calcification. VIF binds to CaSR and inhibits vascular calcification, by decreasing the production of ROS and the activation of various cascades in the cells, which in turn are involved in the expression of various genes related to vascular calcification (Figure 40). Therefore, VIF is a candidate for the development of a drug for the prevention and therapy of vascular calcification in patients with increased vascular calcification, such as patients with CKD, and offers a promising perspective for the future.

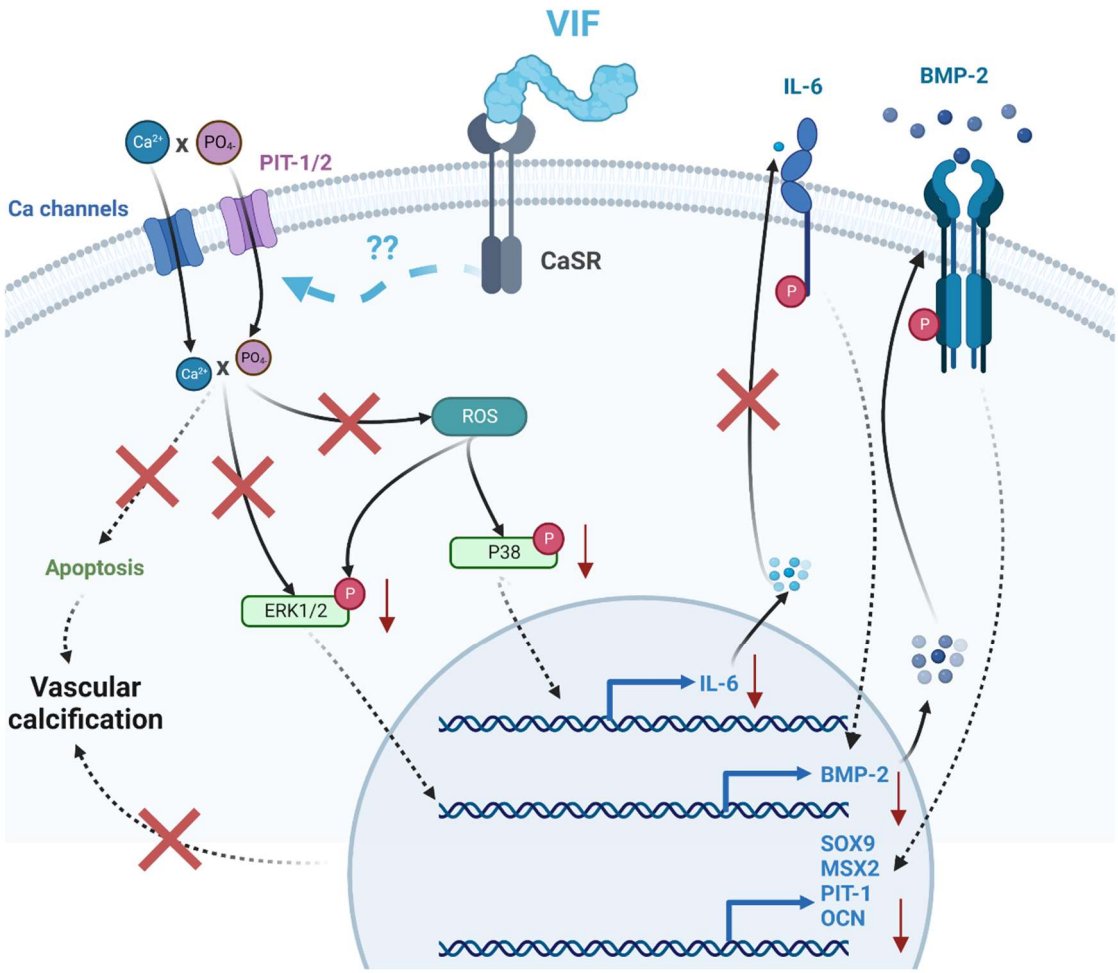

Figure 40: Schematic representation of VIF mechanism to inhibit vascular calcification in smooth muscle cells. VIF binds to calcium sensing receptor (CaSR) and inhibits vascular calcification. Hence, VIF prevents the production of ROS, activation of MAP kinases, secretion of inflammatory cytokines and therefore impeding the activation of genes related to the development of vascular calcification in the SMC.

- **In this thesis reasons behind vitamin K deficiency in CKD have been found: Downregulation of the enzymes HMGCR, VKORC1 and NQO1 in kidneys leads to a decreased vitamin K2 concentration, in the isoform MK4, and an increase in the degree of calcification in CKD kidneys.**

- **Furthermore, a new inhibitor of vascular calcification has been identified and characterised: VIF inhibits the development of vascular calcification, by acting as a possible calcimimetic of CaSR. VIF reduces ROS production and the activation of various cascades in the cells, which in turn are involved in the expression of various genes related to vascular calcification.**

Chapter 6

Summary

6. SUMMARY

This thesis focuses on vascular calcification in chronic kidney disease. Therefore, an explanation for the deficiency of the vascular calcification inhibitor vitamin K in these patients was investigated, and in addition, new mediators in this pathological process were studied.

In the first part of the thesis, we could observe in CKD animal model experiments that intake of the vitamin K2 isoform MK4 is significantly reduced in the context of CKD, in contrast to vitamin K1. This reveals novel directions of therapy to treat the absolute or relative (functional) vitamin K deficiency in CKD patients by supplementation therapies.

Furthermore, at the protein level we found a decrease in the enzymes HMGCR, VKORC1 and NQO1 in our CKD rat model, which negatively correlates with the degree of calcification in the kidneys. These enzymes are involved in vitamin K related processes: HMGCR is needed for the conversion of vitamin K1 to vitamin K2, and VKORC1 and NQO1 are involved in the vitamin K recycling cycle; therefore, a decrease in these enzymes might be directly linked to the deficiency of vitamin K found in CKD patients. Further studies to elucidate the decrease in the expression of these enzymes in CKD should be addressed.

In the second part of the thesis, a novel inhibitor of vascular calcification was found “VIF”. VIF has proven to be a potent inhibitor of vascular calcification in *in vitro, ex vivo* and *in vivo* models. The underlying mechanism has been described in this thesis: VIF is able to reduce the production of ROS, and the secretion of inflammatory cytokines and therefore, to impede the progression of calcification pathways. Calcium-sensing receptor is the VIF binding partner, so VIF is suggested to act as a calcimimetic of this receptor, leading to a more positive calcification outcome.

The results of this thesis revealed new reasons behind the vitamin K deficiency in CKD patients. These should be taken into account in the supplementation approaches in clinic for a better outcome of the therapy. In addition, we have found a new mediator of vascular calcification, that could open new opportunities for the development of drugs in patients with a higher risk of this pathological mechanism like CKD patients.

Chapter 7

Societal impact

7. SOCIETAL IMPACT

Research in the biomedicine field is meant to improve people's lives in the way of looking for new treatments and cures against different diseases, the research is focused on understanding why these diseases develop and how to stop them.

Chronic kidney disease (CKD) and cardiovascular diseases (CVD) are major causes of human deaths worldwide each year [1,2,10]. As it has been described in this thesis, CVD and CKD are very closely linked, and one is a risk factor for the other and vice versa. When a patient suffers from CKD and CVD at the same time it is called "cardio renal syndrome". This syndrome is influenced by different pathological mechanisms, and vascular calcification is one of the main mechanisms that worsens the patients' prognosis [8]. Vascular calcification is an active process highly regulated by different inducers and inhibitors, an imbalance of these regulators triggers the development of vascular calcification [53]. One of these inhibitors is vitamin K, and it is known that patients with CKD have a vitamin K deficiency [146].

Therefore, in this thesis CKD models and CKD patients were studied to unravel the reason for the vitamin K2 deficiency in CKD patients. Furthermore, this thesis focused on a new mediator of vascular calcification, finding VIF as a strong inhibitor of this pathological process.

The findings of this thesis show that in *in vivo* models of CKD, there is a decrease in the vitamin K2 concentration, the MK4 isoform, in the kidneys of CKD models compared to the control ones. MK4 is linked to the inhibition of vascular calcification by the carboxylation of vitamin K-dependent proteins [55]. Our findings should be taken into consideration in the clinical supplementation approaches for CKD patients, since a deficiency in the transport and uptake of this isoform has been described by our group [120]. The MK4 deficiency might be related to the decreased expression of HMGCR, an enzyme involved in the conversion of vitamin K1 to vitamin K2, which was observed in CKD models in this thesis. Moreover, a decreased VKORC1 and NQO1 expression, enzymes involved in the vitamin recycling cycle, has also been shown in CKD models in this thesis. The expression of the enzymes HMGCR, VKORC1 and NQO1 negatively correlates with calcium deposition in kidneys. The data in this thesis explain the increased vascular calcification found in CKD patients, due to an impairment in the vitamin K metabolism, which hinders the carboxylation of VKDP. Although differences found in CKD patients were not significant, they show a tendency similar to the CKD models, which probably will be confirmed with a higher number of samples to analyse. All these results suggest a change should be considered in the clinical supplementation strategies when vitamin K is given to CKD patients, since the incorporation and transport of vitamin K2 isoforms

is also decreased in these patients [120]. Therefore, these findings reveal a new field to improve the clinic approaches, for example using adjuvants that help the vitamin K2 transport, especially to the kidney where MK4 concentrations are decreased.

The other discovery in this thesis is the new inhibitor of vascular calcification ´VIF´. VIF has shown to have a potent inhibitory effect *in vitro*, *ex vivo* and *in vivo* in the development of vascular calcification. The results of this thesis point to VIF as a possible calcimimetic of the calcium sensing receptor (CaSR). VIF is an endogenous inhibitor of vascular calcification, that can contra-regulate it. Clinical trials to investigate a correlation between vascular calcification in CKD patients and VIF should be performed to demonstrate this in more detail. Our findings open up the field for new therapeutic approaches against vascular calcification, where no effective treatment has been found yet. More studies are needed to analyse the benefit of the use of VIF as a drug, or its small active fragment (VIF 22-28 aa). This smaller fragment has better pharmacologic properties to be produced (paper under submission), but the same potency to inhibit vascular calcification.

All these novel findings have been presented and discussed in different international conferences and meetings, through posters and oral presentations. Furthermore, data from the first part of this thesis have been published in a peer-reviewed journal.

Chapter 8

References

8. REFERENCES

1. Eckardt, K. U. *et al.* Evolving importance of kidney disease: From subspecialty to global health burden. *Lancet* 382, 158–169 (**2013**).
2. Bikbov, B. *et al.* Global, regional, and national burden of chronic kidney disease, 1990–2017: a systematic analysis for the Global Burden of Disease Study 2017. *Lancet* 395, 709–733 (**2020**).
3. Gansevoort, R. T. *et al.* Chronic kidney disease and cardiovascular risk: epidemiology, mechanisms, and prevention. *Lancet* 382, 339–352 (**2013**).
4. Levey, A. S. *et al.* A New Equation to Estimate Glomerular Filtration Rate. *Ann. Intern. Med.* 150, 604–12 (**2009**).
5. How to Classify CKD | National Kidney Foundation. https://www.kidney.org/professionals/explore-your-knowledge/how-to-classify-ckd.
6. Denic, A., Glassock, R. J. & Rule, A. D. Structural and functional changes with the aging kidney. *Adv. Chronic Kidney Dis.* 23, 19–28 (**2016**).
7. Van Der Velde, M. *et al.* Lower estimated glomerular filtration rate and higher albuminuria are associated with all-cause and cardiovascular mortality. A collaborative meta-analysis of high-risk population cohorts. *Kidney Int.* 79, 1341–1352 (**2011**).
8. Alani, H., Tamimi, A. & Tamimi, N. Cardiovascular co-morbidity in chronic kidney disease: Current knowledge and future research needs. *World J. Nephrol.* 3, 156–168 (**2014**).
9. Paloian, N. J. & Giachelli, C. M. A current understanding of vascular calcification in CKD. *Am. J. Physiol. Renal Physiol.* 307, 891–900 (**2014**).
10. WHO | Cardiovascular diseases (CVDs). *WHO* (**2018**).
11. WHO, W. H. O. Global Atlas on Cardiovascular disease prevention and control. 155 (**2011**).
12. Marx, N. *et al.* Mechanisms of cardiovascular complications in chronic kidney disease: research focus of the Transregional Research Consortium SFB TRR219 of the University Hospital Aachen (RWTH) and the Saarland University. *Clin. Res. Cardiol.* 107, 120–126 (**2018**).
13. Visseren, F. L. J. *et al.* 2021 ESC Guidelines on cardiovascular disease prevention in clinical practiceDeveloped by the Task Force for cardiovascular disease prevention in clinical practice with representatives of the European Society of Cardiology and 12 medical societies With th. *Eur. Heart J.* 42, 3227–3337 (**2021**).
14. Bhargava, S., de la Puente-Secades, S., Schurgers, L. & Jankowski, J. Lipids and lipoproteins in cardiovascular diseases : a classification. *Trends Endocrinol. Metab.*

33, 409–423 (**2022**).

15. Soppert, J., Lehrke, M., Marx, N., Jankowski, J. & Noels, H. Lipoproteins and lipids in cardiovascular disease: from mechanistic insights to therapeutic targeting. *Adv. Drug Deliv. Rev.* 159, 4–33 (**2020**).
16. Wang, J. *et al.* New insights into the pathophysiological mechanisms underlying cardiorenal syndrome. *Aging (Albany. NY).* 12, 12422–12431 (**2020**).
17. Ronco, C. & Di Lullo, L. Cardiorenal Syndrome. *Heart Fail. Clin.* 10, 251–280 (**2014**).
18. London, G. M. *et al.* Arterial media calcification in end-stage renal disease: impact on all-cause and cardiovascular mortality. *Nephrol. Dial. Transplant.* 18, 1731–1740 (**2003**).
19. Paloian, N. J. & Giachelli, C. M. A current understanding of vascular calcification in CKD. *Am. J. Physiol. Renal Physiol.* 307, F891-900 (**2014**).
20. Lee, S. J., Lee, I. K. & Jeon, J. H. Vascular calcification—new insights into its mechanism. *International Journal of Molecular Sciences* vol. 21 2685 (**2020**).
21. Rennenberg, R. J. M. W. *et al.* Vascular calcifications as a marker of increased cardiovascular risk: A meta-analysis. *Vasc. Health Risk Manag.* 5, 185–197 (**2009**).
22. Di Bartolo, B. A. *et al.* TRAIL-deficiency accelerates vascular calcification in atherosclerosis via modulation of RANKL. *PLoS One* 8, e74211 (**2013**).
23. Kraus, M. A., Kalra, P. A., Hunter, J., Menoyo, J. & Stankus, N. The prevalence of vascular calcification in patients with end-stage renal disease on hemodialysis: a cross-sectional observational study. *Ther. Adv. Chronic Dis.* 6, 84 (**2015**).
24. Blaha, M. *et al.* Absence of Coronary Artery Calcification and All-Cause Mortality. *JACC Cardiovasc. Imaging* 2, 692–700 (**2009**).
25. Bardeesi, A. S. A. *et al.* A novel role of cellular interactions in vascular calcification. *J. Transl. Med.* 15, 95 (**2017**).
26. Hammes, M. Hemodynamic and Biologic Determinates of Arteriovenous Fistula Outcomes in Renal Failure Patients. *Biomed Res. Int.* 2015, 7 (**2015**).
27. Otsuka, F., Sakakura, K., Yahagi, K., Joner, M. & Virmani, R. Has our understanding of calcification in human coronary atherosclerosis progressed? *Arterioscler. Thromb. Vasc. Biol.* 34, 724–36 (**2014**).
28. Leopold, J. A. Vascular calcification: Mechanisms of vascular smooth muscle cell calcification. *Trends Cardiovasc. Med.* 25, 267–74 (**2015**).
29. Mizobuchi, M., Towler, D. & Slatopolsky, E. Vascular Calcification: The Killer of Patients with Chronic Kidney Disease. *J. Am. Soc. Nephrol.* 20, 1453–1464 (**2009**).
30. Reid, D. G. *et al.* Lipids in biocalcification: contrasts and similarities between intimal and medial vascular calcification and bone by NMR. *J. Lipid Res.* 53, 1569–1575 (**2012**).

31. Li, N. *et al.* Vascular adventitia calcification and its underlying mechanism. *PLoS One* 10, 1–12 (**2015**).
32. Himmelsbach, A., Ciliox, C. & Goettsch, C. Cardiovascular Calcification in Chronic Kidney Disease-Therapeutic Opportunities. *Toxins (Basel).* 12, 181 (**2020**).
33. Disthabanchong, S. Vascular calcification in chronic kidney disease: Pathogenesis and clinical implication. *World J. Nephrol.* 1, 43–53 (**2012**).
34. Bundy, J. D. *et al.* Risk factors for progression of coronary artery calcification in patients with chronic kidney disease: the CRIC study. *Atherosclerosis* 271, 53 (**2018**).
35. Lu, K. C., Wu, C. C., Yen, J. F. & Liu, W. C. Vascular calcification and renal bone disorders. *Sci. World J.* 2014, (**2014**).
36. Holmar, J. *et al.* Uremic Toxins Affecting Cardiovascular Calcification: A Systematic Review. *Cells* 9, 1–22 (**2020**).
37. Blaine, J., Chonchol, M. & Levi, M. Renal Control of Calcium, Phosphate, and Magnesium Homeostasis. *Clin. J. Am. Soc. Nephrol.* 10, 1257–1272 (**2015**).
38. Nguyen, N. T. *et al.* Oxidative stress by Ca2+ overload is critical for phosphate-induced vascular calcification. *Am. J. Physiol. - Hear. Circ. Physiol.* 319, H1302–H1312 (**2020**).
39. Alam, M. U. *et al.* Calcification is associated with loss of functional calcium-sensing receptor in vascular smooth muscle cells. *Cardiovasc. Res.* 81, 260–268 (**2009**).
40. Lopez-Fernandez, I., Schepelmann, M., Brennan, S. C., Yarova, P. L. & Riccardi, D. The calcium-sensing receptor: one of a kind. *Exp. Physiol.* 100, 1392–1399 (**2015**).
41. Voelkl, J. *et al.* Signaling pathways involved in vascular smooth muscle cell calcification during hyperphosphatemia. *Cell. Mol. Life Sci.* 1–15 (**2019**).
42. Hénaut, L. *et al.* Calcimimetics increase CaSR expression and reduce mineralization in vascular smooth muscle cells: mechanisms of action. *Cardiovasc. Res.* 101, 256–265 (**2014**).
43. Molostvov, G., Hiemstra, T. F., Fletcher, S., Bland, R. & Zehnder, D. Arterial expression of the calcium-sensing receptor is maintained by physiological pulsation and protects against calcification. *PLoS One* 10, 1–18 (**2015**).
44. Ritter, C. S. & Slatopolsky, E. In-Depth Review Phosphate Toxicity in CKD: The Killer among Us. *Clin J Am Soc Nephrol* 11, 1088–1100 (**2016**).
45. Azpiazu, D., Gonzalo, S., González-Parra, E., Egido, J. & Villa-Bellosta, R. Role of pyrophosphate in vascular calcification in chronic kidney disease. *Nefrología* 38, 250–257 (**2018**).
46. Villa-Bellosta, R. New insights into endogenous mechanisms of protection against arterial calcification. *Atherosclerosis* 306, 68–74 (**2020**).
47. Panh, L. *et al.* Coronary artery calcification: From crystal to plaque rupture. *Arch.*

Cardiovasc. Dis. 110, 550–561 (**2017**).

48. Kutikhin, A. G. *et al.* Calciprotein Particles: Balancing Mineral Homeostasis and Vascular Pathology. *Arterioscler. Thromb. Vasc. Biol.* 41, 1607–1624 (**2021**).
49. Miura, Y. *et al.* Identification and quantification of plasma calciprotein particles with distinct physical properties in patients with chronic kidney disease. *Sci. Rep.* 8, 1256 (**2018**).
50. Martínez-Moreno, J. M. *et al.* High phosphate induces a pro-inflammatory response by vascular smooth muscle cells and modulation by vitamin D derivatives. *Clin. Sci.* 131, 1449–1463 (**2017**).
51. Hnaut, L. & Massy, Z. A. New insights into the key role of interleukin 6 in vascular calcification of chronic kidney disease. *Nephrol. Dial. Transplant.* 33, 543–548 (**2018**).
52. Blanc, A., Pandey, N. R. & Srivastava, A. K. Distinct Roles of Ca2+, Calmodulin, and Protein Kinase C in H2O2-Induced Activation of ERK1/2, p38 MAPK, and Protein Kinase B Signaling in Vascular Smooth Muscle Cells. *Antioxid. Redox Signal.* 6, 353–366 (**2004**).
53. Schlieper, G., Schurgers, L., Brandenburg, V., Reutelingsperger, C. & Floege, J. Vascular calcification in chronic kidney disease: an update. *Nephrol. Dial. Transplant.* 31, 31–39 (**2016**).
54. Wen, L., Chen, J., Duan, L. & Li, S. Vitamin K-dependent proteins involved in bone and cardiovascular health. *Mol. Med. Rep.* 18, 3–15 (**2018**).
55. Nakagawa, K., Okubo, Y. & Masuyama, R. Vitamin Status and Mineralized Tissue Development. *Curr. Oral Heal. Reports* 5, 89–95 (**2018**).
56. Kaesler, N. *et al.* Impaired vitamin K recycling in uremia is rescued by vitamin K supplementation. *Kidney Int.* 86, 286–293 (**2014**).
57. Shioi, A., Morioka, T., Shoji, T. & Emoto, M. The Inhibitory Roles of Vitamin K in Progression of Vascular Calcification. *Nutrients* 12, 583 (**2020**).
58. Chiyoya, M. *et al.* Matrix Gla protein negatively regulates calcification of human aortic valve interstitial cells isolated from calcified aortic valves. *J. Pharmacol. Sci.* 136, 257–265 (**2018**).
59. Dahlberg, S. *et al.* Desphospho-Uncarboxylated Matrix-Gla Protein Is Increased Postoperatively in Cardiovascular Risk Patients. *Nutrients* 10, 46 (**2018**).
60. Cranenburg, E. C. M. *et al.* The circulating inactive form of matrix Gla Protein (ucMGP) as a biomarker for cardiovascular calcification. *J. Vasc. Res.* 45, 427–36 (**2008**).
61. Schurgers, L. J. *et al.* The Circulating Inactive Form of Matrix Gla Protein Is a Surrogate Marker for Vascular Calcification in Chronic Kidney Disease: A Preliminary Report. *Clin. J. Am. Soc. Nephrol.* 5, 568–75 (**2010**).

62. Lees, J. S., Chapman, F. A., Witham, M. D., Jardine, A. G. & Mark, P. B. Vitamin K status, supplementation and vascular disease: a systematic review and meta-analysis. *Heart* 105, 938–945 (**2018**).
63. Shea, M. K. *et al.* Circulating Uncarboxylated Matrix Gla Protein Is Associated with Vitamin K Nutritional Status, but Not Coronary Artery Calcium, in Older Adults. *J. Nutr.* 141, 1529 (**2011**).
64. Thijssen, H. H. W., Vervoort, L. M. T., Schurgers, L. J. & Shearer, M. J. Menadione is a metabolite of oral vitamin K. 95, 260–266 (**2006**).
65. Hirota, Y. *et al.* Menadione (vitamin K3) is a catabolic product of oral phylloquinone (vitamin K1) in the intestine and a circulating precursor of tissue menaquinone-4 (vitamin K2) in rats. *J. Biol. Chem.* 288, 33071–33080 (**2013**).
66. Halder, M. *et al.* Vitamin K: Double Bonds beyond Coagulation Insights into Differences between Vitamin K1 and K2 in Health and Disease. *Int. J. Mol. Sci.* 20, (**2019**).
67. Schwalfenberg, G. K. Vitamins K1 and K2: The Emerging Group of Vitamins Required for Human Health. *J. Nutr. Metab.* (**2017**).
68. Hirota, Y. *et al.* Functional characterization of the vitamin K2 biosynthetic enzyme UBIAD1. *PLoS One* 10, 1–24 (**2015**).
69. Schumacher, M. M., Jun, D. J., Johnson, B. M. & DeBose-Boyd, R. A. UbiA prenyltransferase domain-containing protein-1 modulates HMG-CoA reductase degradation to coordinate synthesis of sterol and nonsterol isoprenoids. *J. Biol. Chem.* 293, 312–323 (**2018**).
70. Schumacher, M. M. & Debose-Boyd, R. A. Posttranslational Regulation of HMG CoA Reductase, the Rate-Limiting Enzyme in Synthesis of Cholesterol. *Annu. Rev. Biochem.* 90, 659–679 (**2021**).
71. Zhelyazkova-Savova, M. D. *et al.* Statins, vascular calcification, and vitamin K-dependent proteins: Is there a relation? *Kaohsiung J. Med. Sci.* 37, 624–631 (**2021**).
72. Grzejszczak, P. & Kurnatowska, I. Role of Vitamin K in CKD: Is Its Supplementation Advisable in CKD Patients? *Kidney Blood Press. Res.* 46, 523–530 (**2021**).
73. Cranenburg, E. C. M. *et al.* Vitamin K intake and status are low in hemodialysis patients. *Kidney Int.* 82, 605–610 (**2012**).
74. Schurgers, L. J. Vitamin K: Key vitamin in controlling vascular calcification in chronic kidney disease. *Kidney International* vol. 83 782–784 (**2013**).
75. Dai, L. *et al.* Sevelamer Use in End-Stage Kidney Disease (ESKD) Patients Associates with Poor Vitamin K Status and High Levels of Gut-Derived Uremic Toxins: A Drug–Bug Interaction? *Toxins (Basel).* 12, 351 (**2020**).
76. Cozzolino, M. *et al.* Current therapy in ckd patients can affect vitamin k status.

Nutrients 12, 6–10 (**2020**).

77. Schlieper, G. *et al.* Circulating Nonphosphorylated Carboxylated Matrix Gla Protein Predicts Survival in ESRD. *J. Am. Soc. Nephrol.* 22, 387–395 (**2011**).
78. de Vriese, A. S. *et al.* Multicenter randomized controlled trial of Vitamin K antagonist replacement by rivaroxaban with or without vitamin K2 in hemodialysis patients with atrial fibrillation: The Valkyrie study. *J. Am. Soc. Nephrol.* 31, 186–196 (**2020**).
79. Kurnatowska, I. *et al.* Effect of vitamin K2 on progression of atherosclerosis and vascular calcification in nondialyzed patients with chronic kidney disease stages 3-5. *Pol. Arch. Med. Wewn.* 125, 631–640 (**2015**).
80. Zwakenberg, S. R. *et al.* The effect of menaquinone-7 supplementation on vascular calcification in patients with diabetes: A randomized, double-blind, placebo-controlled trial. *Am. J. Clin. Nutr.* 110, 883–890 (**2019**).
81. Witham, M. D. *et al.* Vitamin K supplementation to improve vascular stiffness in CKD: The K4Kidneys randomized controlled trial. *J. Am. Soc. Nephrol.* 31, 2434–2445 (**2020**).
82. Schurgers, L. J. *et al.* Regression of warfarin-induced medial elastocalcinosis by high intake of vitamin K in rats. *Blood* 109, 2823–31 (**2007**).
83. Saritas, T. *et al.* Vitamin K1 and progression of cardiovascular calcifications in hemodialysis patients: The VitaVasK randomized controlled trial. *Clin. Kidney J.* 0, 1–12 (**2022**).
84. Vossen, L. M. *et al.* Menaquinone-7 Supplementation to Reduce Vascular Calcification in Patients with Coronary Artery Disease: Rationale and Study Protocol (VitaK-CAC Trial). *Nutrients* 7, 8905–8915 (**2015**).
85. Neves, P. O., Andrade, J. & Monção, H. Coronary artery calcium score: current status. *Radiol. Bras.* 50, 182 (**2017**).
86. Kakani, E., Elyamny, M., Ayach, T. & El-Husseini, A. Pathogenesis and management of vascular calcification in CKD and dialysis patients. *Semin. Dial.* 00, 1–9 (**2019**).
87. Bover, J. *et al.* Detection of cardiovascular calcifications: Is it a useful tool for nephrologists? *Nefrologia* 36, 587–596 (**2016**).
88. Bover, J. *et al.* Clinical Approach to Vascular Calcification in Patients With Non-dialysis Dependent Chronic Kidney Disease: Mineral-Bone Disorder-Related Aspects. *Front. Med.* 8, 642718 (**2021**).
89. Pasch, A. *et al.* Nanoparticle-based test measures overall propensity for calcification in serum. *J. Am. Soc. Nephrol.* 23, 1744–1752 (**2012**).
90. Ruderman, I., Holt, S. G., Hewitson, T. D., Smith, E. R. & Toussaint, N. D. Current and potential therapeutic strategies for the management of vascular calcification in patients with chronic kidney disease including those on dialysis. *Semin. Dial.* 31, 487–

499 (**2018**).

91. Hannan, F. M., Olesen, M. K. & Thakker, R. V. Calcimimetic and calcilytic therapies for inherited disorders of the calcium-sensing receptor signalling pathway. *Br. J. Pharmacol.* 175, 4083 (**2018**).
92. Caffarelli, C., Montagnani, A., Nuti, R. & Gonnelli, S. Bisphosphonates, atherosclerosis and vascular calcification: update and systematic review of clinical studies. *Clin. Interv. Aging* 12, 1819–1828 (**2017**).
93. Zeper, L. W. & de Baaij, J. H. F. Magnesium and calciprotein particles in vascular calcification: the good cop and the bad cop. *Curr. Opin. Nephrol. Hypertens.* 28, 368–374 (**2019**).
94. Diaz-Tocados, J. M. *et al.* Dietary magnesium supplementation prevents and reverses vascular and soft tissue calcifications in uremic rats. *Kidney Int.* 92, 1084–1099 (**2017**).
95. Bressendorff, I. *et al.* Oral Magnesium Supplementation in Chronic Kidney Disease Stages 3 and 4: Efficacy, Safety, and Effect on Serum Calcification Propensity—A Prospective Randomized Double-Blinded Placebo-Controlled Clinical Trial. *Kidney Int. Reports* 2, 380 (**2017**).
96. Bressendorff, I., Hansen, D., Schou, M., Pasch, A. & Brandi, L. The effect of increasing dialysate magnesium on serum calcification propensity in subjects with end stage kidney disease: A randomized, controlled clinical trial. *Clin. J. Am. Soc. Nephrol.* 13, 1373–1380 (**2018**).
97. Bressendorff, I., Hansen, D., Schou, M., Kragelund, C. & Brandi, L. The effect of magnesium supplementation on vascular calcification in chronic kidney disease—a randomised clinical trial (MAGiCAL-CKD): essential study design and rationale. *BMJ Open* 7, (**2017**).
98. Drueke, T. B. & Massy, Z. A. Role of vitamin D in vascular calcification: bad guy or good guy? *Nephrol. Dial. Transplant.* 27, 1704–1707 (**2012**).
99. Wang, J., Zhou, J. J., Robertson, G. R. & Lee, V. W. Vitamin D in Vascular Calcification: A Double-Edged Sword? *Nutrients* 10, 652 (**2018**).
100. Perelló, J. *et al.* Mechanism of action of SNF472, a novel calcification inhibitor to treat vascular calcification and calciphylaxis. *Br. J. Pharmacol.* 177, 4400 (**2020**).
101. Sinha, S. *et al.* The CALCIPHYX study: a randomized, double-blind, placebo-controlled, Phase 3 clinical trial of SNF472 for the treatment of calciphylaxis. *Clin. Kidney J.* 15, 136–144 (**2021**).
102. Mahata, S. K. & Corti, A. Chromogranin A and its fragments in cardiovascular, immunometabolic, and cancer regulation. *Ann. N.Y. Acad. Sci* 1455, 34–58 (**2019**).
103. Fasciotto, B. H., Denny, J. C., Greeley, G. H. & Cohn, D. V. Processing of

chromogranin A in the parathyroid: generation of parastatin-related peptides. *Peptides* 21, 1389–1401 (**2000**).

104. Ghinassi, B., Di Baldassarre, A., Izzicupo, P., D'amico, M. A. & Manzoli, L. Biological function and clinical relevance of chromogranin A and derived peptides. *Endocr. Connect.* 3, R45–R54 (**2014**).
105. Orth-Alampour, S. *et al.* Prevention of vascular calcification by the endogenous chromogranin A-derived mediator that inhibits osteogenic transdifferentiation. *Basic Res. Cardiol.* 116, 57 (**2021**).
106. Salem, S. *et al.* Identification of the Vasoconstriction-Inhibiting Factor (VIF), a potent endogenous cofactor of angiotensin II acting on the angiotensin II type 2 receptor. *Circulation* 131, 1426–1434 (**2015**).
107. Kukida, M. *et al.* AT2 receptor stimulation inhibits phosphate-induced vascular calcification. *Kidney Int.* 95, 138–148 (**2019**).
108. Bai, H. Y., Shan, B. S. & Jiang, Y. N. The protective effects of renin–angiotensin system compont on vascular calcification. *J. Hum. Hypertens.* 35, 410–418 (**2021**).
109. Herencia, C. *et al.* Angiotensin II prevents calcification in vascular smooth muscle cells by enhancing magnesium influx. *Eur. J. Clin. Invest.* 45, 1129–1144 (**2015**).
110. Herrmann, J., Babic, M., Tölle, M., van der Giet, M. & Schuchardt, M. Research Models for Studying Vascular Calcification. *International journal of molecular sciences* vol. 21 (**2020**).
111. Holmar, J. *et al.* Development, establishment and validation of in vitro and ex vivo assays of vascular calcification. *Biochem. Biophys. Res. Commun.* 530, 462–470 (**2020**).
112. Shioi, A. *et al.* β-Glycerophosphate Accelerates Calcification in Cultured Bovine Vascular Smooth Muscle Cells. *Arterioscler. Thromb. Vasc. Biol.* 15, 2003–2009 (**1995**).
113. Leopold, J. A. Vascular Calcification: An Age-Old Problem of Old Age. *Circulation* 127, 2380 (**2013**).
114. Cozzolino, M. *et al.* Vitamin K in Chronic Kidney Disease. *Nutrients* 11, 1–11 (**2019**).
115. Niederhoffer, N., Bobryshev, Y. V, Lartaud-Idjouadiene, I., Giummelly, P. & Atkinson, J. Aortic calcification produced by vitamin D3 plus nicotine. *J. Vasc. Res.* 34, 386–98 (**1997**).
116. Gaillard, V. *et al.* Renal function and structure in a rat model of arterial calcification and increased pulse pressure. *Am. J. Physiol. - Ren. Physiol.* 295, 1222–1229 (**2008**).
117. Chirumamilla, C. S. *et al.* Profiling activity of cellular kinases in migrating T-cells. *Methods Mol. Biol.* 1930, 99–113 (**2019**).
118. Vanholder, R., Pletinck, A., Schepers, E. & Glorieux, G. Biochemical and clinical

impact of organic uremic retention solutes: A comprehensive update. *Toxins (Basel).* 10, 33 (**2018**).

119. Gajjala, P. R., Fliser, D., Speer, T., Jankowski, V. & Jankowski, J. Emerging role of post-translational modifications in chronic kidney disease and cardiovascular disease. *Nephrol. Dial. Transplant.* 30, 1814–1824 (**2015**).
120. Kaesler, N. *et al.* Altered vitamin K biodistribution and metabolism in experimental and human chronic kidney disease. *Kidney Int.* 101, 338–348 (**2022**).
121. Kalra, S. S. & Shanahan, C. M. Vascular calcification and hypertension: Cause and effect. *Ann. Med.* 44, S85-92 (**2012**).
122. Yang, Y. *et al.* AKT-independent activation of p38 MAP kinase promotes vascular calcification. *Redox Biol.* 16, 97 (**2018**).
123. Lee, G. L. *et al.* TLR2 promotes vascular smooth muscle cell chondrogenic differentiation and consequent calcification via the concerted actions of osteoprotegerin suppression and IL-6-Mediated RANKL induction. *Arterioscler. Thromb. Vasc. Biol.* 39, 432–445 (**2019**).
124. Reynolds, J. L. *et al.* Human vascular smooth muscle cells undergo vesicle-mediated calcification in response to changes in extracellular calcium and phosphate concentrations: a potential mechanism for accelerated vascular calcification in ESRD. *J. Am. Soc. Nephrol.* 15, 2857–2867 (**2004**).
125. Proudfoot, D. *et al.* Apoptosis regulates human vascular calcification in vitro: Evidence for initiation of vascular calcification by apoptotic bodies. *Circ. Res.* 87, 1055–1062 (**2000**).
126. Ciceri, P. *et al.* Iron citrate reduces high phosphate-induced vascular calcification by inhibiting apoptosis. *Atherosclerosis* 254, 93–101 (**2016**).
127. Aghagolzadeh, P. *et al.* Calcification of vascular smooth muscle cells is induced by secondary calciprotein particles and enhanced by tumor necrosis factor-α. *Atherosclerosis* 251, 404–414 (**2016**).
128. McCabe, K. M. *et al.* Vitamin K Metabolism in a Rat Model of Chronic Kidney Disease. *Am. J. Nephrol.* 45, 4–13 (**2017**).
129. Moghadam, B. F. & Fereidoni, M. Neuroprotective effect of menaquinone-4 (MK-4) on transient global cerebral ischemia/ reperfusion injury in rat. *PLoS One* 15, 1–30 (**2020**).
130. Nakagawa, K. *et al.* Identification of UBIAD1 as a novel human menaquinone-4 biosynthetic enzyme. *Nature* 468, 117–121 (**2010**).
131. Nickerson, M. L. *et al.* The UBIAD1 Prenyltransferase Links Menaquione-4 Synthesis to Cholesterol Metabolic Enzymes. *Hum. Mutat.* 34, 317–329 (**2013**).
132. Shavit, L., Jaeger, P. & Unwin, R. J. What is nephrocalcinosis? *Kidney Int.* 88, 35–43

(**2015**).

133. Hawkins, C. L. Protein carbamylation: a key driver of vascular calcification during chronic kidney disease. *Kidney Int.* 94, 12–14 (**2018**).
134. Mori, D. *et al.* Protein carbamylation exacerbates vascular calcification. *Kidney Int.* 94, 72–90 (**2018**).
135. Chen, X. *et al.* Naturally occurring UBIAD1 mutations differentially affect menaquinone biosynthesis and vitamin K-dependent carboxylation. *FEBS J.* 289, 2613–2627 (**2021**).
136. Sarosiak, A. *et al.* High expression of Matrix Gla Protein in Schnyder corneal dystrophy patients points to an active role of vitamin K in corneal health. *Acta Ophthalmol.* 99, e171–e177 (**2021**).
137. Michaux, A. *et al.* Missense mutation of VKORC1 leads to medial arterial calcification in rats. *Sci. Rep.* 8, 13733 (**2018**).
138. Hu, B. *et al.* Involvement of VKORC1 in the inhibition of calcium oxalate crystal formation in HK-2 cells. *J. Huazhong Univ. Sci. Technol.* 34, 376–381 (**2014**).
139. Thul, P. J. *et al.* A subcellular map of the human proteome. *Science (80-.).* 356, (**2017**).
140. Klinkhammer, B. M. *et al.* Current kidney function parameters overestimate kidney tissue repair in reversible experimental kidney. *Kidney Int.* 10, 307–320 (**2022**).
141. Nelson, A. J. *et al.* Targeting Vascular Calcification in Chronic Kidney Disease. *JACC Basic to Transl. Sci.* 5, 398–412 (**2020**).
142. Evenepoel, P. *et al.* Microscopic nephrocalcinosis in chronic kidney disease patients. *Nephrol. Dial. Transplant.* 30, 843–848 (**2015**).
143. Orth-Alampour, S. *et al.* Prevention of vascular calcification by the endogenous chromogranin A-derived mediator that inhibits osteogenic transdifferentiation. *Basic Res. Cardiol. 2021* 116, 1–24 (**2021**).
144. Alexander, M. R. & Owens, G. K. Epigenetic Control of Smooth Muscle Cell Differentiation and Phenotypic Switching in Vascular Development and Disease. *Annu. Rev. Physiol.* 74, 13–40 (**2012**).
145. Mendoza, F. J. *et al.* Effect of calcium and the calcimimetic AMG 641 on matrix-Gla protein in vascular smooth muscle cells. *Calcif. Tissue Int.* 88, 169–178 (**2011**).
146. Holden, R. M. *et al.* Vitamins K and D status in stages 3-5 chronic kidney disease. *Clin. J. Am. Soc. Nephrol.* 5, 590–7 (**2010**).

Chapter 9

List of figures

9. LIST OF FIGURES

Chapter 10

List of tables

10. LIST OF TABLES

Chapter 11

About the author

11. ABOUT THE AUTHOR

Sofía de la Puente-Secades was born on August 16th 1993 in Oviedo (Asturias, Spain). In this small city in the north of Spain, she did all her primary, secondary and university studies. At the University of Oviedo, she successfully completed her Bachelor in Biotechnology in 2015 with the bachelor thesis titled '*The effect of DMSO in the secondary metabolism of Streptomyces'*, and one year later she obtained the Master of Science in Biomedicine and Molecular Oncology with a master thesis on *'Lung Cancer in Electroplating workers with mutations in DNA repair genes'*. During the Bachelor's, Sofía had her first experience abroad, studying for 6 months in Mexico in the Tecnológico de Monterrey (Campus Puebla). After fulfilling her university studies, she moved to Madrid to work for two years in the´ Medical-Chemistry Institute´ of the ´Spanish National Research Council´ as a research assistant. During these two years , she worked under the supervision of Dr. Ana San-Félix on different projects on the research of antiviral and antibacterial drugs, performing organic chemical synthesis and bioinformatics research at the same time. Moreover, during this time she was a co-author of two papers *'A Novel Class of Cationic and Non-Peptidic Small Molecules as Hits for the Development of Antimicrobial Agents'* Jiménez A. *et al* 2018, and *'Double Arylation of the Indole Side Chain of Tri- and Tetrapodal Tryptophan Derivatives Renders Highly Potent HIV-1 and EV-A71 Entry Inhibitors'* Martí-Marí O. *et al.* 2021 and co-inventor of a patent to synthesis '*Peptides containing D-alanine (D-Ala) or related amino alcohols*'. After these two years, she realised research is what she loved, she was looking forward to having her own project and coming back to the biological field. That is why Sofia decided to move to Aachen. In Aachen she joined the Institute of Molecular Cardiovascular Research (IMCAR) in the Uniklinik-RWTH Aachen, after being awarded with a Marie Skłodowska-Curie Actions-ITN CaReSyAn (CArdioREnal SYndrome Analysis) under the supervision of Prof. Joachim Jankowski and Prof. Juergen Flöge. Sofía's PhD project is focused on vascular calcification in cardio-renal syndrome, with a special focus on vitamin K deficiency and the search for new mediators. During her PhD, Sofía performed a secondment in the Cardiovascular Research Institute Maastricht (CARIM) in the Netherlands, in the lab of Prof. Leon Schurgers, focused on vitamin K and vascular calcification. The research of her PhD thesis is described in detail in this thesis entitled ***'Vascular calcification in chronic kidney disease: vitamin K deficiency and new mediators'.***

Chapter 12

Publications

12. PUBLICATIONS

1. Holmar, J.*, de la Puente-Secades, S.*, Floege, J., Noels, H., Jankowski, J., Orth-Alampour, S. Uremic Toxins Affecting Cardiovascular Calcification: A Systematic Review. *Cells* 9, 1–22 (**2020**). *equal contribution

2. Kaesler, N., Schreibing, F., Speer, T., Puente-Secades, S de la. *et al.* Altered vitamin K biodistribution and metabolism in experimental and human chronic kidney disease. *Kidney Int.* 101, 338–348 (**2022**).

3. Bhargava, S., de la Puente-Secades, S., Schurgers, L., Jankowski, J. Lipids and lipoproteins in cardiovascular diseases : a classification. *Trends Endocrinol. Metab.* 33, 409–423 (**2022**).

4. de la Puente-Secades, S., Mikolajetz, D. *et al.* VIF: A new chromogranin A-derived peptidic inhibitor of vascular calcification. Under submission

Chapter 13

Conferences and workshops

13. CONFERENCES AND WORKSHOPS

- Poster presentation at Aachen Conference on Cardiorenal Disease and Diabetes in October 2022 titled "*VIF: A new peptidic inhibitor of vascular calcification derived from chromogranin A"*

- Oral presentation award and poster presentation at ESAO-EUTox Summer School in September 2022 titled "*VIF: A new peptidic inhibitor of vascular calcification derived from chromogranin A"*

- Poster presentation at ESAO-EUTox Summer School in September 2022 titled "*Vitamin K deficiency in CKD beyond the diet: vitamin K relating enzymes"*

- Poster presentation at SFB/TRR219 Winter School in May 2022 titled "*VIF: A new chromogranin A derived peptidic inhibitor of vascular calcification"*

- Poster presentation at SFB/TRR219 Winter School in May 2022 titled "*Vitamin K deficiency in CKD beyond the diet: expression of vitamin K converting enzymes"*

- "Business & Entrepreneurship" online workshop in Nov-Dec 2020 organized by Karolinska Institute (Sweden)

- Participation in "Career and scientific workshop" in October 2020 organized by SFB/TRR219

- "Statistics in Biomedicine" workshop in June 2020 organized by ITN CaReSyAn

- Poster presentation at SFB/TRR219 Winter School in February 2020 titled "*Vitamin K and vascular calcification: why there is Vitamin K deficiency in CKD?"*

- "Proteomics/peptidomics analyses: principles, methodologies & application in CKD" workshop in February 2019 by ITN CaReSyAn

- Poster presentation at Vascular Medicine and Atherosclerosis Congress (VMAC) in May 2019, titled *"Vascular calcification in CRS: identification of new pathological mediators"*

- Poster presentation at SFB/TRR219 Winter School in January 2019 titled *"Vascular calcification in CRS: identification of new pathological mediators"*

- Poster presentation at SFB/TRR219 Winter School in August 2018 titled *"Vascular calcification in CRS: identification of new pathological mediators"*

Chapter 14

Acknowledgements

14. ACKNOWLEDGEMENTS

Four years of my life are compiled in these pages. For a long time, I have imagined how my own research project would look like, and now I could say that I am completely satisfied and happy about the result.

First of all, I would like to thank Prof. Dr. Joachim Jankowski for giving me the opportunity to have my own project, and the chance to develop as a researcher at his institute. Furthermore, he gave me the freedom, as well as the proper guidance to achieve this thesis. On the same line, I would like to thank Prof. Dr. Jürgen Floege for his guidance in a project completely new for me and for always give the best advices. I would like to thank both Prof. Dr. Joachim Jankowski and Prof. Dr. Jürgen Floege for giving me the opportunity of been an ITN Marie-Curie fellow for CaReSyAn, and all the good things that this fellowship implied. Of course, I could not forget to thank PD Dr. Heidi Noels who was the first person I had contact with about this project, and thanks to her dedication and effort, we managed to bring the project forward, even dealing with a pandemic in the meantime.

Special words are for Dr. Setareh Orth-Alampour, without her, nothing from this thesis would have been possible. I would like to thank her for being kind, patient, and always available for all my questions, which of course, were always a lot. As we say at IMCAR, she is my lab-Mama, and I couldn't have a better one, she showed me how to be independent, critical, detailed and all the adjectives that a good scientist needs. At the beginning I called her my supervisor, but at the end, we were two colleagues working hand by hand as a team with really successful results.
In addition, I would like to thank Dr. Nadine Kaesler for introducing me into the world of vitamin K and its metabolism, and for giving me the opportunity of contributing to vitamin K research in CKD.

I would like to thank the collaborators that helped me on this project, Dr. Julianne Hermann from IMCAR for the MALDI imaging of post-translational modifications, Dr. Nathalie Gayrard from INSERM in Montpellier for carrying out the *in vivo* experiments for VIF, Dr. Emiel P.C. van der Vorst from IMCAR for performing the kinases arrays, Dr. Sinna Koppert from Biointerface Laboratory in Aachen for introducing me to the world of Calciprotein particles, and Prof. Dr. Vera Jankowski for her hours working on Mas-Spec to bring the best outcome of this project.

Many thanks to Prof. Dr. Leon Schurgers and all his lab members, particularly Niko Rapp, from CARIM in Maastricht, who helped me to develop in the world of vascular calcification during the months I stayed with them, and further with multiple on-line discussions.
My CaReSyAn ESRs family from so many different countries, I think there could not be a better team against cardiorenal syndrome. And even if the COVID-19 did not allow us to meet as much as we wanted, I am pretty sure our paths will meet again, Giulia, Valeria, Ana, Niko, Sam, Irene, Jeppe, Eleni, Tina and Rogier.

Of course many thanks to all the IMCAR members for welcoming me from day one, and all the members from the Nephrology department in Uniklinik Aachen, who helped me in any moment of need. Special thanks to the calcification group, Dr. Shruti Bhargava, Dr. Zhuojun Wu, Dr. Jana Holmar, Amina and Svea, whose help was essential to build this project. Also to Yuan and Roya, the technicians who gave me their assistant when needed. To Dr. Wendy Theelen for her great contribution and help during the last days before finalising this thesis. But particular mention goes to Dustin, who started as my first master student to be supervised, and now has become one of the major supports I had during my PhD, not only inside, but also outside the lab.

However, the work of this 4 years could have not been done without the support of my “International office”. An office where not only good or bad results were shared, but also good and bad days, a lot of fun and funny moments. They were the people that supported me in the first moments after something went wrong in the lab, and the first people that were happy about my achievements. I apologise for all my “confrontations” with the computer, but I’m pretty sure that now you are all much more fluent in Spanish. Thank you Dustin, Michaela, Federica, Kai, Sandra, Constance, Wendy, Jana, Caro…and everyone that during these four years came by our office. But special words go to my twin-ESR Giulia. My twin-ESR because I think it is fortunate to have shared with you these 4 years, from day 0 till now. And not only for expending 8 h per day, 5 days per week, but also for all the hours outside the office. We have had each other’s back, and even being so different we have matched so well.

Many thanks to all my German colleagues, for helping me not only in the lab and particularly with German-language problems, but also for amazing evenings after work, Christian, Sonja, T.Schulz and Erik.

Mention to Sandra Knarren, our secretary but also our problem-solver. My life in Aachen would have been much harder without her.

Last but not least, cannot forget all the people, that being completely out of this science world, have supported, listened and helped me during these four years. Of course my family first, my parents and brother, who supported me from the moment I left my home in Spain, and have shared and understood every instant from my life in Aachen from the distance. Gracias por estar siempre ahí y apoyarme en todas mi decisiones. To my Spanish friends and their support from far away, but special mention to *Las Sabias*, Ana and Laura, who even being spread around Europe, it feels like we meet every day, they knew when was the perfect moment to take a break in the lab, travel around the world and come back full of energy. To Elena for being the artist of the cover of this thesis and being able to capture all my ideas.
And to Tim R., for being my daily support.